Spring 2023

Efficient High Order Ensemble for Fluid Flow

John Carter
Missouri University of Science and Technology

Department: Mathematics and Statistics

EFFICIENT HIGH ORDER ENSEMBLE METHODS FOR FLUID FLOW

by

JOHN AUSTIN CARTER

A DISSERTATION

Presented to the Graduate Faculty of the

MISSOURI UNIVERSITY OF SCIENCE AND TECHNOLOGY

In Partial Fulfillment of the Requirements for the Degree

DOCTOR OF PHILOSOPHY

in

MATHEMATICS WITH COMPUTATIONAL AND APPLIED EMPHASIS

2023

Approved by:

Daozhi Han, Advisor
Nan Jiang, Co-Advisor
Xiaoming He
Yanzhi Zhang
John Singler
Guirong Yan

PUBLICATION DISSERTATION OPTION

This dissertation consists of the following three articles, formatted in the style used by the Missouri University of Science and Technology.

Paper I: Pages 3-21 have been accepted by Numerical Methods for Partial Differential Equations Journal.

Paper II: Pages 22-59 have been accepted by Journal of Scientific Computing.

Paper III: Pages 60-73 are intended for submission to Journal of Scientific Computing.

ABSTRACT

This thesis proposes efficient ensemble-based algorithms for solving the full and reduced Magnetohydrodynamics (MHD) equations. The proposed ensemble methods require solving only one linear system with multiple right-hand sides for different realizations, reducing computational cost and simulation time. Four algorithms utilize a Generalized Positive Auxiliary Variable (GPAV) approach and are demonstrated to be second-order accurate and unconditionally stable with respect to the system energy through comprehensive stability analyses and error tests. Two algorithms make use of Artificial Compressibility (AC) to update pressure and a solenoidal constraint for the magnetic field. Numerical simulations are provided to illustrate theoretical results and demonstrate the efficiency and long-time accuracy of the proposed algorithms.

ACKNOWLEDGMENTS

I would like to thank my close friends in and outside academia who were with me through so much. In particular, thanks to my roommates and life-long friends Xuejian Li, Austin Vandegriffe and Louis Steinmiester, who could always offer advice, discuss world-events, and quip jokes often needed. I thank my wife Jialin for being with me through good and bad times, a partner with whom to find solutions for everything life brought. Thanks to Yumeng Wang for great friendship and competitive sports, my officemate Rukman for philosophical conversations, and Shiping for time we spent learning that teaching is the best way to learn. I thank my parents for their support and willingness to help and, on occasion, offering a place to relax in their countryside homestead.

Thanks to my advisor, Dr. Han, for giving his all to direct me even through events such as the Covid 19 pandemic. Thanks to Dr. Zhang for offering the most sincere advice, analyzing life in many aspects and extracting meaningful veiwpoints to a level I'll always remember. A considerate heart and earnestly caring for students' futures, I hope I may learn to guide people similarly. Thanks to my co-advisor, Dr. Jiang, for giving me direction in research. Even as I branch out, these foundations will always remain pivotal. A big thanks to Dr. Singler and Dr. He for much of my academic coursework that has transferred to research in numerous ways. Thanks to Dr. Yan for following my work and offering questions from useful perspectives.

Finally, I thank my grandfather, Dean, for instilling a tendency to veiw everyone as a kindred spirit, helping when possible and holding this notion that we can more readily move towards peace when we can be mindful for the peace of others. He was a testament that even through great suffering, believing in your work and focusing on your path can wrought a beacon of content and ambition that shows upon you and those around you. With what I've been given, may I continue along his path and allow that beacon to shine farther.

This work was partially supported by the US National Science Foundation grants DMS-1720001, DMS-1912715, and DMS-2120413.

TABLE OF CONTENTS

Page

LIST OF ILLUSTRATIONS

Figure Page

PAPER I

PAPER II

PAPER III

LIST OF TABLES

1. INTRODUCTION

In most applications, methods for modeling fluid flow can be highly sensitive due to imperfect initial conditions and parameters. These errors cause deviations that increase over time and propagate throughout the simulation domain, leading to inaccurate long-term predictions. Uncertainty quantification (UQ) is one field that aims to remedy this, often through statistical approaches. Ensemble-based UQ methods combine the results of multiple calculations with slightly different initial conditions and forcing terms to improve the accuracy of long-term predictions. However, for large-scale simulations, it is not feasible to obtain predictions one-by-one for a large ensemble of parameters at a high spatial resolution within a specific time window.

The purpose of this thesis is to introduce efficient second-order numerical schemes involving an ensemble mean for the magnetohydrodynamics equations (MHD). The ensemble mean addresses the computational burden associated with solving PDEs for each realization. This is done by considering all realizations sharing the same coefficient matrix, and efficient block-solvers can then be applied to the resulting single linear system with multiple right-hand sides. This approach enables us to compute a large ensemble for a prescribed accuracy with limited computational resources.

In this thesis, we focus on developing efficient second-order ensemble methods for MHD flow simulations. Section 2 presents our paper focused on an ensemble mean algorithm for solving the reduced MHD at small magnetic reynolds number, and presents extensive error and stability analysis, along with numerical tests to verify results. Section 3 presents our paper describing two ensemble algorithms for the full MHD combined with a scalar auxiliary variable (SAV) technique to explicitly discretize nonlinear terms while maintaining unconditional stability with respect to a modified system energy equation. Section 4 describes extending the approach in Section 3 to a scheme that utilizes artificial

compressibility to separate the velocity and magnetic field equations from the pressure and solenoidal constraint equations respectively. Finally, Section 4 will conclude and discuss future potential directions.

Overall, this thesis aims to contribute to provide new insights into the use of ensemble methods for practical and computationally efficient simulations.

PAPER

I. NUMERICAL ANALYSIS OF A SECOND ORDER ENSEMBLE METHOD FOR EVOLUTIONARY MHD EQUATIONS AT SMALL MAGNETIC REYNOLDS NUMBER

J. A. Carter, J. Nan
Department of Computational & Applied Mathematics
Missouri University of Science and Technology
Rolla, Missouri 65409–0050
Tel: 573–341–6622, Fax: 573–341–4115
Email: jachdm@mst.edu

ABSTRACT

We study a second order ensemble method for fast computation of an ensemble of MHD flows at small magnetic Reynolds number. Computing an ensemble of flow equations with different input parameters is a common procedure for uncertainty quantification in many engineering applications, for which the computational cost can be prohibitively expensive for nonlinear complex systems. We propose an ensemble algorithm that requires only solving one linear system with multiple right-hands instead of solving multiple different linear systems, which significantly reduces the computational cost and simulation time. Comprehensive stability and error analyses are presented proving conditional stability and second order in time convergent. Numerical tests are provided to illustrate theoretical results and demonstrate the efficiency of the proposed algorithm.

Keywords: MHD, low magnetic Reynolds number, uncertainty quantification, ensemble algorithm, finite element method, partitioned method

1.1. INTRODUCTION

Uncertainty quantification (UQ) is critical to effective flow simulations with uncertain model inputs such as initial conditions, forcing functions and other model parameters. The main challenge for studying efficient UQ methods is the excessive computational cost. Ensemble-based UQ methods are nonintrusive in the sense that they require the solution of a set of deterministic PDEs corresponding to different parameter samples and legacy flow solvers can be used without modifications. These methods require little coding efforts and some require much less realizations to achieve certain accuracy, proving to be effective in many applications. Nevertheless, for large-scale simulations, it is not realistic to run simulations over a large ensemble of parameters at a high spatial resolution and obtain predictions within a certain time window, which is essential for important applications such as numerical weather prediction. Ensemble methods have been developed in recent years aiming to address this issue. The idea is that if all realizations share the same coefficient matrix, efficient block solvers can be applied to solve the resulting single linear system with multiple right-hand sides. In [1], the first ensemble method was developed for solving the Navier-Stokes equations, which cleverly split the nonlinear term into two parts, the mean and the fluctuation. The mean doesn't depend on the ensemble index and thus is the same for all realizations, while the fluctuation term that does depend on the ensemble index was lagged to the previous timestep and thus can be moved to the right-hand side of the equation without affecting the coefficient matrix. All realizations can then be solved at one pass with efficient block solvers greatly reducing the averaged computational cost for each realization, making the algorithm well-suited for applications that require computing a large ensemble for a prescribed accuracy but have limited computer resources. This algorithm has been further tested for high-Reynolds number flows [2, 3], turbulent flows [4, 5] and other flow models [6–10]. It has been demonstrated to be highly computationally efficient used in conjunction with UQ methods such as the Monte Carlo method [8, 11, 12], multilevel Monte Carlo [13], pseudo-spectral stochastic collocation [14], and the proper orthogonal

decomposition (POD) technique [15–17]. In this report, we study a second order ensemble algorithm for Magnetohydrodynamics (MHD) flows at small magnetic Reynolds number and develop a second order accurate ensemble algorithm for fast computation.

1.1.1. GOVERNING EQUATIONS.

1.1.1.1. Reduced MHD. Magnetohydrodynamics (MHD) flows occur in many important applications such as plasmas, astrophysics, planetary science and metallized industry. For liquid metals, the induced magnetic field is negligible compared with the imposed magnetic field leading to a reduced MHD model. Let Ω be a bounded Lipschitz domain in R^d $(d = 3)$. Herein we consider computing the reduced MHD system J times with different initial conditions and/or body forces. The solution (u_j, p_j, ϕ_j) of j-th realization, which corresponds to the initial condition $u_j^0(x)$ and body force $f_j(x,t)$, satisfies, for $j = 1, 2, ..., J$,

$$\begin{cases} \frac{1}{N}\left(u_{j,t} + u_j \cdot \nabla u_j\right) - \frac{1}{M^2}\triangle u_j + \nabla p_j = f_j + \left(B \times \nabla \phi_j + B \times (B \times u_j)\right), \\ \Delta \phi_j = \nabla \cdot (u_j \times B) \text{ and } \nabla \cdot u_j = \nabla \cdot B = 0 \quad \forall (x,t) \in \Omega \times (0,T], \\ u_j = B = 0 \quad \forall (x,t) \in \partial\Omega \times (0,T], \\ u_j(x,0) = u_j^0(x) \quad \forall x \in \Omega, \\ \phi_j(x,0) = \phi_j^0(x) \quad \forall x \in \Omega. \end{cases} \tag{1.1}$$

Here $u_j(x,t)$ is the fluid velocity, $p_j(x,t)$ the pressure and $\phi_j(x,t)$ the electric potential. The body force $f_j(x,t)$ and imposed static magnetic field $B_j(x)$ are given, M is the Hartmann number given by $M = \tilde{B}L\sqrt{\frac{\sigma}{\rho\nu}}$ and N is the interaction parameter given by $N = \sigma\tilde{B}^2\frac{L}{\rho U}$, in which $\tilde{B}$ is the characteristic magnetic field, ρ is the density, ν is the kinematic viscosity, σ is the electrical conductivity, U is a typical velocity of the motion, and L is the characteristic length scale.

1.1.1.2. Ensemble. We define the ensemble mean and the fluctuation of the velocity u_j^n and the electric potential ϕ_j^n respectively

$$\bar{u}^n = \frac{1}{J}\sum_{j=1}^{J}(2u_j^n - u_j^{n-1}) \quad \text{and} \quad \bar{\phi}^n = \frac{1}{J}\sum_{j=1}^{J}(2\phi_j^n - \phi_j^{n-1}), \tag{mean}$$

$$u_j'^n = 2u_j^n - u_j^{n-1} - \bar{u}^n \quad \text{and} \quad \phi_j'^n = 2\phi_j^n - \phi_j^{n-1} - \bar{\phi}^n, \tag{fluctuation}$$

where $u_j^n = u_j(x, t^n)$, $\phi_j^n = \phi_j(x, t^n)$ and $t^n = n\Delta t$ $(n = 0, 1, 2, ...)$.

1.1.2. ALGORITHM. We then propose a second order, partitioned ensemble algorithm given by

Sub-problem 1: Given u_j^n and ϕ_j^n, find u_j^{n+1} and p_j^{n+1} satisfying

$$\begin{cases} \dfrac{1}{N}\left(\dfrac{3u_j^{n+1} - 4u_j^n + u_j^{n-1}}{2\Delta t}\right) + \dfrac{1}{N}\bar{u}^n \cdot \nabla u_j^{n+1} + \dfrac{1}{N}u_j'^n \cdot \nabla(2u_j^n - u_j^{n-1}) \\ -\dfrac{1}{M^2}\Delta u_j^{n+1} + \nabla p_j^{n+1} = f_j^{n+1} + \left(B \times \nabla(2\phi_j^n - \phi_j^{n-1}) + B \times \left(B \times u_j^{n+1}\right)\right), \\ \nabla \cdot u_j^{n+1} = 0. \end{cases}$$

Sub-problem 2: Given u_j^{n+1}, find ϕ_j^{n+1} satisfying

$$\Delta\phi_j^{n+1} = \nabla \cdot (u_j^{n+1} \times B).$$

1.2. PRELIMINARIES

1.2.1. NOTATION. Throughout this paper the $L^2(\Omega)$ norm of scalars, vectors, and tensors will be denoted by $\|\cdot\|$ with the usual L^2 inner product denoted by $(\cdot, \cdot)$. $H^k(\Omega)$ is the Sobolev space $W_2^k(\Omega)$, with norm $\|\cdot\|_k$. For functions $v(x, t)$ defined on $(0, T)$, we define the norms, for $1 \le m < \infty$,

$$\|v\|_{\infty,k} := \operatorname*{ess\,sup}_{[0,T]} \|v(\cdot, t)\|_k \qquad \text{and} \qquad \|v\|_{m,k} := \left(\int_0^T \|v(\cdot, t)\|_k^m \, dt\right)^{1/m}.$$

The function spaces we consider are:

$$
\begin{aligned}
X &:= H_0^1(\Omega)^d = \left\{ v \in L^2(\Omega)^d : \nabla v \in L^2(\Omega)^{d\times d} \text{ and } v = 0 \text{ on } \partial\Omega \right\}, \\
Q &:= L_0^2(\Omega) = \left\{ q \in L^2(\Omega) : \int_\Omega q \, dx = 0 \right\}, \\
S &:= H_0^1(\Omega) = \left\{ \phi \in L^2(\Omega) : \nabla\phi \in L^2(\Omega) \text{ and } \phi = 0 \text{ on } \partial\Omega \right\}, \\
V &:= \{ v \in X : (\nabla \cdot v, q) = 0, \forall q \in Q \}.
\end{aligned}
$$

The norm on the dual space of X is defined by

$$
\|f\|_{-1} = \sup_{0\neq v\in X} \frac{(f,v)}{\|\nabla v\|}.
$$

A weak formulation of the reduced MHD equations is: Find $u : [0,T] \to X$, $p : [0,T] \to Q$, and $\phi : [0,T] \to S$ for a.e. $t \in (0,T]$ satisfying

$$
\begin{aligned}
&\frac{1}{N}\left(u_{j,t}, v\right) + \frac{1}{N}\left(u_j \cdot \nabla u_j, v\right) + \frac{1}{M^2}\left(\nabla u_j, \nabla v\right) - \left(p_j, \nabla\cdot v\right) \\
&\qquad + \left(-\phi_j + u_j \times B, v \times B\right) = \left(f_j, v\right), \quad \forall v \in X, \\
&\left(\nabla \cdot u_j, q\right) = 0, \quad \forall q \in Q, \\
&-\left(\nabla\phi_j, \nabla\psi\right) + \left(u_j \times B, \nabla\psi\right) = 0, \quad \forall \psi \in S.
\end{aligned}
\tag{1.2}
$$

We denote conforming velocity, pressure, potential finite element spaces based on an edge-to-edge triangulation ($d = 2$) or tetrahedralization ($d = 3$) of Ω with maximum element diameter h by

$$
X_h \subset X, Q_h \subset Q, S_h \subset S.
$$

We also assume the finite element spaces (X_h, Q_h) satisfy the usual discrete inf-sup /LBB^h condition for stability of the discrete pressure, see [18] for more on this condition. Taylor-Hood elements, e.g., [19], [18], are one such choice used in the tests in Section 5. We

assume the mesh and finite element spaces satisfy the standard inverse inequality

$$h\|\nabla v_h\| \leq C_{(inv)}\|v_h\|. \tag{1.3}$$

that is known to hold for standard finite element spaces with locally quasi-uniform meshes [19]. We also define the standard explicitly skew-symmetric trilinear form

$$b^*(u,v,w) := \frac{1}{2}(u\cdot\nabla v, w) - \frac{1}{2}(u\cdot\nabla w, v),$$

and note by the divergence theorem,

$$b^*(u,v,w) = (u\cdot\nabla v, w) + \frac{1}{2}(\nabla\cdot u, w\cdot v). \tag{1.4}$$

Also, by [20] we have the following bounds

$$b^*(u,v,w) \leq C\|\nabla u\|\|\nabla v\|\|\nabla w\|, \quad \forall\, u,v,w \in X, \tag{1.5}$$

$$b^*(u,v,w) \leq C\|\nabla u\|\|\nabla v\|\left(\|\nabla w\|\|w\|\right)^{1/2}, \quad \forall\, u,v,w \in X, \tag{1.6}$$

$$b^*(u,v,w) \leq C(\|\nabla u\|\|u\|)\|\nabla v\|\|\nabla w\|, \quad \forall\, u,v,w \in X. \tag{1.7}$$

1.3. PROBLEM FORMULATION

1.3.1. FULLY DISCRETIZED ALGORITHM. The full discretization of the proposed partitioned ensemble algorithm is Sub-problem 1: Given $u_{j,h}^n \in X_h$ and $\phi_{j,h}^n \in S_h$, find $u_{j,h}^{n+1} \in X_h$ and $p_{j,h}^{n+1} \in Q_h$ satisfying

$$\begin{cases} \frac{1}{N}\left(\frac{3u_j^{n+1} - 4u_j^n + u_j^{n-1}}{2\Delta t}, v_h\right) + \frac{1}{N}b^*(\bar{u}_h^n, u_{j,h}^{n+1}, v_h) \\ + \frac{1}{N}b^*(u'^n_{j,h}, 2u_{j,h}^n - u_{j,h}^{n-1}, v_h) + \frac{1}{M^2}(\nabla u_{j,h}^{n+1}, \nabla v_h) - (p_{j,h}^{n+1}, \nabla \cdot v_h) \\ \qquad + \left(-\nabla(2\phi_{j,h}^n - \phi_{j,h}^{n-1}) + u_{j,h}^{n+1} \times B, v_h \times B\right) = \left(f_j^{n+1}, v_h\right), \qquad \forall v_h \in X_h, \\ \left(\nabla \cdot u_{j,h}^{n+1}, q_h\right) = 0, \qquad \forall q_h \in Q_h. \end{cases} \tag{1.8}$$

Sub-problem 2: Given $u_{j,h}^{n+1} \in X_h$, find $\phi_{j,h}^{n+1} \in S_h$ satisfying

$$\left(-\nabla\phi_{j,h}^{n+1} + u_{j,h}^{n+1} \times B, \nabla\psi_h\right) = 0, \qquad \forall \psi_h \in S_h. \tag{1.9}$$

1.3.2. ALGORITHM WITH REGULARIZATION. Herein we define an eddy viscosity term, following [2]. The proceeding regularization will be critically useful for computations involving large Re, and will eliminate one timestep condition, forcing less restriction on Δt. We present the following eddy viscosity term:

$$\nu_T(u'_{j,h}, t^n) = \mu|u'^n_{j,h}|^2\Delta t.$$

With the addition of this term to Algorithm 1.3.1, the ensemble algorithm with regularization is Sub-problem 1: Given $u_{j,h}^n \in X_h$ and $\phi_{j,h}^n \in S_h$, find $u_{j,h}^{n+1} \in X_h$ and $p_{j,h}^{n+1} \in Q_h$ satisfying

$$\begin{cases} \frac{1}{N}\left(\frac{3u_j^{n+1}-4u_j^n+u_j^{n-1}}{2\Delta t}, v_h\right) + \frac{1}{N}b^*(\bar{u}_h^n, u_{j,h}^{n+1}, v_h) + \frac{1}{N}b^*(u_{j,h}'^n, 2u_{j,h}^n - u_{j,h}^{n-1}, v_h) \\ \qquad + \frac{1}{M^2}(\nabla u_{j,h}^{n+1}, \nabla v_h) - (p_{j,h}^{n+1}, \nabla \cdot v_h) + \frac{1}{N}(\nu_T(u'_{j,h}, t^n)\nabla u_{j,h}^{n+1}, \nabla v_h) \\ \qquad + \left(-\nabla(2\phi_{j,h}^n - \phi_{j,h}^{n-1}) + u_{j,h}^{n+1} \times B, v_h \times B\right) = \left(f_j^{n+1}, v_h\right), \qquad \forall v_h \in X_h, \\ \left(\nabla \cdot u_{j,h}^{n+1}, q_h\right) = 0, \qquad \forall q_h \in Q_h. \end{cases} \tag{1.10}$$

Sub-problem 2: Given $u_{j,h}^{n+1} \in X_h$, find $\phi_{j,h}^{n+1} \in S_h$ satisfying

$$\left(-\nabla\phi_{j,h}^{n+1} + u_{j,h}^{n+1} \times B, \nabla\psi_h\right) = 0, \qquad \forall \psi_h \in S_h. \tag{1.11}$$

1.4. STABILITY

1.4.1. STABILITY OF ALGORITHM WITHOUT REGULARIZATION. Algorithm 1.3.1 is long time, nonlinearly stable under two timestep conditions.

Consider the method with a standard spacial discretization with mesh size h. Suppose the following timestep conditions hold

$$\Delta t < \left[4N\|B\|_{L^\infty}^2(1 + C_p^2M^2\|B\|_{L^\infty}^2)\right]^{-1}, \tag{1.12}$$

$$C\frac{M^2}{N}\frac{\Delta t}{h}\|\nabla(2u_{j,h}^n - u_{j,h}^{n-1} - \bar{u}_h^n)\|^2 \leq 1, \qquad j = 1, ..., J, \tag{1.13}$$

then, for any $n \geq 1$

$$\begin{aligned}
&\frac{1}{2N}\|u_{j,h}^n\|^2 + \frac{1}{2N}\|2u_{j,h}^n - u_{j,h}^{n-1}\|^2 + \sum_{k=1}^{n-1}\frac{\Delta t}{4M^2}\|\nabla u_{j,h}^{k+1}\|^2 \qquad (1.14)\\
&+ \Delta t\sum_{k=1}^{n-1}\|-\nabla(2\phi_{j,h}^k - \phi_{j,h}^{k-1}) + u_{j,h}^{k+1}\times B\|^2\\
&+ \Delta t\sum_{k=1}^{n-1}\|-\nabla(2\phi_{j,h}^k - \phi_{j,h}^{k-1}) + (2u_{j,h}^k - u_{j,h}^{k-1})\times B\|^2\\
&\leq \frac{1}{2N}\|u_{j,h}^1\|^2 + \frac{1}{2N}\|2u_{j,h}^1 - u_{j,h}^0\|^2 + 2\Delta t\sum_{k=1}^{n-1}M^2\|f_j^{k+1}\|_{-1}^2\,.
\end{aligned}$$

1.4.2. STABILITY OF ALGORITHM WITH REGULARIZATION. Consider Algorithm 1.3.2 with a standard spacial discretization with mesh size h. Suppose the following timestep condition holds

$$\Delta t < \left[2 + 2N\|B\|_{L^\infty}^2(1 + C_p^2M^2\|B\|_{L^\infty}^2)\right]^{-1}. \qquad (1.15)$$

Directly, nonlinear long time stability holds if

$$\nabla\cdot u_{j,h}'^n = 0 \quad \text{and} \quad \mu > \frac{1}{2}. \qquad (1.16)$$

In addition to having one less time-step condition than Theorem 1.4, if we compare the similar condition (1.12) to (1.15) we see for M or N sufficiently large,

$$\left[4N\|B\|_{L^\infty}^2(1 + C_p^2M^2\|B\|_{L^\infty}^2)\right]^{-1} < \left[2 + 2N\|B\|_{L^\infty}^2(1 + C_p^2M^2\|B\|_{L^\infty}^2)\right]^{-1},$$

placing even less restriction on Δt.

1.5. ERROR ANALYSIS

Here we provide an error estimate of the proposed method under both of the same time-step conditions (with possibly different constant C in the condition). Assuming that X_h and Q_h satisfy the LBB^h condition, Subproblem 1 in Algorithm 1.3.1 is equivalent to: Given $u^n_{j,h} \in V_h$and $\phi^n_{j,h} \in S_h$, for $n = 0, 1, ..., \tilde{N} - 1$ find $u^{n+1}_{j,h} \in V_h$ such that

$$\begin{aligned}
&\frac{1}{N}\left(\frac{3u^{n+1}_{j,h} - 4u^n_{j,h} + u^{n-1}_{j,h}}{2\Delta t}, v_h\right) + \frac{1}{N}b^*(\bar{u}^n_h, u^{n+1}_{j,h}, v_h) \\
&+ \frac{1}{N}b^*(u'^n_{j,h}, 2u^n_{j,h} - u^{n-1}_{j,h}, v_h) + \frac{1}{M^2}(\nabla u^{n+1}_{j,h}, \nabla v_h) \\
&\quad + \left(-\nabla(2\phi^n_{j,h} + \phi^{n-1}_{j,h}) - u^{n+1}_{j,h} \times B, v_h \times B\right) = \left(f^{n+1}_j, v_h\right), \qquad \forall v_h \in V_h. \qquad (1.17)
\end{aligned}$$

We define the discrete norms as

$$|||v|||_{\infty,k} = \max_{0\le n\le \tilde{N}} \|v^n\|_k \qquad \text{and} \qquad |||v|||_{m,k} := \left(\sum_{n=1}^{\tilde{N}-1} \|v^n\|^m_k \Delta t\right)^{1/m},$$

where $v^n = v(t^n)$ and $t^n = n\Delta t$.

The discrete Gronwall inequality [21] will be used in the analysis.

Let $D \ge 0$ and $\kappa_n, A_n, B_n, C_n \ge 0$ for any integer $n \ge 0$ and satisfy

$$A_{\tilde{N}} + \Delta t \sum_{n=0}^{\tilde{N}} B_n \le \Delta t \sum_{n=0}^{\tilde{N}} \kappa_n A_n + \Delta t \sum_{n=0}^{\tilde{N}} C_n + D \text{ for } \tilde{N} \ge 0. \qquad (1.18)$$

Suppose that for all n, $\Delta t\kappa_n \le 1$, and set $g_n = (1 - \Delta t\kappa_n)^{-1}$. Then,

$$A_{\tilde{N}} + \Delta t \sum_{n=0}^{\tilde{N}} B_n \le exp(\Delta t \sum_{n=0}^{\tilde{N}} g_n\kappa_n)[\Delta t \sum_{n=0}^{\tilde{N}} C_n + D] \text{ for } \tilde{N} \ge 0.$$

To analyze the rate of convergence of the approximation, we assume the following regularity for the exact solutions:

$$
\begin{aligned}
&u_j \in L^\infty(0,T;H^{k+1}(\Omega)) \cap H^1(0,T;H^{k+1}(\Omega)) \cap H^2(0,T;L^2(\Omega)),\\
&p_j \in L^2(0,T;H^{s+1}), \quad \text{and} \quad f_j \in L^2(0,T;L^2(\Omega)),\\
&\phi_j \in L^\infty(0,T;H^{m+1}(\Omega)) \cap H^1(0,T,H^1(\Omega)).
\end{aligned}
$$

We further assume the finite element spaces satisfy the approximation properties of piecewise polynomials on quasiuniform meshes

$$\inf_{v_h \in X_h} \|v - v_h\| \le Ch^{k+1}\|u\|_{k+1} \qquad \forall v \in [H^{k+1}(\Omega)]^d, \tag{1.19}$$

$$\inf_{v_h \in X_h} \|\nabla(v - v_h)\| \le Ch^{k}\|v\|_{k+1} \qquad \forall v \in [H^{k+1}(\Omega)]^d, \tag{1.20}$$

$$\inf_{q_h \in Q_h} \|q - q_h\| \le Ch^{s+1}\|p\|_{s+1} \qquad \forall q \in H^{s+1}(\Omega), \tag{1.21}$$

$$\inf_{\psi_h \in S_h} \|\psi - \psi_h\| \le Ch^{m+1}\|\psi\|_{m+1} \qquad \forall \psi \in H^{m+1}(\Omega), \tag{1.22}$$

$$\inf_{\psi_h \in S_h} \|\nabla(\psi - \psi_h)\| \le Ch^{m}\|\psi\|_{m+1} \qquad \forall \psi \in H^{m+1}(\Omega), \tag{1.23}$$

where the generic constant $C > 0$ is independent of mesh size h. An example for which the LBB_h stability condition and the approximation properties are satisfied is the finite elements pair (P^{k+1}–P^k–P^{k+1}), $k \ge 1$. For finite element methods see [18, 20, 22, 23] for more details.

The discretely divergence free subspace of X_h is

$$V_h : = \{v_h \in X_h : (\nabla \cdot v_h, q_h) = 0 \ , \forall q_h \in Q_h\}.$$

Let $e^n_{u,j} = u^n_j - u^n_{j,h}$ and $e^n_{\phi,j} = \phi^n_j - \phi^n_{j,h}$ denote the approximation error of the jth simulation at the time instance t^n. We then have the following error estimates.

[Convergence of Algorithm 1.3.1] For all $j = 1, \ldots, J$, if the following timestep conditions hold

$$\Delta t < \left(4N\|B\|_{L^\infty}^2(1 + C_p^2 M^2 \|B\|_{L^\infty}^2)\right)^{-1}, \tag{1.24}$$

$$C\frac{M^2}{N}\frac{\Delta t}{h}\|\nabla(2u_{j,h}^n - u_{j,h}^{n-1} - \bar{u}_h^n)\|^2 \leq 1, \qquad j = 1, ..., J, \tag{1.25}$$

then there exists a positive constant C independent of the timestep such that

$$\begin{aligned}
&\|2e_{u,j}^n - e_{u,j}^{n-1}\|^2 + \|e_{u,j}^n\|^2 + \frac{3N\Delta t}{7M^2}\|\nabla e_{u,j}^n\|^2 + \frac{3N\Delta t}{14M^2}\|\nabla e_{u,j}^{n-1}\|^2 + 2N\Delta t\sum_{l=1}^{n-1}\|e_{u,j}^{l+1} \times B\|^2 \\
&+ 2N\Delta t\sum_{l=1}^{n-1}\|-\nabla(2e_{\phi,j}^l - e_{\phi,j}^{l-1}) + (2e_{u,j}^l - e_{u,j}^{l-1}) \times B\|^2 + N\Delta t\sum_{l=1}^{n-1}\|\nabla(2e_{\phi,j}^l - e_{\phi,j}^{l-1})\|^2 \\
&\leq e^{\frac{T\tilde{C}}{1-\Delta t\tilde{C}}}\Bigg\{\|2e_{u,j}^1 - e_{u,j}^0\|^2 + \|e_{u,j}^1\|^2 + \frac{3N\Delta t}{7M^2}\|\nabla e_{u,j}^1\|^2 + \frac{3N\Delta t}{14M^2}\left(\|\nabla e_{u,j}^0\|^2\right) \\
&\quad + \frac{C^4M^6\Delta t}{16C_0^3N^3}\left(2\|e_{u,j}^1\|^2 + \|e_{u,j}^0\|^2\right) + CNh^{2k+2}\|B\|_{L^\infty}^2\|u_j\|_{2,k+1}^2 + \frac{Ch^{2k}M^2}{N}\|u_j\|_{2,k+1}^2 \\
&\quad + \frac{Ch^{2k}N}{M^2}\|u_j\|_{2,k+1}^2 + Ch^{2k}N\|u_j\|_{2,k+1}^2 + \frac{56C^2M^2}{3N}h^{2k}\|u_j\|_{4,k+1}^4 + \frac{56C^2M^3}{3N}h^{2k} \\
&\quad + \frac{CM^2(\Delta t)^4}{N}\|\nabla u_{j,tt}\|_{2,0}^2 + Ch^{2k+1}(\Delta t)^3\|u_{j,tt}\|_{2,k+1}^2 + Ch(\Delta t)^3\|\nabla u_{j,tt}\|_{2,0}^2 \\
&\quad + Ch^{2s+2}NM^2\|p_j\|_{2,s+1}^2 + \frac{Ch^{2k+2}M^2}{N}\|u_{j,t}\|_{2,k+1}^2 + \frac{CM^2(\Delta t)^4}{N}\|u_{j,ttt}\|_{2,0}^2 \\
&\quad + Ch^{2m}\|\phi_j\|_{2,m+1}^2 + N(\Delta t)^2\|\nabla\phi_{j,t}\|_{2,0}^2\Bigg\} + Ch^{2k+2}\|u_j\|_{\infty,k+1}^2 \\
&\quad + \frac{CNh^{2k}\Delta t}{M^2}\|u_j\|_{\infty,k+1}^2 + CNh^{2k+2}\Delta t\|B\|_{L^\infty}^2\|u_j\|_{2,k+1}^2 + CNh^{2m}\Delta t\|\phi_j\|_{2,m+1}^2 \\
&\quad + CNh^{2k+2}\|B\|_{L^\infty}^2\|u_j\|_{2,k+1}^2.
\end{aligned} \tag{1.26}$$

1.6. NUMERICAL TESTS

This section will present numerical results for (1.3.1) to demonstrate the stability and convergence proven previously. Numerical results will also be presented for stability of (1.3.2). Throughout these tests we'll use the finite element triplet (P^2–P^1–P^2), and the finite element software package FEniCS [24].

1.6.1. CONVERGENCE TEST. To verify the convergence rates proven in section 1.4.1, and predicted error of $O(\Delta t^2 + h^2)$, we will use a variation of the test problem in [25]. Take the time interval $0 \leq t \leq 1$, $M = 20$, $N = 16$, $\Omega = [0, \pi]^2$, and the imposed magnetic field $B = (0, 0, 1)$. Define the true solution (u, p, ϕ) as

$$\begin{cases} u_\epsilon = (25\cos(2x)\sin(2y), -2\sin(2x)\cos(2y), 0)(1+\epsilon)e^{-5t}, \\ p = 0, \\ \phi_\epsilon = (\cos(2x)\cos(2y) + x^2 - y^2)(1+\epsilon)e^{-5t}, \end{cases} \tag{1.27}$$

where ϵ is a given perturbation. For this problem we will consider two perturbations $\epsilon_1 = 10^{-1}$ and $\epsilon_2 = -10^{-1}$. The boundary conditions are set at $u_h = u_\epsilon$ and $\phi_h = \phi_\epsilon$ on $\delta\Omega$. The source terms and initial conditions implemented correspond with the exact solution for the given perturbation. Because the exact solutions decay exponentially with time, we will utilize the relative error in our numerical tests to accurately demonstrate the performance, defined as

$$\|v - v_h\|_{k_{rel}} = \frac{\|v - v_h\|_k}{\|v\|_k}. \tag{1.28}$$

The results are displayed in tables (1.1)-(1.4), where convergence rates appear to match expectations.

Table 1.1. Error and convergence rates for the first ensemble member in u_h and ∇u_h.

h	Δt	$\|u_1 - u_{1,h}\|_{\infty,0_{rel}}$	Rate	$\|\nabla u_1 - \nabla u_{1,h}\|_{2,0_{rel}}$	Rate
1/5	1/40	3.861 e+0	—	1.278 e+0	—
1/10	1/80	1.021 e+0	1.919	3.353 e-1	1.931
1/20	1/160	2.638 e-1	1.952	8.541 e-2	1.973
1/40	1/320	6.720 e-2	1.973	2.157 e-2	1.986
1/80	1/640	1.696 e-2	1.986	5.410 e-3	1.995

Table 1.2. Error and convergence rates for the first ensemble member in ϕ_h and $\nabla \phi_h$.

h	Δt	$\|\phi_1 - \phi_{1,h}\|_{\infty,0_{rel}}$	Rate	$\|\nabla \phi_1 - \nabla \phi_{1,h}\|_{2,0_{rel}}$	Rate
1/5	1/40	7.117 e-1	—	3.509 e-1	—
1/10	1/80	1.864 e-1	1.933	9.033 e-2	1.958
1/20	1/160	4.823 e-2	1.950	2.301 e-2	1.973
1/40	1/320	1.232 e-2	1.969	5.820 e-3	1.983
1/80	1/640	3.119 e-3	1.982	1.463 e-3	1.992

Table 1.3. Error and convergence rates for the second ensemble member in u_h and ∇u_h.

h	Δt	$\|u_2 - u_{2,h}\|_{\infty,0_{rel}}$	Rate	$\|\nabla u_2 - \nabla u_{2,h}\|_{2,0_{rel}}$	Rate
1/5	1/40	3.878 e+0	—	1.285 e+0	—
1/10	1/80	1.027 e+0	1.917	3.375 e-1	1.929
1/20	1/160	2.655 e-1	1.952	8.603 e-2	1.972
1/40	1/320	6.764 e-2	1.973	2.172 e-2	1.986
1/80	1/640	1.706 e-2	1.987	5.443 e-3	1.997

Table 1.4. Error and convergence rates for the second ensemble member in ϕ_h and $\nabla\phi_h$.

h	Δt	$\|\phi_2 - \phi_{2,h}\|_{\infty,0_{rel}}$	Rate	$\|\nabla\phi_2 - \nabla\phi_{2,h}\|_{2,0_{rel}}$	Rate
1/5	1/40	7.140 e-1	—	3.524 e-1	—
1/10	1/80	1.872 e-1	1.931	9.088 e-2	1.955
1/20	1/160	4.846 e-2	1.950	2.316 e-2	1.972
1/40	1/320	1.238 e-2	1.969	5.858 e-3	1.983
1/80	1/640	3.134 e-3	1.982	1.472 e-3	1.993

1.6.2. EFFICIENCY TEST. In this experiment we repeat the numerical method used above with the same problem, except we analyze 11 perturbations $\epsilon_i = 10^{-1} - 0.009 * i$, $i = 0, \ldots, 10$. To see how efficient our ensemble approach is, we compare the performance speed and accuracy of Algorithm 1.3.1 with the corresponding nonensemble IMEX method, where linear systems for each perturbation are solved in serial. To do this, we list the CPU runtime in seconds and accuracy of the averages $\bar{u}^n$ and $\bar{\phi}^n$ for each computation. Each approach will make use of the MUMPS LU solver [[26], [27]]. As can be seen in the tables (1.5) and (1.6) below, the second order ensemble method obtains almost the same accuracy as the nonensemble method, while requiring significantly less runtime.

Table 1.5. Error and CPU time for computing $\bar{u}_h$ and $\bar{\phi}_h$ with Algorithm 1.3.1.

h	Δt	$\|\bar{u} - \bar{u}_{en,h}\|_{\infty,0_{rel}}$	$\|\bar{\phi} - \bar{\phi}_{en,h}\|_{\infty,0_{rel}}$	CPU time (s)
1/5	1/40	6.847 e+0	1.358 e+0	1.311 e+1
1/10	1/80	1.518 e+0	2.817 e-1	7.915 e+1
1/20	1/160	3.547 e-1	7.044 e-2	5.857 e+2
1/40	1/320	9.230 e-2	2.241 e-2	4.592 e+3
1/80	1/640	2.604 e-2	8.914 e-3	3.662 e+4

Table 1.6. Error and CPU time for computing $\bar{u}_h$ and $\bar{\phi}_h$ serially with nonensemble method.

h	Δt	$\|\bar{u} - \bar{u}_{ser,h}\|_{\infty,0_{rel}}$	$\|\bar{\phi} - \bar{\phi}_{ser,h}\|_{\infty,0_{rel}}$	CPU time (s)
1/5	1/40	6.847 e+0	1.358 e+0	1.426 e+1
1/10	1/80	1.518 e+0	2.817 e-1	8.985 e+1
1/20	1/160	3.547 e-1	7.044 e-2	6.583 e+2
1/40	1/320	9.230 e-2	2.241 e-2	5.410 e+3
1/80	1/640	2.604 e-2	8.914 e-3	4.652 e+4

1.6.3. STABILITY TEST. Here we analyze the stability of the second order ensemble method. We'll use a test example from [28] for the flow of liquid aluminum at 700° Celsius, with electric conductivity $\sigma = 4.1 \times 10^6$mho/m, kinematic viscosity $\nu = 6 \times 10^{-7}$m^2/s, density $\rho = 2400$kg/m^3 and magnetic diffusivity $\eta = 1.94 \times 10^{-1}$m^2/s. Also, the characteristic length, velocity and magnetic field are $L = 0.1$m, $u = 0.1$m/s, and $B = 1$T correspondingly. We'll exclude external energy and body forces so that in observation if the method is stable, the system energy should decay to zero as time passes. Fix the static magnetic field at $B = (0, 0, 1)$ and Let $0 \le t \le 1$ and $\Omega = [0, 10^{-1}]^2$. Then we have $Re = 16667$, $R_m = 0.051496$, $M = 5336$ and $N = 1708$. Set f and all boundary conditions to zero, and initial conditions

$$u_0(x, y, \epsilon) = (10\pi \cos(10\pi x) \sin(10\pi y), -10 \sin(10\pi x) \cos(10\pi y), 0)(1 + \epsilon),$$
$$\phi_0(x, y, \epsilon) = (\cos(10\pi x) \cos(10\pi y) + x^2 - y^2)(1 + \epsilon).$$

We will test several sets of (ϵ_1, ϵ_2) to observe how stability is affected by different perturbations. Fixing $h = 1/10$, we compute the average energy $E^n = \frac{1}{2}\|\bar{\phi}^n\|^2 + \frac{1}{2}\|\bar{u}^n\|^2$ for multiple timesteps and graph the results in log-log plots in Figures

(1.1a), (1.1b) and (1.1c). Eventually for small enough timestep, we begin to see decent results as the stability timestep conditions (1.12) and (1.13) are satisfied and the energy indeed goes to zero.

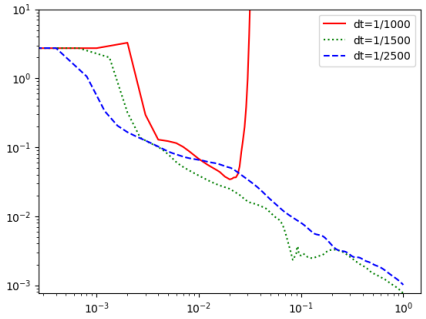

(a) Decay of the system energy with $\epsilon_1 = 10^{-1}$ and $\epsilon_2 = 10^{-2}$.

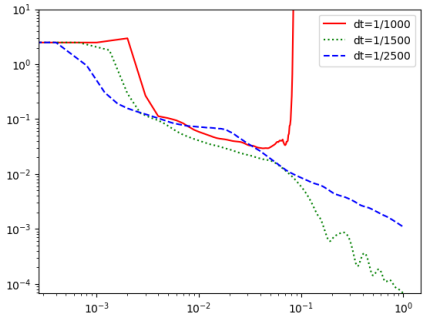

(b) Decay of the system energy with $\epsilon_1 = 10^{-2}$ and $\epsilon_2 = 10^{-3}$.

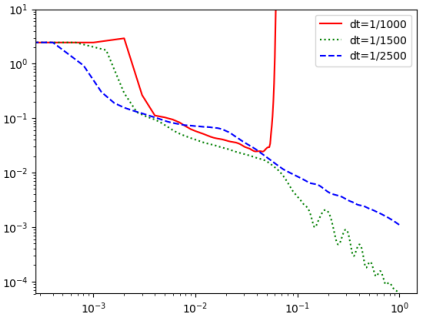

(c) Decay of the system energy with $\epsilon_1 = 10^{-2}$ and $\epsilon_2 = -10^{-2}$.

Figure 1.1. Log-log plots of decay of the system energy for Algorithm 1.3.1 with varying perturbations.

These results indicate the method is not very optimally stable, but requires a small timestep or some size constraints on Re. Next observe in Figures (1.2a), (1.2b) and (1.2c) the stability results under the same test problem for Algorithm 1.3.2 with regularization, where we've set $\mu = 0.55$,

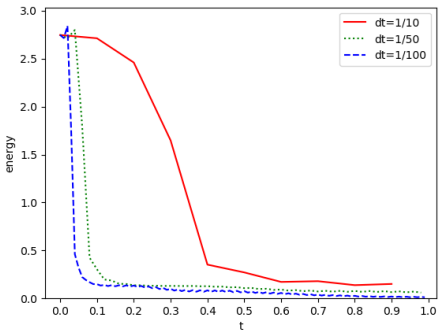

(a) Decay of the system energy with $\epsilon_1 = 10^{-1}$ and $\epsilon_2 = 10^{-2}$.

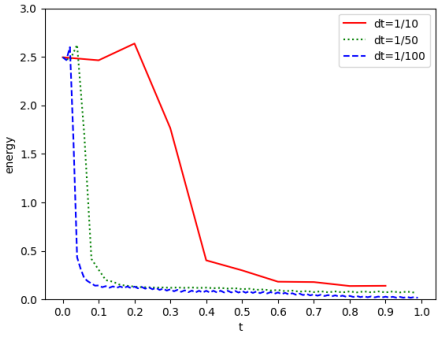

(b) Decay of the system energy with $\epsilon_1 = 10^{-2}$ and $\epsilon_2 = 10^{-3}$.

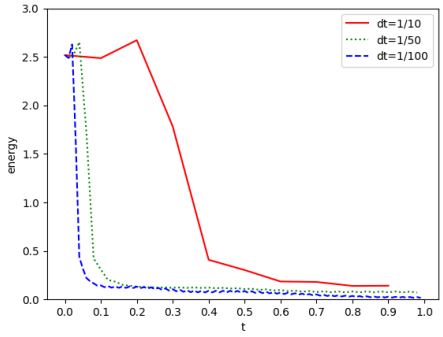

(c) Decay of the system energy with $\epsilon_1 = 10^{-2}$ and $\epsilon_2 = -10^{-2}$.

Figure 1.2. Decay of the system energy for Algorithm 1.3.2 with varying perturbations.

Here the timestep condition (1.15) is satisfied rather easily, as results become sufficiently stable even at $\Delta t = 1/100$.

1.7. CONCLUSIONS

This paper has presented the second order ensemble algorithm applied to the reduced MHD equations, and demonstrated the stability and convergence rate of the method under two time-step conditions. We've shown with the addition of an eddy viscosity term one time-step condition can be removed and stability ensured. This can be useful when dealing

with high Reynolds number where a sufficiently small time discretization may be too computationally expensive for Algorithm 1.3.1. Numerical experiments verify expectations of our ensemble approach and show promising results in terms of accuracy and computational time costs.

II. SECOND ORDER, UNCONDITIONALLY STABLE, LINEAR ENSEMBLE ALGORITHMS FOR THE MAGNETOHYDRODYNAMICS EQUATIONS

J. A. Carter, D. Han, J. Nan
Department of Computational & Applied Mathematics
Missouri University of Science and Technology
Rolla, Missouri 65409–0050
Tel: 573–341–6622, Fax: 573–341–4115
Email: jachdm@mst.edu

ABSTRACT

We propose two unconditionally stable, linear ensemble algorithms with precomputable shared coefficient matrices across different realizations for the magnetohydrodynamics equations. The viscous terms are treated by a standard perturbative discretization. The nonlinear terms are discretized fully explicitly within the framework of the generalized positive auxiliary variable approach (GPAV). Artificial viscosity stabilization that modifies the kinetic energy is introduced to improve accuracy of the GPAV ensemble methods. Numerical results are presented to demonstrate the accuracy and robustness of the ensemble algorithms.

Keywords: MHD, SAV, uncertainty quantification, ensemble algorithm, unconditional stability

1.1. INTRODUCTION

Magnetohydrodynamics (MHD) flow describes electrically conducting fluid moving through a magnetic field. It has important applications in fusion technology, submarine propulsion system, liquid metals in magnetic pumps, and so on. The mathematical model comprises the Navier-Stokes equations for fluid flow and Maxwell's equations for electromagnetics. In practical applications, the problem parameters such as viscosity and magnetic

resistivity, external body forcing and initial conditions, are invariably subject to uncertainty. To quantify the impact of uncertainty and develop high-fidelity numerical simulations, one usually computes the flow ensembles in which the MHD equations are solved repeatedly with different inputs. The aim of this article is to develop efficient second-order accurate ensemble algorithms that are unconditionally stable and suitable for long-time simulations.

Ensemble methods have been extensively developed for solving the Navier-Stokes equations and related fluid models [7, 29–37]. The central idea in these ensemble methods is a perturbative time discretization that utilizes the ensemble mean corrected by explicit treatment of the fluctuations in time marching of each realization. As a result, at each time step the coefficient matrix of the resulting linear systems is identical for all realizations, saving both storage and computational cost. Moreover, under some constraint on the time-step and the size of fluctuations it is shown that the ensemble algorithms are long-time stable. A similar ensemble method is developed in [38] and [39] for solving a reduced MHD system at low magnetic Reynolds number. Based on the Elsasser formulation [40] and the perturbative time discretization, a first-order decoupled and unconditionally stable ensemble algorithm is proposed and analyzed in [41, 42] for solving the full MHD model. An artificial eddy viscosity term is employed to ensure unconditional stability. Due to the usage of Elsasser variables, the method appears to be limited to the case of Dirichlet boundary conditions.

Further computational efficiency gains can be achieved by fully explicit discretization of the nonlinear terms so that the exact same coefficient matrix is shared across different time steps in ensemble simulations. This approach would often incur a CFL condition that hinders the efficiency of the algorithm for long-time simulation or for problems involving multiple scales. One remedy is the introduction of a Lagrange multiplier for enforcement of the underlying energy estimate (energy dissipation or conservation). This idea leads to recent development of the so-called Invariant Energy Quadratization (IEQ) method [43–46], and the Scalar Auxiliary Variable (SAV) approach [47, 48] for solving phase field models.

Extensions of these methods are reported in [49–52] on the design of linear, decoupled, unconditionally stable numerical schemes for solving general nonlinear equations satisfying an energy law. Based on the SAV approach proposed in [49], a stabilized SAV ensemble algorithm is developed in [53] for parameterized flow problems where superior accuracy is observed thanks to a penalization of the kinetic energy causing the high frequency mode to quickly roll-off in the energy spectrum [54]. Stability and error analysis of a SAV method for the MHD equations is recently conducted in [55].

In this article we propose two linear, second-order accurate, unconditionally stable ensemble methods with shared coefficient matrix across different realizations and time steps for solving the MHD model. The parameters are treated by the usual perturbative method. We employ the Generalized Positive Auxiliary Variable framework (GPAV) from [50] in the discretization of the nonlinear terms. The advantages of the GPAV method include: linearity of the algebra equation for the scalar variable; provable positivity of the scalar variable; and flexibility in handling complex boundary conditions. These Lagrange multiplier type approaches often suffer from poor accuracy especially for long time simulation of advection-dominated flow, cf. [56] for a careful benchmark comparison study of the SAV approach. This drop in accuracy is also discussed and demonstrated in the numerical tests from [50]. In [57] a post-processing procedure is introduced to improve accuracy of the SAV method for the Cahn-Hilliard equation. In our method we adopt the stabilization technique of artificial viscosity that proves robust and efficient in past studies [53, 54]. The stabilization introduces a penalty term in the kinetic energy which leads to a quick roll-off of the under-resolved modes in the energy spectrum thus curtailing the inertial range and making the system more computable, cf. [54]. This mechanism is well-known in the Navier-Stokes-α model for large eddy simulation of turbulence [58, 59]. We perform extensive numerical tests to gauge the accuracy, efficiency and robustness of the proposed ensemble methods.

1.1.1. GOVERNING EQUATIONS.

1.1.1.1. MHD. We consider solving J times the following MHD equations: for $j = 1, 2, ..., J$,

$$\begin{cases} \boldsymbol{u}_{j,t} + \boldsymbol{u}_j \cdot \nabla \boldsymbol{u}_j - s\boldsymbol{B}_j \cdot \nabla \boldsymbol{B}_j - \nu_j \Delta \boldsymbol{u}_j + \nabla p_j = \boldsymbol{f}_j \text{ in } \Omega \times (0,T), \\ \nabla \cdot \boldsymbol{u}_j = 0, \text{ in } \Omega \times (0,T), \\ \boldsymbol{B}_{j,t} + \boldsymbol{u}_j \cdot \nabla \boldsymbol{B}_j - \boldsymbol{B}_j \cdot \nabla \boldsymbol{u}_j - \gamma_j \Delta \boldsymbol{B}_j + \nabla \lambda_j = \nabla \times \boldsymbol{g}_j \text{ in } \Omega \times (0,T), \\ \nabla \cdot \boldsymbol{B}_j = 0, \text{ in } \Omega \times (0,T), \\ \boldsymbol{u}_j(x,0) = \boldsymbol{u}_j^0(x), \text{ in } \Omega, \quad \boldsymbol{B}_j(x,0) = \boldsymbol{B}_j^0(x), \text{ in } \Omega. \end{cases} \tag{1.1}$$

Here $\boldsymbol{u}_j$ is the fluid velocity, p_j the pressure, $\boldsymbol{B}_j$ the magnetic field and λ_j is a Lagrange multiplier corresponding to the solenoidal constraint on $\boldsymbol{B}_j$ [41]. The body force $\boldsymbol{f}_j(x,t)$ and $\nabla \times \boldsymbol{g}_j$ are given, s is the coupling number, ν_j is the kinematic viscosity, and γ_j is the magnetic resistivity. Dirichlet boundary conditions will be imposed for both $\boldsymbol{u}_j$ and $\boldsymbol{B}_j$, though the numerical methods are also applicable to other boundary conditions including $\nabla \times \boldsymbol{B}_j = 0$ on $\partial\Omega$. Note that we have adopted an equivalent formulation of the MHD equations, cf. [41, 42, 60, 61].

1.1.1.2. Ensemble and Approximations. We define the ensemble mean and the fluctuation of the viscosity terms ν_j^n and the electric potential γ_j^n at timestep n respectively

$$\bar{\nu}^n = \frac{1}{J}\sum_{j=1}^{J} \nu_j^n \quad \text{and} \quad \bar{\gamma}^n = \frac{1}{J}\sum_{j=1}^{J} \gamma_j^n, \tag{mean}$$

$$\nu_j'^n = \nu_j^n - \bar{\nu}^n \quad \text{and} \quad \gamma_j'^n = \gamma_j^n - \bar{\gamma}^n, \tag{fluctuation}$$

$$\nu'_{\max} = \max_j \max_{x\in\Omega} |\nu_j'^n(x)| \quad \text{and} \quad \gamma'_{\max} = \max_j \max_{x\in\Omega} |\gamma_j'^n(x)|,$$

where in our considerations $\nu_j^n = \nu_j$, $\gamma_j^n = \gamma_j$ are constants and $t_n = n\Delta t$ $(n = 0, 1, 2, ...)$. Define

$$\boldsymbol{v}^{n+1/2} = \frac{1}{2}(\boldsymbol{v}^{n+1} + \boldsymbol{v}^n), \qquad \tilde{\boldsymbol{v}}^{n+1/2} = 2\boldsymbol{v}^{n-1/2} - \boldsymbol{v}^{n-3/2}, \tag{1.2}$$

$$\overset{*}{\boldsymbol{v}}^{n+1/2} = \frac{3}{2}\boldsymbol{v}^n - \frac{1}{2}\boldsymbol{v}^{n-1}, \qquad \tilde{\boldsymbol{v}}^{n+1} = 2\boldsymbol{v}^n - \boldsymbol{v}^{n-1}. \tag{1.3}$$

1.1.1.3. Relevant Functions and Equations. We define a shifted energy of the form

$$E_j(t) = E[\boldsymbol{u}_j, \boldsymbol{B}_j] = \int_\Omega \frac{1}{2}|\boldsymbol{u}_j|^2 d\Omega + \int_\Omega \frac{s}{2}|\boldsymbol{B}_j|^2 d\Omega + C_0, \tag{1.4}$$

where $E[\boldsymbol{u}_j, \boldsymbol{B}_j]$ is the total kinetic energy of the system, which for physical examples is bounded from below, and C_0 is an arbitrarily small positive constant chosen in such a way that $E_j(t) > 0$ for $0 \le t \le T$. Next, let $\mathcal{F}$ be any one-to-one increasing differentiable function with $\mathcal{F}^{-1} = \mathcal{G}$ such that

$$\begin{cases} \mathcal{F}(\chi) > 0, & \chi > 0, \end{cases} \tag{1.5}$$

$$\begin{cases} \mathcal{G}(\chi) > 0, & \chi > 0. \end{cases} \tag{1.6}$$

The scalar variable $R_j(t)$ is defined by

$$R_j(t) = \mathcal{G}(E_j), \tag{1.7}$$

$$E_j(t) = \mathcal{F}(R_j). \tag{1.8}$$

With E_j as in (1.4), $R_j(t)$ then satisfies

$$\mathcal{F}'(R_j)\frac{dR_j}{dt} = \int_\Omega \boldsymbol{u}_j \cdot \frac{\partial \boldsymbol{u}_j}{\partial t} d\Omega + \int_\Omega s\boldsymbol{B}_j \cdot \frac{\partial \boldsymbol{B}_j}{\partial t} d\Omega. \tag{1.9}$$

Since $\frac{\mathcal{F}(R_j)}{E_j} = 1$ for all j, we may write

$$
\begin{aligned}
\mathcal{F}'(R_j)\frac{dR_j}{dt} &= \int_\Omega \left[\boldsymbol{u}_j \cdot \frac{\partial \boldsymbol{u}_j}{\partial t} + s\boldsymbol{B}_j \cdot \frac{\partial \boldsymbol{B}_j}{\partial t} \right] d\Omega \\
&\quad + \left[\frac{\mathcal{F}(R_j)}{E_j} - 1 \right] \left[\int_\Omega \boldsymbol{u}_j \cdot \left(\nu_j \Delta \boldsymbol{u}_j - \nabla p_j + \boldsymbol{f}_j \right) d\Omega \right. \\
&\quad \left. + \int_\Omega s\boldsymbol{B}_j \cdot \left(\gamma_j \Delta \boldsymbol{B}_j - \nabla \lambda_j + \nabla \times \boldsymbol{g}_j \right) d\Omega \right] \\
&\quad + \frac{\mathcal{F}(R_j)}{E_j} \left[\int_\Omega \boldsymbol{u}_j \cdot [\boldsymbol{B}_j \cdot \nabla \boldsymbol{B}_j - \boldsymbol{u}_j \cdot \nabla \boldsymbol{u}_j] d\Omega \right. \\
&\quad - \int_\Omega \boldsymbol{u}_j \cdot [\boldsymbol{B}_j \cdot \nabla \boldsymbol{B}_j - \boldsymbol{u}_j \cdot \nabla \boldsymbol{u}_j] d\Omega \\
&\quad + \int_\Omega s\boldsymbol{B}_j \cdot [\boldsymbol{B}_j \cdot \nabla \boldsymbol{u}_j - \boldsymbol{u}_j \cdot \nabla \boldsymbol{B}_j] d\Omega \\
&\quad \left. - \int_\Omega s\boldsymbol{B}_j \cdot [\boldsymbol{B}_j \cdot \nabla \boldsymbol{u}_j - \boldsymbol{u}_j \cdot \nabla \boldsymbol{B}_j] d\Omega \right] \\
&= \int_\Omega \left[\boldsymbol{u}_j \cdot \frac{\partial \boldsymbol{u}_j}{\partial t} + s\boldsymbol{B}_j \cdot \frac{\partial \boldsymbol{B}_j}{\partial t} \right] d\Omega \\
&\quad - \int_\Omega \boldsymbol{u}_j \cdot \left(\nu_j \Delta \boldsymbol{u}_j - \nabla p_j + \frac{\mathcal{F}(R_j)}{E_j} [\boldsymbol{B}_j \cdot \nabla \boldsymbol{B}_j - \boldsymbol{u}_j \cdot \nabla \boldsymbol{u}_j] + \boldsymbol{f}_j \right) d\Omega \\
&\quad - \int_\Omega s\boldsymbol{B}_j \cdot \left(\gamma_j \Delta \boldsymbol{B}_j - \nabla \lambda_j + \frac{\mathcal{F}(R_j)}{E_j} [\boldsymbol{B}_j \cdot \nabla \boldsymbol{u}_j \right. \\
&\quad \left. - \boldsymbol{u}_j \cdot \nabla \boldsymbol{B}_j] + \nabla \times \boldsymbol{g}_j \right) d\Omega + \frac{\mathcal{F}(R_j)}{E_j} \left[\int_\Omega \boldsymbol{u}_j \cdot [\boldsymbol{B}_j \cdot \nabla \boldsymbol{B}_j \right. \\
&\quad - \boldsymbol{u}_j \cdot \nabla \boldsymbol{u}_j + \nu_j \Delta \boldsymbol{u}_j - \nabla p_j + \boldsymbol{f}_j] d\Omega \\
&\quad \left. + \int_\Omega s\boldsymbol{B}_j \cdot [\boldsymbol{B}_j \cdot \nabla \boldsymbol{u}_j - \boldsymbol{u}_j \cdot \nabla \boldsymbol{B}_j + \gamma_j \Delta \boldsymbol{B}_j - \nabla \lambda_j + \nabla \times \boldsymbol{g}_j] d\Omega \right]
\end{aligned}
\tag{1.10}
$$

Note that all the additional terms above amount to adding zero to (1.9). Using integration by parts we get the equality

$$
\begin{aligned}
&\int_\Omega \boldsymbol{u}_j \cdot [\boldsymbol{B}_j \cdot \nabla \boldsymbol{B}_j - \boldsymbol{u}_j \cdot \nabla \boldsymbol{u}_j + \nu_j \Delta \boldsymbol{u}_j - \nabla p_j + \boldsymbol{f}_j] d\Omega \\
&\quad + \int_\Omega s\boldsymbol{B}_j \cdot [\boldsymbol{B}_j \cdot \nabla \boldsymbol{u}_j - \boldsymbol{u}_j \cdot \nabla \boldsymbol{B}_j + \gamma_j \Delta \boldsymbol{B}_j - \nabla \lambda_j + \nabla \times \boldsymbol{g}_j] d\Omega
\end{aligned}
\tag{1.11}
$$

$$= -\int_\Omega (\nu_j|\nabla \boldsymbol{u}_j|^2 + s\gamma_j|\nabla \boldsymbol{B}_j|^2)d\Omega + \int_\Omega (\boldsymbol{f}_j \cdot \boldsymbol{u}_j + s(\nabla \times \boldsymbol{g}_j)\cdot \boldsymbol{B}_j)d\Omega$$
$$+ \int_\Gamma B_S(\boldsymbol{u}_j, \boldsymbol{B}_j)d\Gamma,$$

where $B_S(\boldsymbol{u}_j, \boldsymbol{B}_j)$ represents the forcing terms on the boundary, defined as

$$B_S(\boldsymbol{u}_j, \boldsymbol{B}_j) = \int_\Gamma \bigg(-\frac{1}{2}|\boldsymbol{u}_j|^2\boldsymbol{u}_j - \frac{s}{2}|\boldsymbol{B}_j|^2\boldsymbol{u}_j + \nu_j \nabla \boldsymbol{u}_j \cdot \boldsymbol{u}_j - p_j\boldsymbol{u}_j \tag{1.12}$$
$$+ s(\boldsymbol{B}_j \cdot \boldsymbol{u}_j)\boldsymbol{B}_j + s\gamma_j \nabla \boldsymbol{B}_j \cdot \boldsymbol{B}_j - s\lambda_j \boldsymbol{B}_j \bigg) \cdot \hat{n} \; d\Gamma$$

and $\hat{n}$ is the unit normal vector to the boundary. We use this equality and write

$$\mathcal{F}'(R_j)\frac{dR_j}{dt} = \int_\Omega \left[\boldsymbol{u}_j \cdot \frac{\partial \boldsymbol{u}_j}{\partial t} + s\boldsymbol{B}_j \cdot \frac{\partial \boldsymbol{B}_j}{\partial t} \right] d\Omega \tag{1.13}$$
$$- \int_\Omega \boldsymbol{u}_j \cdot \left(\nu_j \Delta \boldsymbol{u}_j - \nabla p_j + \frac{\mathcal{F}(R_j)}{E_j}[\boldsymbol{B}_j \cdot \nabla \boldsymbol{B}_j - \boldsymbol{u}_j \cdot \nabla \boldsymbol{u}_j] + \boldsymbol{f}_j \right) d\Omega$$
$$- \int_\Omega s\boldsymbol{B}_j \cdot \left(\gamma_j \Delta \boldsymbol{B}_j - \nabla \lambda_j + \frac{\mathcal{F}(R_j)}{E_j}[\boldsymbol{B}_j \cdot \nabla \boldsymbol{u}_j - \boldsymbol{u}_j \cdot \nabla \boldsymbol{B}_j] + \nabla \times \boldsymbol{g}_j \right) d\Omega$$
$$+ \frac{\mathcal{F}(R_j)}{E_j} \bigg[-\int_\Omega (\nu_j|\nabla \boldsymbol{u}_j|^2 + s\gamma_j|\nabla \boldsymbol{B}_j|^2)d\Omega$$
$$+ \int_\Omega (\boldsymbol{f}_j \cdot \boldsymbol{u}_j + s(\nabla \times \boldsymbol{g}_j)\cdot \boldsymbol{B}_j)d\Omega + \int_\Gamma B_S(\boldsymbol{u}_j, \boldsymbol{B}_j)d\Gamma \bigg]$$
$$+ \left[1 - \frac{\mathcal{F}(R_j)}{E_j} \right] \left| \int_\Omega (\boldsymbol{f}_j \cdot \boldsymbol{u}_j + s(\nabla \times \boldsymbol{g}_j)\cdot \boldsymbol{B}_j)d\Omega + \int_\Gamma B_S(\boldsymbol{u}_j, \boldsymbol{B}_j)d\Gamma \right|.$$

As will be seen later, we consider this reformulation (including the addition of the terms within absolute value brackets) as a means of constructing numerical schemes that inherit unconditional stability with respect to the modified energy $\mathcal{F}(R_j)$ and guaranteed positivity of a computed scalar variable ξ_j to be defined.

1.1.2. CRANK-NICOLSON ALGORITHM. With Dirichlet boundary conditions, a Crank-Nicolson scheme for 1.1 becomes Given $\boldsymbol{u}_j^n$, $\boldsymbol{B}_j^n$, q_j^n and p_j^n, find $\boldsymbol{u}_j^{n+1}$, $\boldsymbol{B}_j^{n+1}$, q_j^{n+1} and p_j^{n+1} satisfying

$$\left(\frac{u_j^{n+1}-u_j^n}{\Delta t}\right) = -\xi_j\left(\tilde{\boldsymbol{u}}_j^{n+1/2}\cdot\nabla\right)\tilde{\boldsymbol{u}}_j^{n+1/2} + s\xi_j\left(\tilde{\boldsymbol{B}}_j^{n+1/2}\cdot\nabla\right)\tilde{\boldsymbol{B}}_j^{n+1/2} + \bar{\nu}^n\Delta u_j^{n+1/2} \tag{1.14}$$

$$+ \nu_j'^n\Delta\tilde{\boldsymbol{u}}_j^{n+1/2} - \nabla p_j^{n+1/2} + \boldsymbol{f}_j^{n+1/2},$$

$$\nabla\cdot u_j^{n+1} = 0, \tag{1.15}$$

$$\left(\frac{\boldsymbol{B}_j^{n+1}-\boldsymbol{B}_j^n}{\Delta t}\right) = \xi_j\left(\tilde{\boldsymbol{B}}_j^{n+1/2}\cdot\nabla\right)\tilde{\boldsymbol{u}}_j^{n+1/2} - \xi_j\left(\tilde{\boldsymbol{u}}_j^{n+1/2}\cdot\nabla\right)\tilde{\boldsymbol{B}}_j^{n+1/2} + \bar{\gamma}^n\Delta\boldsymbol{B}_j^{n+1/2} \tag{1.16}$$

$$+ \gamma_j'^n\Delta\tilde{\boldsymbol{B}}_j^{n+1/2} - \nabla\lambda_j^{n+1/2} + \nabla\times\boldsymbol{g}_j^{n+1/2},$$

$$\nabla\cdot\boldsymbol{B}_j^{n+1} = 0, \tag{1.17}$$

$$\xi_j = \frac{\mathcal{F}(R_j^{n+1})}{E(\bar{\boldsymbol{u}}_j^{n+1},\bar{\boldsymbol{B}}_j^{n+1})}, \tag{1.18}$$

$$E(\bar{\boldsymbol{u}}_j^{n+1},\bar{\boldsymbol{B}}_j^{n+1}) = \frac{1}{2}\|\bar{\boldsymbol{u}}_j^{n+1}\|^2 + \frac{s}{2}\|\bar{\boldsymbol{B}}_j^{n+1}\|^2 + C_0, \tag{1.19}$$

$$\begin{aligned}\frac{\mathcal{F}(R_j^{n+1})-\mathcal{F}(R_j^n)}{\Delta t} &= \int_\Omega u_j^{n+1/2}\cdot\left(\frac{u_j^{n+1}-u_j^n}{\Delta t}\right)d\Omega \\ &+ \int_\Omega s\boldsymbol{B}_j^{n+1/2}\cdot\left(\frac{\boldsymbol{B}_j^{n+1}-\boldsymbol{B}_j^n}{\Delta t}\right)d\Omega \\ &- \int_\Omega u_j^{n+1/2}\cdot\Bigg[-\xi_j\left(\tilde{\boldsymbol{u}}_j^{n+1/2}\cdot\nabla\right)\tilde{\boldsymbol{u}}_j^{n+1/2} + s\xi_j\left(\tilde{\boldsymbol{B}}_j^{n+1/2}\cdot\nabla\right)\tilde{\boldsymbol{B}}_j^{n+1/2} \\ &+ \bar{\nu}^n\Delta u_j^{n+1/2} + \nu_j'^n\Delta\tilde{\boldsymbol{u}}_j^{n+1/2} - \nabla p_j^{n+1/2} + \boldsymbol{f}_j^{n+1/2}\Bigg]d\Omega \\ &- \int_\Omega s\boldsymbol{B}_j^{n+1/2}\cdot\Bigg[\xi_j\left(\tilde{\boldsymbol{B}}_j^{n+1/2}\cdot\nabla\right)\tilde{\boldsymbol{u}}_j^{n+1/2} - \xi_j\left(\tilde{\boldsymbol{u}}_j^{n+1/2}\cdot\nabla\right)\tilde{\boldsymbol{B}}_j^{n+1/2} \\ &+ \bar{\gamma}^n\Delta\boldsymbol{B}_j^{n+1/2} + \gamma_j'^n\Delta\tilde{\boldsymbol{B}}_j^{n+1/2} - \nabla\lambda_j^{n+1/2} + \nabla\times\boldsymbol{g}_j^{n+1/2}\Bigg]d\Omega \\ &+ \xi_j\Bigg[-\int_\Omega\left(\nu_j|\nabla\bar{\boldsymbol{u}}_j^{n+1/2}|^2 + s\gamma_j|\nabla\bar{\boldsymbol{B}}_j^{n+1/2}|^2\right)d\Omega + \int_\Omega\boldsymbol{f}_j^{n+1/2}\cdot\bar{\boldsymbol{u}}_j^{n+1/2}d\Omega \\ &+ \int_\Omega s(\nabla\times\boldsymbol{g}_j^{n+1/2})\cdot\bar{\boldsymbol{B}}_j^{n+1/2}d\Omega + \int_\Gamma B_S(\bar{\boldsymbol{u}}_j^{n+1/2},\bar{\boldsymbol{B}}_j^{n+1/2})d\Gamma\Bigg]\end{aligned} \tag{1.20}$$

$$+ (1-\xi_j)\Bigg| \int_\Omega \boldsymbol{f}_j^{n+1/2} \cdot \bar{\boldsymbol{u}}_j^{n+1/2} d\Omega$$
$$+ \int_\Omega s(\nabla \times \boldsymbol{g}_j^{n+1/2}) \cdot \bar{\boldsymbol{B}}_j^{n+1/2} d\Omega + \int_\Gamma B_S(\bar{\boldsymbol{u}}_j^{n+1/2}, \bar{\boldsymbol{B}}_j^{n+1/2}) d\Gamma \Bigg|.$$

Here $\bar{\boldsymbol{u}}_j^{n+1}$, $\bar{\boldsymbol{u}}_j^{n+1/2}$, $\bar{\boldsymbol{B}}_j^{n+1}$ and $\bar{\boldsymbol{B}}_j^{n+1/2}$ are second order approximations of u_j^{n+1}, $u_j^{n+1/2}$, $\boldsymbol{B}_j^{n+1}$, and $\boldsymbol{B}_j^{n+1/2}$ that will be defined later.

1.1.3. BDF2 ALGORITHM. for Dirichlet boundary conditions, a BDF2 scheme is Given $\boldsymbol{u}_j^n$, $\boldsymbol{B}_j^n$, q_j^n and p_j^n, find $\boldsymbol{u}_j^{n+1}$, $\boldsymbol{B}_j^{n+1}$, q_j^{n+1} and p_j^{n+1} satisfying

$$\left(\frac{3u_j^{n+1} - 4u_j^n + u_j^{n-1}}{2\Delta t}\right) = -\xi_j \left(\tilde{\boldsymbol{u}}_j^{n+1} \cdot \nabla\right) \tilde{\boldsymbol{u}}_j^{n+1} + s\xi_j \left(\tilde{\boldsymbol{B}}_j^{n+1} \cdot \nabla\right) \tilde{\boldsymbol{B}}_j^{n+1} + \bar{\nu}^n \Delta u_j^{n+1} \tag{1.21}$$
$$+ \nu_j'^n \Delta \tilde{\boldsymbol{u}}_j^{n+1} - \nabla p_j^{n+1} + \boldsymbol{f}_j^{n+1},$$

$$\nabla \cdot u_j^{n+1} = 0, \tag{1.22}$$

$$\left(\frac{3\boldsymbol{B}_j^{n+1} - 4\boldsymbol{B}_j^n + \boldsymbol{B}_j^{n-1}}{2\Delta t}\right) = \xi_j \left(\tilde{\boldsymbol{B}}_j^{n+1} \cdot \nabla\right) \tilde{\boldsymbol{u}}_j^{n+1} - \xi_j \left(\tilde{\boldsymbol{u}}_j^{n+1} \cdot \nabla\right) \tilde{\boldsymbol{B}}_j^{n+1} + \bar{\gamma}^n \Delta \boldsymbol{B}_j^{n+1} \tag{1.23}$$
$$+ \gamma_j'^n \Delta \tilde{\boldsymbol{B}}_j^{n+1} - \nabla \lambda_j^{n+1} + \nabla \times \boldsymbol{g}_j^{n+1},$$

$$\nabla \cdot \boldsymbol{B}_j^{n+1} = 0, \tag{1.24}$$

$$\xi_j = \frac{\mathcal{F}(\overset{*}{R}_j^{n+3/2})}{E(\bar{\boldsymbol{u}}_j^{n+3/2}, \bar{\boldsymbol{B}}_j^{n+3/2})}, \tag{1.25}$$

$$E(\bar{\boldsymbol{u}}_j^{n+3/2}, \bar{\boldsymbol{B}}_j^{n+3/2}) = \frac{1}{2}\|\bar{\boldsymbol{u}}_j^{n+3/2}\|^2 + \frac{s}{2}\|\bar{\boldsymbol{B}}_j^{n+3/2}\|^2 + C_0, \tag{1.26}$$

$$\frac{\mathcal{F}(\overset{*}{R}_j^{n+3/2}) - \mathcal{F}(\overset{*}{R}_j^{n+1/2})}{\Delta t} = \int_\Omega u_j^{n+1} \cdot \left(\frac{3u_j^{n+1} - 4u_j^n + u_j^{n-1}}{2\Delta t}\right) d\Omega \tag{1.27}$$
$$+ \int_\Omega s\boldsymbol{B}_j^{n+1} \cdot \left(\frac{3\boldsymbol{B}_j^{n+1} - 4\boldsymbol{B}_j^n + \boldsymbol{B}_j^{n-1}}{2\Delta t}\right) d\Omega$$
$$- \int_\Omega u_j^{n+1} \cdot \Bigg[- \xi_j \left(\tilde{\boldsymbol{u}}_j^{n+1} \cdot \nabla\right) \tilde{\boldsymbol{u}}_j^{n+1} + s\xi_j \left(\tilde{\boldsymbol{B}}_j^{n+1} \cdot \nabla\right) \tilde{\boldsymbol{B}}_j^{n+1}$$

$$
\begin{aligned}
&+ \bar{\nu}^n \Delta u_j^{n+1} + \nu_j'^n \Delta \tilde{\boldsymbol{u}}_j^{n+1} - \nabla p_j^{n+1} + \boldsymbol{f}_j^{n+1} \Big] d\Omega \\
&- \int_\Omega s\boldsymbol{B}_j^{n+1} \cdot \Big[\xi_j \left(\tilde{\boldsymbol{B}}_j^{n+1} \cdot \nabla \right) \tilde{\boldsymbol{u}}_j^{n+1} - \xi_j \left(\tilde{\boldsymbol{u}}_j^{n+1} \cdot \nabla \right) \tilde{\boldsymbol{B}}_j^{n+1} \\
&+ \bar{\gamma}^n \Delta \boldsymbol{B}_j^{n+1} + \gamma_j'^n \Delta \tilde{\boldsymbol{B}}_j^{n+1} - \nabla \lambda_j^{n+1} + \nabla \times \boldsymbol{g}_j^{n+1} \Big] d\Omega \\
&+ \xi_j \Big[- \int_\Omega \left(\nu_j |\nabla \bar{\boldsymbol{u}}_j^{n+1}|^2 + s\gamma_j |\nabla \bar{\boldsymbol{B}}_j^{n+1}|^2 \right) d\Omega + \int_\Omega \boldsymbol{f}_j^{n+1} \cdot \bar{\boldsymbol{u}}_j^{n+1} d\Omega \\
&+ \int_\Omega s(\nabla \times \boldsymbol{g}_j^{n+1}) \cdot \bar{\boldsymbol{B}}_j^{n+1} d\Omega + \int_\Gamma B_S(\bar{\boldsymbol{u}}_j^{n+1}, \bar{\boldsymbol{B}}_j^{n+1}) d\Gamma \Big] \\
&+ (1 - \xi_j) \Big| \int_\Omega \boldsymbol{f}_j^{n+1} \cdot \bar{\boldsymbol{u}}_j^{n+1} d\Omega + \int_\Omega s(\nabla \times \boldsymbol{g}_j^{n+1}) \cdot \bar{\boldsymbol{B}}_j^{n+1} d\Omega + \int_\Gamma B_S(\bar{\boldsymbol{u}}_j^{n+1}, \bar{\boldsymbol{B}}_j^{n+1}) d\Gamma \Big|.
\end{aligned}
$$

Similarly $\bar{\boldsymbol{u}}_j^{n+1}$, $\bar{\boldsymbol{u}}_j^{n+3/2}$, $\bar{\boldsymbol{B}}_j^{n+1}$ and $\bar{\boldsymbol{B}}_j^{n+3/2}$ are second order approximations of u_j^{n+1}, $u_j^{n+3/2}$, $\boldsymbol{B}_j^{n+1}$, and $\boldsymbol{B}_j^{n+3/2}$ to be defined later.

1.2. PRELIMINARIES

1.2.1. NOTATION. Throughout this paper the $L^2(\Omega)$ norm of scalars, vectors, and tensors will be denoted by $\|\cdot\|$ with the usual L^2 inner product denoted by $(\cdot,\cdot)$. $H^k(\Omega)$ is the Sobolev space $W_2^k(\Omega)$, with norm $\|\cdot\|_k$. For functions $v(x,t)$ defined on $(0,T)$, we define the norms, for $1 \le m < \infty$,

$$
\|v\|_{\infty,k} := EssSup_{[0,T]} \|v(\cdot,t)\|_k \qquad \text{and} \qquad \|v\|_{m,k} := \Big(\int_0^T \|v(\cdot,t)\|_k^m \, dt \Big)^{1/m}.
$$

The function spaces we consider are:

$$
\begin{aligned}
X &:= H_0^1(\Omega)^d = \left\{ v \in L^2(\Omega)^d : \nabla v \in L^2(\Omega)^{d\times d} \text{ and } v = 0 \text{ on } \partial\Omega \right\}, \\
Q &:= L_0^2(\Omega) = \left\{ q \in L^2(\Omega) : \int_\Omega q \, dx = 0 \right\}, \\
V &:= \{ v \in X : (\nabla \cdot v, q) = 0, \forall q \in Q \}.
\end{aligned}
$$

A weak formulation of the full MHD equations is: Find $\boldsymbol{u}_j : [0,T] \to X$, $p_j : [0,T] \to Q$, $\boldsymbol{B}_j : [0,T] \to X$ and $\lambda_j : [0,T] \to Q$ satisfying

$$
\begin{aligned}
&\left(\boldsymbol{u}_{j,t}, \boldsymbol{v}\right) + \left(\boldsymbol{u}_j \cdot \nabla \boldsymbol{u}_j, \boldsymbol{v}\right) - s\left(\boldsymbol{B}_j \cdot \nabla \boldsymbol{B}_j, \boldsymbol{v}\right) \\
&\quad + \nu_j \left(\nabla \boldsymbol{u}_j, \nabla \boldsymbol{v}\right) - \left(p_j, \nabla \cdot \boldsymbol{v}\right) = \left(\boldsymbol{f}_j, \boldsymbol{v}\right), \quad \forall \boldsymbol{v} \in X, \\
&\left(\nabla \cdot \boldsymbol{u}_j, l\right) = 0, \quad \forall l \in Q, \\
&\left(\boldsymbol{B}_{j,t}, \boldsymbol{\chi}\right) + \left(\boldsymbol{u}_j \cdot \nabla \boldsymbol{B}_j, \boldsymbol{\chi}\right) - \left(\boldsymbol{B}_j \cdot \nabla \boldsymbol{u}_j, \boldsymbol{\chi}\right) \\
&\quad + \gamma_j \left(\nabla \boldsymbol{B}_j, \nabla \boldsymbol{\chi}\right) - \left(\lambda_j, \nabla \cdot \boldsymbol{\chi}\right) = \left(\nabla \times \boldsymbol{g}_j, \boldsymbol{\chi}\right), \quad \forall \boldsymbol{\chi} \in X, \\
&\left(\nabla \cdot \boldsymbol{B}_j, \psi\right) = 0, \quad \forall \psi \in Q.
\end{aligned}
$$

We denote conforming velocity, pressure, potential finite element spaces based on an edge to edge triangulation ($d = 2$) or tetrahedralization ($d = 3$) of Ω with maximum element diameter h by

$$X_h \subset X \, , Q_h \subset Q.$$

We also assume the finite element spaces (X_h, Q_h) satisfy the usual discrete inf-sup /LBB^h condition for stability of the discrete pressure, see [62] for more on this condition. Taylor-Hood elements, e.g., [63], [62], are one such choice used in the tests in Section 1.6. We define the trilinear form

$$b(u, v, w) := (u \cdot \nabla v, w).$$

1.3. PROBLEM FORMULATION

1.3.1. FULLY DISCRETIZED ALGORITHMS. The full discretization of the proposed partitioned ensemble algorithm with Crank-Nicolson scheme is: Given $u_{j,h}^n$, $\boldsymbol{B}_{j,h}^n$, $p_{j,h}^n$ and $\lambda_{j,h}^n$, find $u_{j,h}^{n+1}$, $\boldsymbol{B}_{j,h}^{n+1}$, $p_{j,h}^{n+1}$ and $\lambda_{j,h}^{n+1}$ satisfying for any $\boldsymbol{v_h}, \boldsymbol{\chi_h} \in X_h$ and $l_h, \psi_h \in Q_h$,

$$\begin{aligned}\left(\frac{u_{j,h}^{n+1}-u_{j,h}^n}{\Delta t}, \boldsymbol{v_h}\right) &= -\xi_j b(\tilde{\boldsymbol{u}}_{j,h}^{n+1/2}, \tilde{\boldsymbol{u}}_{j,h}^{n+1/2}, \boldsymbol{v_h}) + s\xi_j b(\tilde{\boldsymbol{B}}_{j,h}^{n+1/2}, \tilde{\boldsymbol{B}}_{j,h}^{n+1/2}, \boldsymbol{v_h}) \\ &- \bar{\nu}^n \left(\nabla u_{j,h}^{n+1/2}, \nabla \boldsymbol{v_h}\right) - \nu_j'^n \left(\nabla \tilde{\boldsymbol{u}}_{j,h}^{n+1/2}, \nabla \boldsymbol{v_h}\right) + \left(p_{j,h}^{n+1/2}, \nabla \cdot \boldsymbol{v_h}\right) \\ &- \alpha h \left(\nabla(u_{j,h}^{n+1}-u_{j,h}^n), \nabla \boldsymbol{v_h}\right) + \left(\boldsymbol{f}_{j,h}^{n+1/2}, \boldsymbol{v_h}\right),\end{aligned} \tag{1.28}$$

$$\left(\nabla \cdot u_{j,h}^{n+1}, l_h\right) = 0, \tag{1.29}$$

$$\begin{aligned}\left(\frac{\boldsymbol{B}_{j,h}^{n+1}-\boldsymbol{B}_{j,h}^n}{\Delta t}, \boldsymbol{\chi_h}\right) &= \xi_j b(\tilde{\boldsymbol{B}}_{j,h}^{n+1/2}, \tilde{\boldsymbol{u}}_{j,h}^{n+1/2}, \boldsymbol{\chi_h}) - \xi_j b(\tilde{\boldsymbol{u}}_{j,h}^{n+1/2}, \tilde{\boldsymbol{B}}_{j,h}^{n+1/2}, \boldsymbol{\chi_h}) \\ &- \bar{\gamma}^n \left(\nabla \boldsymbol{B}_{j,h}^{n+1/2}, \nabla \boldsymbol{\chi_h}\right) - \gamma_j'^n \left(\nabla \tilde{\boldsymbol{B}}_{j,h}^{n+1/2}, \nabla \boldsymbol{\chi_h}\right) + \left(\lambda_{j,h}^{n+1/2}, \nabla \cdot \boldsymbol{\chi_h}\right) \\ &- \alpha_M h \left(\nabla(\boldsymbol{B}_{j,h}^{n+1}-\boldsymbol{B}_{j,h}^n), \nabla \boldsymbol{\chi_h}\right) + \left(\nabla \times \boldsymbol{g}_{j,h}^{n+1/2}, \boldsymbol{\chi_h}\right),\end{aligned} \tag{1.30}$$

$$\left(\nabla \cdot \boldsymbol{B}_{j,h}^{n+1}, \psi_h\right) = 0, \tag{1.31}$$

$$\xi_j = \frac{\mathcal{F}(R_{j,h}^{n+1})}{E(\bar{\boldsymbol{u}}_{j,h}^{n+1}, \bar{\boldsymbol{B}}_{j,h}^{n+1})}, \tag{1.32}$$

$$E(\bar{\boldsymbol{u}}_{j,h}^{n+1}, \bar{\boldsymbol{B}}_{j,h}^{n+1}) = \frac{1}{2}\|\bar{\boldsymbol{u}}_{j,h}^{n+1}\|^2 + \frac{s}{2}\|\bar{\boldsymbol{B}}_{j,h}^{n+1}\|^2 + C_0, \tag{1.33}$$

$$\begin{aligned}\frac{\mathcal{F}(R_{j,h}^{n+1}) - \mathcal{F}(R_{j,h}^n)}{\Delta t} &= \left(\frac{u_{j,h}^{n+1}-u_{j,h}^n}{\Delta t}, u_{j,h}^{n+1/2}\right) + s\left(\frac{\boldsymbol{B}_{j,h}^{n+1}-\boldsymbol{B}_{j,h}^n}{\Delta t}, \boldsymbol{B}_{j,h}^{n+1/2}\right) \\ &+ \xi_j b(\tilde{\boldsymbol{u}}_{j,h}^{n+1/2}, \tilde{\boldsymbol{u}}_{j,h}^{n+1/2}, u_{j,h}^{n+1/2}) - s\xi_j b(\tilde{\boldsymbol{B}}_{j,h}^{n+1/2}, \tilde{\boldsymbol{B}}_{j,h}^{n+1/2}, u_{j,h}^{n+1/2}) + \bar{\nu}^n \|\nabla u_{j,h}^{n+1/2}\|^2 \\ &+ \nu_j'^n \left(\nabla \tilde{\boldsymbol{u}}_{j,h}^{n+1/2}, \nabla u_{j,h}^{n+1/2}\right) - \left(p_{j,h}^{n+1/2}, \nabla \cdot u_{j,h}^{n+1/2}\right) \\ &+ \alpha h \left(\nabla(u_{j,h}^{n+1}-u_{j,h}^n), \nabla u_{j,h}^{n+1/2}\right) - \left(\boldsymbol{f}_{j,h}^{n+1/2}, u_{j,h}^{n+1/2}\right) \\ &- s\xi_j b(\tilde{\boldsymbol{B}}_{j,h}^{n+1/2}, \tilde{\boldsymbol{u}}_{j,h}^{n+1/2}, \boldsymbol{B}_{j,h}^{n+1/2}) + s\xi_j b(\tilde{\boldsymbol{u}}_{j,h}^{n+1/2}, \tilde{\boldsymbol{B}}_{j,h}^{n+1/2}, \boldsymbol{B}_{j,h}^{n+1/2}) + s\bar{\gamma}^n \|\nabla \boldsymbol{B}_{j,h}^{n+1/2}\|^2\end{aligned} \tag{1.34}$$

$$
\begin{aligned}
&+ s\gamma_j'^n \left(\nabla \boldsymbol{B}_{j,h}^{n+1/2}, \nabla \boldsymbol{B}_{j,h}^{n+1/2}\right) - s\left(\lambda_{j,h}^{n+1/2}, \nabla \cdot \boldsymbol{B}_{j,h}^{n+1/2}\right) \\
&+ s\alpha_M h \left(\nabla(\boldsymbol{B}_{j,h}^{n+1} - \boldsymbol{B}_{j,h}^{n}), \nabla \boldsymbol{B}_{j,h}^{n+1/2}\right) - s\left(\nabla \times \boldsymbol{g}_{j,h}^{n+1/2}, \boldsymbol{B}_{j,h}^{n+1/2}\right) \\
&+ \xi_j \Bigg[- \int_\Omega \left(\nu_j |\nabla \bar{\boldsymbol{u}}_{j,h}^{n+1/2}|^2 + s\gamma_j |\nabla \bar{\boldsymbol{B}}_{j,h}^{n+1/2}|^2\right) d\Omega + \int_\Omega \boldsymbol{f}_{j,h}^{n+1/2} \cdot \bar{\boldsymbol{u}}_{j,h}^{n+1/2} d\Omega \\
&+ \int_\Omega s(\nabla \times \boldsymbol{g}_{j,h}^{n+1/2}) \cdot \bar{\boldsymbol{B}}_{j,h}^{n+1/2} d\Omega + \int_\Gamma B_S(\bar{\boldsymbol{u}}_{j,h}^{n+1/2}, \bar{\boldsymbol{B}}_{j,h}^{n+1/2}) d\Gamma \Bigg] \\
&+ (1-\xi_j) \Bigg| \int_\Omega \boldsymbol{f}_{j,h}^{n+1/2} \cdot \bar{\boldsymbol{u}}_{j,h}^{n+1/2} d\Omega + \int_\Omega s(\nabla \times \boldsymbol{g}_{j,h}^{n+1/2}) \cdot \bar{\boldsymbol{B}}_{j,h}^{n+1/2} d\Omega \\
&+ \int_\Gamma B_S(\bar{\boldsymbol{u}}_{j,h}^{n+1/2}, \bar{\boldsymbol{B}}_{j,h}^{n+1/2}) d\Gamma \Bigg|.
\end{aligned}
$$

The full discretization of the proposed partitioned ensemble algorithm with BDF2 scheme is Given $u_{j,h}^{n-1}$, $u_{j,h}^{n}$, $\boldsymbol{B}_{j,h}^{n-1}$, $\boldsymbol{B}_{j,h}^{n}$, find $u_{j,h}^{n+1}$, $\boldsymbol{B}_{j,h}^{n+1}$, $p_{j,h}^{n+1}$ and $\lambda_{j,h}^{n+1}$ satisfying for any $\boldsymbol{v_h}, \boldsymbol{\chi_h} \in X_h$ and $l_h, \psi_h \in Q_h$,

$$
\begin{aligned}
&\left(\frac{3u_{j,h}^{n+1} - 4u_{j,h}^{n} + u_{j,h}^{n-1}}{2\Delta t}, \boldsymbol{v_h}\right) = -\xi_j b(\tilde{\boldsymbol{u}}_{j,h}^{n+1}, \tilde{\boldsymbol{u}}_{j,h}^{n+1}, \boldsymbol{v_h}) + s\xi_j b(\tilde{\boldsymbol{B}}_{j,h}^{n+1}, \tilde{\boldsymbol{B}}_{j,h}^{n+1}, \boldsymbol{v_h}) \\
&\quad - \bar{\nu}^n \left(\nabla u_{j,h}^{n+1}, \nabla \boldsymbol{v_h}\right) - \nu_j'^n \left(\nabla \tilde{\boldsymbol{u}}_{j,h}^{n+1}, \nabla \boldsymbol{v_h}\right) + \left(p_{j,h}^{n+1}, \nabla \cdot \boldsymbol{v_h}\right) \\
&\quad - \alpha h \left(\nabla(3u_{j,h}^{n+1} - 4u_{j,h}^{n} + u_{j,h}^{n-1}), \nabla \boldsymbol{v_h}\right) + \left(\boldsymbol{f}_{j,h}^{n+1}, \boldsymbol{v_h}\right),
\end{aligned} \tag{1.35}
$$

$$
\left(\nabla \cdot u_{j,h}^{n+1}, l_h\right) = 0, \tag{1.36}
$$

$$
\begin{aligned}
&\left(\frac{3\boldsymbol{B}_{j,h}^{n+1} - 4\boldsymbol{B}_{j,h}^{n} + \boldsymbol{B}_{j,h}^{n-1}}{2\Delta t}, \boldsymbol{\chi_h}\right) = \xi_j b(\tilde{\boldsymbol{B}}_{j,h}^{n+1}, \tilde{\boldsymbol{u}}_{j,h}^{n+1}, \boldsymbol{\chi_h}) - \xi_j b(\tilde{\boldsymbol{u}}_{j,h}^{n+1}, \tilde{\boldsymbol{B}}_{j,h}^{n+1}, \boldsymbol{\chi_h}) \\
&\quad - \bar{\gamma}^n \left(\nabla \boldsymbol{B}_{j,h}^{n+1}, \nabla \boldsymbol{\chi_h}\right) - \gamma_j'^n \left(\nabla \tilde{\boldsymbol{B}}_{j,h}^{n+1}, \nabla \boldsymbol{\chi_h}\right) + \left(\lambda_{j,h}^{n+1}, \nabla \cdot \boldsymbol{\chi_h}\right) \\
&\quad - \alpha_M h \left(\nabla(3\boldsymbol{B}_{j,h}^{n+1} - 4\boldsymbol{B}_{j,h}^{n} + \boldsymbol{B}_{j,h}^{n-1}), \nabla \boldsymbol{\chi_h}\right) + \left(\nabla \times \boldsymbol{g}_{j,h}^{n+1}, \boldsymbol{\chi_h}\right),
\end{aligned} \tag{1.37}
$$

$$
\left(\nabla \cdot \boldsymbol{B}_{j,h}^{n+1}, \psi_h\right) = 0, \tag{1.38}
$$

$$
\xi_j = \frac{\mathcal{F}(\overset{*}{R}_{j,h}^{n+3/2})}{E(\bar{\boldsymbol{u}}_{j,h}^{n+3/2}, \bar{\boldsymbol{B}}_{j,h}^{n+3/2})}, \tag{1.39}
$$

$$E(\bar{\boldsymbol{u}}_{j,h}^{n+3/2}, \bar{\boldsymbol{B}}_{j,h}^{n+3/2}) = \frac{1}{2}\|\bar{\boldsymbol{u}}_{j,h}^{n+3/2}\|^2 + \frac{s}{2}\|\bar{\boldsymbol{B}}_{j,h}^{n+3/2}\|^2 + C_0, \tag{1.40}$$

$$\frac{\mathcal{F}(\overset{*}{R}_{j,h}^{n+3/2}) - \mathcal{F}(\overset{*}{R}_{j,h}^{n+1/2})}{\Delta t} = \left(\frac{3u_{j,h}^{n+1} - 4u_{j,h}^{n} + u_{j,h}^{n-1}}{2\Delta t}, u_{j,h}^{n+1}\right) \tag{1.41}$$

$$\begin{aligned}
&+ s\left(\frac{3\boldsymbol{B}_{j,h}^{n+1} - 4\boldsymbol{B}_{j,h}^{n} + \boldsymbol{B}_{j,h}^{n-1}}{2\Delta t}, \boldsymbol{B}_{j,h}^{n+1}\right) + \xi_j b(\tilde{\boldsymbol{u}}_{j,h}^{n+1}, \tilde{\boldsymbol{u}}_{j,h}^{n+1}, u_{j,h}^{n+1}) \\
&- s\xi_j b(\tilde{\boldsymbol{B}}_{j,h}^{n+1}, \tilde{\boldsymbol{B}}_{j,h}^{n+1}, u_{j,h}^{n+1}) + \bar{\nu}^n \|\nabla u_{j,h}^{n+1}\|^2 + \nu_j'^n \left(\nabla\tilde{\boldsymbol{u}}_{j,h}^{n+1}, \nabla u_{j,h}^{n+1}\right) \\
&- \left(p_{j,h}^{n+1}, \nabla\cdot u_{j,h}^{n+1}\right) + \alpha h\left(\nabla(3u_{j,h}^{n+1} - 4u_{j,h}^{n} + u_{j,h}^{n-1}), \nabla u_{j,h}^{n+1}\right) - \left(\boldsymbol{f}_{j,h}^{n+1}, u_{j,h}^{n+1}\right) \\
&- s\xi_j b(\tilde{\boldsymbol{B}}_{j,h}^{n+1}, \tilde{\boldsymbol{u}}_{j,h}^{n+1}, \boldsymbol{B}_{j,h}^{n+1}) + s\xi_j b(\tilde{\boldsymbol{u}}_{j,h}^{n+1}, \tilde{\boldsymbol{B}}_{j,h}^{n+1}, \boldsymbol{B}_{j,h}^{n+1}) + s\bar{\gamma}^n \|\nabla \boldsymbol{B}_{j,h}^{n+1}\|^2 \\
&+ s\gamma_j'^n \left(\nabla\tilde{\boldsymbol{B}}_{j,h}^{n+1}, \nabla\boldsymbol{B}_{j,h}^{n+1}\right) - s\left(\lambda_{j,h}^{n+1}, \nabla\cdot\boldsymbol{B}_{j,h}^{n+1}\right) \\
&+ s\alpha_M h\left(\nabla(3\boldsymbol{B}_{j,h}^{n+1} - 4\boldsymbol{B}_{j,h}^{n} + \boldsymbol{B}_{j,h}^{n-1}), \nabla\boldsymbol{B}_{j,h}^{n+1}\right) - s\left(\nabla\times\boldsymbol{g}_{j,h}^{n+1}, \boldsymbol{B}_{j,h}^{n+1}\right) \\
&+ \xi_j\Bigg[- \int_\Omega \left(\nu_j|\nabla\bar{\boldsymbol{u}}_{j,h}^{n+1}|^2 + s\gamma_j|\nabla\bar{\boldsymbol{B}}_{j,h}^{n+1}|^2\right) d\Omega + \int_\Omega \boldsymbol{f}_{j,h}^{n+1}\cdot\bar{\boldsymbol{u}}_{j,h}^{n+1} d\Omega \\
&+ \int_\Omega s(\nabla\times\boldsymbol{g}_{j,h}^{n+1})\cdot\bar{\boldsymbol{B}}_{j,h}^{n+1} d\Omega + \int_\Gamma B_S(\bar{\boldsymbol{u}}_{j,h}^{n+1}, \bar{\boldsymbol{B}}_{j,h}^{n+1}) d\Gamma\Bigg] \\
&+ (1-\xi_j)\left|\int_\Omega \boldsymbol{f}_{j,h}^{n+1}\cdot\bar{\boldsymbol{u}}_{j,h}^{n+1} d\Omega + \int_\Omega s(\nabla\times\boldsymbol{g}_{j,h}^{n+1})\cdot\bar{\boldsymbol{B}}_{j,h}^{n+1} d\Omega + \int_\Gamma B_S(\bar{\boldsymbol{u}}_{j,h}^{n+1}, \bar{\boldsymbol{B}}_{j,h}^{n+1}) d\Gamma\right|.
\end{aligned} \tag{1.42}$$

There's also the addition of two regularization terms in Algorithms (1.3.1) and (1.3.1),

$$\begin{cases} \alpha h\Delta(u_{j,h}^{n+1} - u_{j,h}^{n}), \\ \alpha_M h\Delta(\boldsymbol{B}_{j,h}^{n+1} - \boldsymbol{B}_{j,h}^{n}), \end{cases} \text{for CN,} \qquad \begin{cases} \alpha h\Delta(3u_{j,h}^{n+1} - 4u_{j,h}^{n} + u_{j,h}^{n-1}), \\ \alpha_M h\Delta(3\boldsymbol{B}_{j,h}^{n+1} - 4\boldsymbol{B}_{j,h}^{n} + \boldsymbol{B}_{j,h}^{n-1}), \end{cases} \text{for BDF2.} \tag{1.43}$$

1.3.1.1. Regularization. The terms in 1.43 are highly effective at reducing the considerable error that eventually appears when the timestep is not sufficiently refined. Significant improvement in accuracy will be seen later in the numerical tests. It's noted in [54] that this improvement cannot be explained by the stability or error analysis alone. Instead, an explanation is offered through analysis of a modified form of the equations

under consideration. In the modified equations, the addition of the term $-\alpha hk\Delta u_t$ (in the case of velocity) and $-\alpha hk\Delta B_t$ (in the case of magnetic field) are added to the left-hand sides,

$$\begin{cases} \left[\boldsymbol{u}_{j,t} - \alpha hk\Delta \boldsymbol{u}_{j,t}\right] + \boldsymbol{u}_j \cdot \nabla \boldsymbol{u}_j - s\boldsymbol{B}_j \cdot \nabla \boldsymbol{B}_j - \nu_j \Delta \boldsymbol{u}_j + \nabla p_j = \boldsymbol{f}_j \text{ in } \Omega \times (0,T), \\ \nabla \cdot \boldsymbol{u}_j = 0, \text{ in } \Omega \times (0,T), \\ \left[\boldsymbol{B}_{j,t} - s\alpha_M hk\Delta \boldsymbol{B}_{j,t}\right] + \boldsymbol{u}_j \cdot \nabla \boldsymbol{B}_j - \boldsymbol{B}_j \cdot \nabla \boldsymbol{u}_j - \gamma_j \Delta \boldsymbol{B}_j + \nabla \lambda_j = \nabla \times \boldsymbol{g}_j \text{ in } \Omega \times (0,T), \\ \nabla \cdot \boldsymbol{B}_j = 0, \text{ in } \Omega \times (0,T), \\ \boldsymbol{u}_j(x,0) = \boldsymbol{u}_j^0(x), \text{ in } \Omega, \quad \boldsymbol{B}_j(x,0) = \boldsymbol{B}_j^0(x), \text{ in } \Omega. \end{cases} \tag{1.44}$$

This results in a modified kinetic energy corresponding to the equation. In our case, the resulting modified kinetic energy would be

$$\|u(t)\|^2 + \alpha hk\|\nabla u(t)\|^2 + s\|B(t)\|^2 + s\alpha_M hk\|\nabla B(t)\|^2. \tag{1.45}$$

Following Kraichnan's theory [64], it is argued in [54] that the penalty term in the kinetic energy induces an enhanced energy decay rate for numerically under-resolved modes while preserving the correct energy cascade above the cut-off length scale. The quick roll-off in the energy spectrum is also exploited in the Navier-Stokes-α model (NS-α)–a nonlinearly dispersive modification of the Navier-Stokes equations for large eddy simulation of turbulence [58, 59]. This roll-off mechanism shortens the inertial range and makes the system more computable.

1.4. STABILITY OF THE METHOD

1.4.1. CRANK-NICOLSON. With homogeneous boundary conditions and forcing terms equal to zero, Algorithm (1.3.1) is unconditionally stable with respect to the modified energy $\mathcal{F}(R_j)$.

Proof. Stability follows directly from [50]. Set $\boldsymbol{v_h}$ to $u_{j,h}^{n+1/2}$ in (1.28), $\boldsymbol{\chi_h}$ to $s\boldsymbol{B}_{j,h}^{n+1/2}$ in (1.30), add each of these to (1.34) and note (1.29) and (1.31). Then one gets

$$\mathcal{F}(R_{j,h}^{n+1}) - \mathcal{F}(R_{j,h}^{n}) = -\Delta t \frac{\mathcal{F}(R_{j,h}^{n+1})}{E(\bar{\boldsymbol{u}}_{j,h}^{n+1}, \bar{\boldsymbol{B}}_{j,h}^{n+1})} \int_\Omega \left(\nu_j |\nabla \bar{\boldsymbol{u}}_{j,h}^{n+1/2}|^2 + s\gamma_j |\nabla \bar{\boldsymbol{B}}_{j,h}^{n+1/2}|^2 \right) d\Omega \quad (1.46)$$
$$+ \left[1 - \frac{\mathcal{F}(R_{j,h}^{n+1})}{E(\bar{\boldsymbol{u}}_{j,h}^{n+1}, \bar{\boldsymbol{B}}_{j,h}^{n+1})} \right] |S_0| \Delta t + \frac{\mathcal{F}(R_{j,h}^{n+1})}{E(\bar{\boldsymbol{u}}_{j,h}^{n+1}, \bar{\boldsymbol{B}}_{j,h}^{n+1})} S_0 \Delta t.$$

Where $S_0 = \int_\Omega \boldsymbol{f}_{j,h}^{n+1/2} \cdot \bar{\boldsymbol{u}}_{j,h}^{n+1/2} d\Omega + \int_\Omega s(\nabla \times \boldsymbol{g}_{j,h}^{n+1/2}) \cdot \bar{\boldsymbol{B}}_{j,h}^{n+1/2} d\Omega$. Solving for $\mathcal{F}(R_{j,h}^{n+1})$ gives

$$\mathcal{F}(R_{j,h}^{n+1}) = \frac{\mathcal{F}(R_{j,h}^{n}) + |S_0| \Delta t}{1 + \frac{\Delta t}{E(\bar{\boldsymbol{u}}_{j,h}^{n+1}, \bar{\boldsymbol{B}}_{j,h}^{n+1})} \left[\int_\Omega \left(\nu_j |\nabla \bar{\boldsymbol{u}}_{j,h}^{n+1/2}|^2 + s\gamma_j |\nabla \bar{\boldsymbol{B}}_{j,h}^{n+1/2}|^2 \right) d\Omega + (|S_0| - S_0) \right]}. \quad (1.47)$$

If $\boldsymbol{f}_j = 0$ and $\nabla \times \boldsymbol{g}_j = 0$, then $S_0 = 0$ and

$$\mathcal{F}(R_{j,h}^{n+1}) = \frac{\mathcal{F}(R_{j,h}^{n})}{1 + \frac{\Delta t}{E(\bar{\boldsymbol{u}}_{j,h}^{n+1}, \bar{\boldsymbol{B}}_{j,h}^{n+1})} \int_\Omega \left(\nu_j |\nabla \bar{\boldsymbol{u}}_{j,h}^{n+1/2}|^2 + s\gamma_j |\nabla \bar{\boldsymbol{B}}_{j,h}^{n+1/2}|^2 \right) d\Omega}. \quad (1.48)$$

Note the denominator in (1.48) is greater than or equal to 1. By definition (1.5), if $R_{j,h}^0 > 0$, then $\mathcal{F}(R_{j,h}^0) > 0$. In fact $R_{j,h}^0$ would be initialized as $\mathcal{G}(E[\boldsymbol{u}_j^0(x), \boldsymbol{B}_j^0(x)])$, which by definition (1.6) is guaranteed positive. Then by induction for any timestep n, $\mathcal{F}(R_{j,h}^{n+1}) > 0$, giving us

$$0 < \mathcal{F}(R_{j,h}^{n+1}) \leq \mathcal{F}(R_{j,h}^{n}), \qquad n \geq 0. \quad (1.49)$$

This completes the proof. □

1.4.1.1. Crank-Nicolson Scalar Positivity. The scalar ξ_j in (1.58) and R_j^{n+1} in (1.60) are guaranteed to be positive at all timesteps.

Proof. By definition (1.5), $\mathcal{F}(R_j^0) > 0$ so long as $R_j^0 > 0$. It's explained in (1.4.1) that R_j^0 will be positive. The energy function $E(u, B)$ is always positive and $\int_\Omega \left(\nu|\nabla u|^2 + s\gamma|\nabla B|^2\right) d\Omega \geq 0$. Since $|S_0| - S_0 \geq 0$, the initially computed ξ_j is ensured positive. Then by induction, ξ_j at any timestep is guaranteed positive.

Once it's ensured $\xi_j > 0$, from the definition (1.6) we can guarantee R_j^{n+1} in (1.60) is positive. This completes the proof. □

1.4.2. BDF2 STABILITY. With homogeneous boundary conditions and forcing terms equal to zero, Algorithm (1.3.1) is unconditionally stable with respect to the modified energy $\mathcal{F}(R_j)$ as long as the approximations of $R_j(t)$ at timestep $\frac{1}{2}$ are positive. *Proof.* If one sets $\boldsymbol{v_h}$ to $u_{j,h}^{n+1}$ in (1.35) and $\boldsymbol{\chi_h}$ to $s\boldsymbol{B}_{j,h}^{n+1}$ in (1.37), subtracts each of these from (1.41) and notes (1.36) and (1.38), the proof follows identically to [50]. We have

$$\mathcal{F}(\overset{*}{R}_{j,h}^{n+3/2}) - \mathcal{F}(\overset{*}{R}_{j,h}^{n+1/2}) = -\Delta t \frac{\mathcal{F}(\overset{*}{R}_{j,h}^{n+3/2})}{E(\bar{\boldsymbol{u}}_{j,h}^{n+3/2}, \bar{\boldsymbol{B}}_{j,h}^{n+3/2})} \int_\Omega \left(\nu_j|\nabla \bar{\boldsymbol{u}}_{j,h}^{n+1}|^2 + s\gamma_j|\nabla \bar{\boldsymbol{B}}_{j,h}^{n+1}|^2\right) d\Omega \tag{1.50}$$
$$+ \left[1 - \frac{\mathcal{F}(\overset{*}{R}_{j,h}^{n+3/2})}{E(\bar{\boldsymbol{u}}_{j,h}^{n+3/2}, \bar{\boldsymbol{B}}_{j,h}^{n+3/2})}\right] |S_0|\Delta t + \frac{\mathcal{F}(\overset{*}{R}_{j,h}^{n+3/2})}{E(\bar{\boldsymbol{u}}_{j,h}^{n+3/2}, \bar{\boldsymbol{B}}_{j,h}^{n+3/2})} S_0 \Delta t.$$

Where $S_0 = \int_\Omega \boldsymbol{f}_{j,h}^{n+1} \cdot \bar{\boldsymbol{u}}_{j,h}^{n+1} d\Omega + \int_\Omega s(\nabla \times \boldsymbol{g}_{j,h}^{n+1}) \cdot \bar{\boldsymbol{B}}_{j,h}^{n+1} d\Omega$. Solving for $\mathcal{F}(\overset{*}{R}_{j,h}^{n+3/2})$ gives

$$\mathcal{F}(\overset{*}{R}_{j,h}^{n+3/2}) = \frac{\mathcal{F}(\overset{*}{R}_{j,h}^{n+1/2}) + |S_0|\Delta t}{1 + \frac{\Delta t}{E(\bar{\boldsymbol{u}}_{j,h}^{n+3/2}, \bar{\boldsymbol{B}}_{j,h}^{n+3/2})} [\int_\Omega \left(\nu_j|\nabla \bar{\boldsymbol{u}}_{j,h}^{n+1}|^2 + s\gamma_j|\nabla \bar{\boldsymbol{B}}_{j,h}^{n+1}|^2\right) d\Omega + (|S_0| - S_0)]}. \tag{1.51}$$

If $\boldsymbol{f}_j = 0$ and $\nabla \times \boldsymbol{g}_j = 0$, then $S_0 = 0$ and

$$\mathcal{F}(\overset{*}{R}_{j,h}^{n+3/2}) = \frac{\mathcal{F}(\overset{*}{R}_{j,h}^{n+1/2})}{1 + \frac{\Delta t}{E(\bar{\boldsymbol{u}}_{j,h}^{n+3/2}, \bar{\boldsymbol{B}}_{j,h}^{n+3/2})} \int_\Omega \left(\nu_j|\nabla \bar{\boldsymbol{u}}_{j,h}^{n+1}|^2 + s\gamma_j|\nabla \bar{\boldsymbol{B}}_{j,h}^{n+1}|^2\right) d\Omega}. \tag{1.52}$$

The denominator above is greater than or equal to 1. Now by definition (1.5), if it's ensured the approximation of $R_j(t)$ at timestep $1/2$ is positive, i.e. $\overset{*}{R}{}^{1/2}_{j,h} > 0$, then $\mathcal{F}(\overset{*}{R}{}^{1/2}_{j,h}) > 0$. Then by induction for any timestep n, $\mathcal{F}(\overset{*}{R}{}^{n+3/2}_{j,h}) > 0$ and

$$0 < \mathcal{F}(\overset{*}{R}{}^{n+3/2}_{j,h}) \leq \mathcal{F}(\overset{*}{R}{}^{n+1/2}_{j,h}), \qquad n \geq 0. \tag{1.53}$$

This completes the proof. □

1.4.2.1. BDF2 Scalar Positivity. The scalar ξ_j in (1.5.2) and R^{n+1}_j in (1.67) are guaranteed to be positive at all timesteps if the approximation $\overset{*}{R}{}^{1/2}_j > 0$.

Proof. Again by definition (1.5), $\mathcal{F}(\overset{*}{R}{}^{1/2}_j) > 0$ so long as approximation $\overset{*}{R}{}^{1/2}_j > 0$. The argument for positivity of ξ_j proceeds identically to that made in the proof of Theorem (1.4.1.1). Once it's ensured $\xi_j > 0$, again from definition (1.6) we can guarantee $\overset{*}{R}{}^{n+3/2}_j$ in (1.66) is positive. It's also guaranteed R^0_j is positive from the previously stated point that it would be initialized as $\mathcal{G}(E(\boldsymbol{u}^0_j(x), \boldsymbol{B}^0_j(x)))$. Thus we conclude R^{n+1}_j in (1.67) remains positive. This completes the proof. □

Note that for the choice of $\mathcal{F}(\chi) = \chi^2 \geq 0$ for all $\chi \in (-\infty, \infty)$, (1.53) and unconditional stability will hold regardless of whether $\overset{*}{R}{}^{1/2}_{j,h} > 0$.

1.5. IMPLEMENTATION

Since the schemes are linear and the auxiliary variables are scalar functions of time variable, the resulting systems can be solved conveniently by superposition of a series of Stokes-type equations. We illustrate the idea by presenting the algorithms in strong form.

1.5.1. CRANK-NICOLSON. To efficiently implement Algorithm (1.1.2), we proceed in the following manner. Assume

$$u^{n+1}_j = \hat{\boldsymbol{u}}^{n+1}_j + \xi_j \breve{\boldsymbol{u}}^{n+1}_j, \qquad p^{n+1}_j = \hat{p}^{n+1}_j + \xi_j \breve{p}^{n+1}_j,$$
$$\boldsymbol{B}^{n+1}_j = \hat{\boldsymbol{B}}^{n+1}_j + \xi_j \breve{\boldsymbol{B}}^{n+1}_j, \qquad \lambda^{n+1}_j = \hat{\lambda}^{n+1}_j + \xi_j \breve{\lambda}^{n+1}_j.$$

Then solving Algorithm (1.1.2) is equivalent to solving the following subproblems, Given u_j^{n-2}, u_j^{n-1}, u_j^n, $\boldsymbol{B}_j^{n-2}$, $\boldsymbol{B}_j^{n-1}$, $\boldsymbol{B}_j^n$, p_j^n and λ_j^n,
Sub-problem 1: find $\hat{\boldsymbol{u}}_j^{n+1}$, $\hat{\boldsymbol{B}}_j^{n+1}$, $\hat{p}_j^{n+1}$ and $\hat{\lambda}_j^{n+1}$ satisfying

$$\begin{aligned}\frac{1}{\Delta t}\hat{\boldsymbol{u}}_j^{n+1} - \frac{\bar{\nu}^n}{2}\Delta\hat{\boldsymbol{u}}_j^{n+1} + \frac{1}{2}\nabla\hat{p}_j^{n+1} &= \boldsymbol{f}_j^{n+1/2} + \frac{1}{\Delta t}u_j^n + \nu_j'^n\Delta\tilde{\boldsymbol{u}}_j^{n+1/2} \\ &+ \frac{\bar{\nu}^n}{2}\Delta u_j^n - \frac{1}{2}\nabla p_j^n,\end{aligned} \tag{1.54a}$$

$$\nabla\cdot\hat{\boldsymbol{u}}_j^{n+1} = 0, \tag{1.54b}$$

$$\begin{aligned}\frac{1}{\Delta t}\hat{\boldsymbol{B}}_j^{n+1} - \frac{\bar{\gamma}^n}{2}\Delta\hat{\boldsymbol{B}}_j^{n+1} + \frac{1}{2}\nabla\hat{\lambda}_j^{n+1} &= \nabla\times\boldsymbol{g}_j^{n+1/2} + \frac{1}{\Delta t}\boldsymbol{B}_j^n + \frac{\bar{\gamma}^n}{2}\Delta\boldsymbol{B}_j^n \\ &+ \gamma_j'^n\Delta\tilde{\boldsymbol{B}}_j^{n+1/2} - \frac{1}{2}\nabla\lambda_j^n,\end{aligned} \tag{1.54c}$$

$$\nabla\cdot\hat{\boldsymbol{B}}_j^{n+1} = 0, \tag{1.54d}$$

Sub-problem 2: find $\breve{\boldsymbol{u}}_j^{n+1}$, $\breve{\boldsymbol{B}}_j^{n+1}$, $\breve{p}_j^{n+1}$ and $\breve{\lambda}_j^{n+1}$ satisfying

$$\frac{1}{\Delta t}\breve{\boldsymbol{u}}_j^{n+1} - \frac{\bar{\nu}^n}{2}\Delta\breve{\boldsymbol{u}}_j^{n+1} + \frac{1}{2}\nabla\breve{p}_j^{n+1} = s\left(\tilde{\boldsymbol{B}}_j^{n+1/2}\cdot\nabla\right)\tilde{\boldsymbol{B}}_j^{n+1/2} - \left(\tilde{\boldsymbol{u}}_j^{n+1/2}\cdot\nabla\right)\tilde{\boldsymbol{u}}_j^{n+1/2}, \tag{1.55a}$$

$$\nabla\cdot\breve{\boldsymbol{u}}_j^{n+1} = 0, \tag{1.55b}$$

$$\frac{1}{\Delta t}\breve{\boldsymbol{B}}_j^{n+1} + \frac{1}{2}\nabla\breve{\lambda}_j^{n+1} - \frac{\bar{\gamma}^n}{2}\Delta\breve{\boldsymbol{B}}_j^{n+1} = \left(\tilde{\boldsymbol{B}}_j^{n+1/2}\cdot\nabla\right)\tilde{\boldsymbol{u}}_j^{n+1/2} - \left(\tilde{\boldsymbol{u}}_j^{n+1/2}\cdot\nabla\right)\tilde{\boldsymbol{B}}_j^{n+1/2}, \tag{1.55c}$$

$$\nabla\cdot\breve{\boldsymbol{B}}_j^{n+1} = 0. \tag{1.55d}$$

For inhomogeneous Dirichlet boundary conditions, let

$$\hat{\boldsymbol{u}}_j^{n+1} = g(x,t^{n+1}),\quad \breve{\boldsymbol{u}}_j^{n+1} = 0,\quad \hat{\boldsymbol{B}}_j^{n+1} = h(x,t^{n+1}),\quad \breve{\boldsymbol{B}}_j^{n+1} = 0 \quad \text{on } \partial\Omega.$$

We use the following approximations,

$$\begin{cases}\bar{\boldsymbol{v}}_j^{n+1} = \hat{\boldsymbol{v}}_j^{n+1} + \breve{\boldsymbol{v}}_j^{n+1}, & (1.56)\\ \bar{\boldsymbol{v}}_j^{n+1/2} = \dfrac{1}{2}(\bar{\boldsymbol{v}}_j^{n+1} + \boldsymbol{v}^n). & (1.57)\end{cases}$$

This is a reasonable approximation to use since ξ_j is a second order approximation to 1 and is necessary for our equations to result in a linear update of ξ_j. We then update ξ_j as

$$\xi_j = \frac{\mathcal{F}(R_j^n) + |S_0|\Delta t}{E(\bar{\boldsymbol{u}}_j^{n+1}, \bar{\boldsymbol{B}}_j^{n+1}) + \Delta t \int_\Omega \left(\nu|\nabla \bar{\boldsymbol{u}}_j^{n+1/2}|^2 + s\gamma|\nabla \bar{\boldsymbol{B}}_j^{n+1/2}|^2\right) d\Omega + \Delta t(|S_0| - S_0)}, \quad (1.58)$$

where

$$S_0 = \int_\Omega \boldsymbol{f}_j^{n+1/2} \cdot \bar{\boldsymbol{u}}_j^{n+1/2} d\Omega + \int_\Omega s(\nabla \times \boldsymbol{g}_j^{n+1/2}) \cdot \bar{\boldsymbol{B}}_j^{n+1/2} d\Omega + \int_\Gamma B_S(\bar{\boldsymbol{u}}_j^{n+1/2}, \bar{\boldsymbol{B}}_j^{n+1/2}) d\Gamma. \quad (1.59)$$

Notice ξ_j is updated via a linear equation and is very direct. Once we have ξ_j we update

$$R_j^{n+1} = \mathcal{G}\left(\xi_j E(\bar{\boldsymbol{u}}_j^{n+1}, \bar{\boldsymbol{B}}_j^{n+1})\right) \quad (1.60)$$

and proceed to the next timestep iteration. Since ξ_j is a ratio of the SAV to itself, we should expect the result to be close to one. With our ensemble approach in (1.54)-(1.55), all J realizations have the same coefficient matrix in each timestep so should be computationally efficient.

1.5.2. BDF2. For Algorithm (1.1.3), we develop an efficient implementation with the same approach. Note solving Algorithm (1.1.3) is equivalent to the following, Given $\boldsymbol{u}_j^n$, $\boldsymbol{B}_j^n$ and p_j^n, Sub-problem 1: find $\hat{\boldsymbol{u}}_j^{n+1}$, $\hat{\boldsymbol{B}}_j^{n+1}$, $\hat{p}_j^{n+1}$ and $\hat{\lambda}_j^{n+1}$ satisfying

$$\frac{3}{2\Delta t}\hat{\boldsymbol{u}}_j^{n+1} - \bar{\nu}^n \Delta \hat{\boldsymbol{u}}_j^{n+1} + \nabla \hat{p}_j^{n+1} = \boldsymbol{f}_j^{n+1} + \frac{2}{\Delta t}u_j^n - \frac{1}{2\Delta t}u_j^{n-1} + \nu_j'^n \Delta, \quad (1.61a)$$

$$\nabla \cdot \hat{\boldsymbol{u}}_j^{n+1} = 0, \quad (1.61b)$$

$$\frac{3}{2\Delta t}\hat{\boldsymbol{B}}_j^{n+1} - \bar{\gamma}^n \Delta \hat{\boldsymbol{B}}_j^{n+1} + \nabla \hat{\lambda}_j^{n+1} = \nabla \times \boldsymbol{g}_j^{n+1} + \frac{2}{\Delta t}\boldsymbol{B}_j^n - \frac{1}{2\Delta t}\boldsymbol{B}_j^{n-1} + \gamma_j'^n \Delta, \quad (1.61c)$$

$$\nabla \cdot \hat{\boldsymbol{B}}_j^{n+1} = 0, \quad (1.61d)$$

Sub-problem 2: find $\breve{\boldsymbol{u}}_j^{n+1}$, $\breve{\boldsymbol{B}}_j^{n+1}$, $\breve{p}_j^{n+1}$ and $\breve{\lambda}_j^{n+1}$ satisfying

$$\frac{3}{2\Delta t}\breve{\boldsymbol{u}}_j^{n+1} - \bar{\nu}^n \Delta \breve{\boldsymbol{u}}_j^{n+1} + \nabla \breve{p}_j^{n+1} = s\left(\tilde{\boldsymbol{B}}_j^{n+1}\cdot\nabla\right)\tilde{\boldsymbol{B}}_j^{n+1} - \left(\tilde{\boldsymbol{u}}_j^{n+1}\cdot\nabla\right)\tilde{\boldsymbol{u}}_j^{n+1}, \tag{1.62a}$$

$$\nabla\cdot\hat{\boldsymbol{u}}_j^{n+1} = 0, \tag{1.62b}$$

$$\frac{3}{2\Delta t}\breve{\boldsymbol{B}}_j^{n+1} - \bar{\gamma}^n \Delta \breve{\boldsymbol{B}}_j^{n+1} + \nabla \breve{\lambda}_j^{n+1} = \left(\tilde{\boldsymbol{B}}_j^{n+1}\cdot\nabla\right)\tilde{\boldsymbol{u}}_j^{n+1} - \left(\tilde{\boldsymbol{u}}_j^{n+1}\cdot\nabla\right)\tilde{\boldsymbol{B}}_j^{n+1}, \tag{1.62c}$$

$$\nabla\cdot\hat{\boldsymbol{B}}_j^{n+1} = 0. \tag{1.62d}$$

We use the following approximations,

$$\begin{cases} \bar{\boldsymbol{v}}_j^{n+1} = \hat{\boldsymbol{v}}_j^{n+1} + \breve{\boldsymbol{v}}_j^{n+1}, & (1.63)\\ \bar{\boldsymbol{v}}_j^{n+3/2} = \dfrac{3}{2}\bar{\boldsymbol{v}}_j^{n+1} - \dfrac{1}{2}\boldsymbol{v}^n. & (1.64) \end{cases}$$

again noting ξ_j is a second order approximation to 1. We update ξ_j as

$$\xi_j = \frac{\mathcal{F}(\overset{*}{R}_j^{n+1/2}) + |S_0|\Delta t}{E(\bar{\boldsymbol{u}}_j^{n+3/2}, \bar{\boldsymbol{B}}_j^{n+3/2}) + \Delta t\int_\Omega \left(\nu|\nabla\bar{\boldsymbol{u}}_j^{n+1}|^2 + s\gamma|\nabla\bar{\boldsymbol{B}}_j^{n+1}|^2\right)d\Omega + \Delta t(|S_0| - S_0)}, \tag{1.65}$$

where

$$S_0 = \int_\Omega \boldsymbol{f}_j^{n+1}\cdot\bar{\boldsymbol{u}}_j^{n+1}d\Omega + \int_\Omega s(\nabla\times\boldsymbol{g}_j^{n+1})\cdot\bar{\boldsymbol{B}}_j^{n+1}d\Omega + \int_\Gamma B_S(\bar{\boldsymbol{u}}_j^{n+1}, \bar{\boldsymbol{B}}_j^{n+1})d\Gamma.$$

Once we have ξ_j we update R_j^{n+1} as follows:

$$\begin{cases} \overset{*}{R}_j^{n+3/2} = \mathcal{G}\left(\xi_j E(\bar{\boldsymbol{u}}_j^{n+3/2}, \bar{\boldsymbol{B}}_j^{n+3/2})\right), & (1.66)\\ R_j^{n+1} = \dfrac{2}{3}\overset{*}{R}_j^{n+3/2} + \dfrac{1}{3}R_j^n. & (1.67) \end{cases}$$

and proceed to the next timestep iteration.

1.6. NUMERICAL TESTS

This section will present numerical results for Algorithms (1.3.1) and (1.3.1) to demonstrate the expected convergence rates and the stability proven previously. We set $\mathcal{F}(\chi) = \chi^2$ and the corresponding $\mathcal{G}(\chi) = \sqrt{\chi}$ in every experiment. Throughout these tests we'll use the finite element triplet (P^2–P^1–P^2), and the finite element software package FEniCS [24].

1.6.1. CONVERGENCE TEST. To verify the expected convergence rates, we will use a variation of the test problem in [65]. Take the time interval $0 \leq t \leq 1$ and domain $\Omega = [0, 1]^2$. Define the true solution (u, p, B) as

$$\begin{cases} u_\epsilon = \left(y^5 + t^2, x^5 + t^2\right)(1 + \epsilon), \\ p_\epsilon = 10(2x - 1)(2y - 1)(1 + t^2)(1 + \epsilon), \\ B_\epsilon = \left(\sin(\pi y) + t^2, \sin(\pi x) + t^2\right)(1 + \epsilon), \end{cases} \tag{1.68}$$

where ϵ is a given perturbation. For this problem we will consider two perturbations $\epsilon_1 = 10^{-1}$ and $\epsilon_2 = -10^{-1}$. The kinematic viscosity and magnetic resistivity are defined as $\nu_\epsilon = 0.5 \cdot (1 + \epsilon)$ and $\gamma_\epsilon = 0.5 \cdot (1 + \epsilon)$. The source terms and initial conditions correspond with the exact solution for the given perturbation. For each algorithm we initialize u_j, B_j, p_j or λ_j using the exact solution. The results are displayed in tables (1.1)-(1.8) both with regularization and without ($\alpha = \alpha_M = 0$). Under this test, we indeed observe second order convergence with and without regularization. In this particular test on a short time interval, we also observe the algorithm with regularization achieves relatively similar accuracy to the algorithm without.

Table 1.1. Crank-Nicolson error and convergence rates for the first ensemble member in u_h and ∇u_h.

h	Δt	$\|u_1 - u_{1,h}\|_{\infty,0_{rel}}$	Rate	$\|\nabla u_1 - \nabla u_{1,h}\|_{2,0_{rel}}$	Rate
1/10	1/8	9.191 e-4	—	4.985 e-3	—
1/20	1/16	2.088 e-4	2.138	1.399 e-3	1.834
1/40	1/32	4.810 e-5	2.118	3.679 e-4	1.927
1/80	1/64	1.154 e-5	2.060	9.422 e-5	1.965
1/160	1/128	2.889 e-6	1.998	2.384 e-5	1.983
			Reg with $\alpha = \alpha_M = 0.5$		
1/10	1/8	3.912 e-4	—	4.741 e-3	—
1/20	1/16	6.032 e-5	2.697	1.355 e-3	1.807
1/40	1/32	9.532 e-6	2.662	3.579 e-4	1.920
1/80	1/64	2.208 e-6	2.110	9.179 e-5	1.963

Table 1.2. Crank-Nicolson error and convergence rates for the first ensemble member in B_h and ∇B_h.

h	Δt	$\|B_1 - B_{1,h}\|_{\infty,0_{rel}}$	Rate	$\|\nabla B_1 - \nabla B_{1,h}\|_{2,0_{rel}}$	Rate
1/10	1/8	2.566 e-4	—	3.013 e-3	—
1/20	1/16	5.0568 e-5	2.343	8.451 e-4	1.834
1/40	1/32	1.150 e-5	2.136	2.223 e-4	1.927
1/80	1/64	2.746 e-6	2.067	5.694 e-5	1.965
1/160	1/128	6.869 e-7	1.999	1.440 e-5	1.983
			Reg with $\alpha = \alpha_M = 0.5$		
1/10	1/8	1.512 e-4	—	2.909 e-3	—
1/20	1/16	2.138 e-5	2.822	8.298 e-4	1.810
1/40	1/32	3.082 e-6	2.795	2.191 e-4	1.921
1/80	1/64	6.830 e-7	2.174	5.619 e-5	1.964

Table 1.3. Crank-Nicolson error and convergence rates for the second ensemble member in u_h and ∇u_h.

h	Δt	$\|u_2 - u_{2,h}\|_{\infty,0_{rel}}$	Rate	$\|\nabla u_2 - \nabla u_{2,h}\|_{2,0_{rel}}$	Rate
1/10	1/8	2.020 e-3	—	5.498 e-3	—
1/20	1/16	4.897 e-4	2.045	1.433 e-3	1.940
1/40	1/32	9.342 e-5	2.390	3.701 e-4	1.953
1/80	1/64	1.560 e-5	2.582	9.440 e-5	1.971
1/160	1/128	2.923 e-6	2.416	2.385 e-5	1.985
			Reg with $\alpha = \alpha_M = 0.5$		
1/10	1/8	4.070 e-4	—	4.753 e-3	—
1/20	1/16	6.277 e-5	2.697	1.357 e-3	1.809
1/40	1/32	1.134 e-5	2.469	3.584 e-4	1.921
1/80	1/64	2.649 e-6	2.097	9.190 e-5	1.964

Table 1.4. Crank-Nicolson error and convergence rates for the second ensemble member in B_h and ∇B_h.

h	Δt	$\|B_2 - B_{2,h}\|_{\infty,0_{rel}}$	Rate	$\|\nabla B_2 - \nabla B_{2,h}\|_{2,0_{rel}}$	Rate
1/10	1/8	7.455 e-4	—	3.376 e-3	—
1/20	1/16	1.666 e-4	2.162	8.700 e-4	1.956
1/40	1/32	3.097 e-5	2.427	2.239 e-4	1.958
1/80	1/64	5.113 e-6	2.598	5.706 e-5	1.973
1/160	1/128	7.772 e-7	2.718	1.442 e-5	1.985
			Reg with $\alpha = \alpha_M = 0.5$		
1/10	1/8	1.567 e-4	—	2.915 e-3	—
1/20	1/16	2.222 e-5	2.818	8.308 e-4	1.811
1/40	1/32	3.664 e-6	2.600	2.193 e-4	1.922
1/80	1/64	8.188 e-7	2.162	5.622 e-5	1.964

Table 1.5. BDF2 error and convergence rates for the first ensemble member in u_h and ∇u_h.

h	Δt	$\|u_1 - u_{1,h}\|_{\infty,0_{rel}}$	Rate	$\|\nabla u_1 - \nabla u_{1,h}\|_{2,0_{rel}}$	Rate
1/10	1/8	7.413 e-4	—	5.804 e-3	—
1/20	1/16	1.891 e-4	1.971	1.495 e-3	1.957
1/40	1/32	4.790 e-5	1.981	3.793 e-4	1.978
1/80	1/64	1.183 e-5	2.018	9.557 e-5	1.989
1/160	1/128	2.944 e-6	2.006	2.399 e-5	1.994
			Reg with $\alpha = \alpha_M = 0.5$		
1/10	1/8	4.528 e-4	—	5.601 e-3	—
1/20	1/16	6.215 e-5	2.865	1.453 e-3	1.947
1/40	1/32	7.946 e-6	2.968	3.694 e-4	1.976
1/80	1/64	1.339 e-6	2.570	9.310 e-5	1.988

Table 1.6. BDF2 error and convergence rates for the first ensemble member in B_h and ∇B_h.

h	Δt	$\|B_1 - B_{1,h}\|_{\infty,0_{rel}}$	Rate	$\|\nabla B_1 - \nabla B_{1,h}\|_{2,0_{rel}}$	Rate
1/10	1/8	1.868 e-4	—	3.502 e-3	—
1/20	1/16	3.792 e-5	2.301	9.005 e-4	1.960
1/40	1/32	9.133 e-6	2.054	2.285 e-4	1.979
1/80	1/64	2.300 e-6	1.990	5.756 e-5	1.989
1/160	1/128	5.816 e-7	1.983	1.445 e-5	1.994
			Reg with $\alpha = \alpha_M = 0.5$		
1/10	1/8	1.649 e-4	—	3.438 e-3	—
1/20	1/16	2.185 e-5	2.916	8.904 e-4	1.949
1/40	1/32	2.772 e-6	2.978	2.263 e-4	1.976
1/80	1/64	4.182 e-7	2.729	5.705 e-5	1.988

Table 1.7. BDF2 error and convergence rates for the second ensemble member in u_h and ∇u_h.

h	Δt	$\|u_2 - u_{2,h}\|_{\infty,0_{rel}}$	Rate	$\|\nabla u_2 - \nabla u_{2,h}\|_{2,0_{rel}}$	Rate
1/10	1/8	7.762 e-4	—	5.806 e-3	—
1/20	1/16	1.880 e-4	2.045	1.495 e-3	1.957
1/40	1/32	4.699 e-5	2.001	3.795 e-4	1.978
1/80	1/64	1.186 e-5	1.987	9.561 e-5	1.989
1/160	1/128	2.964 e-6	2.001	2.400 e-5	1.994
			Reg with $\alpha = \alpha_M = 0.5$		
1/10	1/8	4.531 e-4	—	5.603 e-3	—
1/20	1/16	6.218 e-5	2.865	1.453 e-3	1.947
1/40	1/32	7.964 e-6	2.965	3.695 e-4	1.976
1/80	1/64	1.547 e-6	2.364	9.314 e-5	1.988

Table 1.8. BDF2 error and convergence rates for the second ensemble member in B_h and ∇B_h.

h	Δt	$\|B_2 - B_{2,h}\|_{\infty,0_{rel}}$	Rate	$\|\nabla B_2 - \nabla B_{2,h}\|_{2,0_{rel}}$	Rate
1/10	1/8	1.918 e-4	—	3.505 e-3	—
1/20	1/16	3.930 e-5	2.287	9.013 e-4	1.960
1/40	1/32	9.605 e-6	2.033	2.287 e-4	1.979
1/80	1/64	2.425 e-6	1.986	5.761 e-5	1.989
1/160	1/128	6.129 e-7	1.984	1.446 e-5	1.994
			Reg with $\alpha = \alpha_M = 0.5$		
1/10	1/8	1.649 e-3	—	3.439 e-3	—
1/20	1/16	2.185 e-4	2.916	8.906 e-4	1.949
1/40	1/32	2.772 e-4	2.978	2.264 e-4	1.976
1/80	1/64	4.880 e-5	2.506	5.706 e-5	1.988

1.6.2. EFFICIENCY TEST. In this experiment we repeat the numerical methods used above with the same problem, except we set $\nu_\epsilon = 1.0 \cdot (1+\epsilon)$, $\gamma_\epsilon = 0.2 \cdot (1+\epsilon)$ and analyze 11 perturbations $\epsilon_i = 10^{-1} - 0.009 * i$, $i = 0, \ldots, 10$. We compare the performance speed and accuracy of Algorithms (1.3.1) and (1.3.1) with the corresponding nonensemble GPAV methods, where no ensemble mean is used and the linear systems for each perturbation are solved in serial. To do this, we list the CPU runtime in seconds and error norm of the average of all 11 velocities and magnetic fields, labeled as $\bar{u}^n$ and $\bar{B}^n$, for each computation. As can be seen in the tables (1.9)-(1.12) below, the second order ensemble methods obtain the same accuracy as the nonensemble trials, while requiring significantly less runtime.

Table 1.9. Error and CPU time for computing $\bar{u}_h$ and $\bar{B}_h$ with Algorithm 1.3.1.

h	Δt	$\|\bar{u} - \bar{u}_{en,h}\|_{\infty,0_{rel}}$	$\|\bar{B} - \bar{B}_{en,h}\|_{\infty,0_{rel}}$	CPU time (s)
1/5	1/40	3.099 e-3	1.220 e-3	2.117 e+0
1/10	1/80	4.782 e-4	1.716 e-4	7.622 e+0
1/20	1/160	6.294 e-5	2.218 e-5	3.911 e+1
1/40	1/320	7.968 e-6	2.802 e-6	2.905 e+2
1/80	1/640	1.005 e-6	4.450 e-7	2.181 e+3

Table 1.10. Error and CPU time for computing $\bar{u}_h$ and $\bar{B}_h$ with nonensemble CN algorithm.

h	Δt	$\|\bar{u} - \bar{u}_{en,h}\|_{\infty,0_{rel}}$	$\|\bar{B} - \bar{B}_{en,h}\|_{\infty,0_{rel}}$	CPU time (s)
1/10	1/80	4.783 e-4	1.718 e-4	1.694 e+1
1/20	1/160	6.294 e-5	2.219 e-5	1.144 e+2
1/40	1/320	7.968 e-6	2.802 e-6	8.362 e+2
1/80	1/640	1.004 e-6	7.730 e-7	6.895 e+3

Table 1.11. Error and CPU time for computing $\bar{u}_h$ and $\bar{B}_h$ with Algorithm 1.3.1.

h	Δt	$\|\bar{u} - \bar{u}_{en,h}\|_{\infty,0_{rel}}$	$\|\bar{B} - \bar{B}_{en,h}\|_{\infty,0_{rel}}$	CPU time (s)
1/5	1/40	3.609 e-3	1.331 e-3	2.768 e+0
1/10	1/80	4.961 e-4	1.750 e-4	8.432 e+0
1/20	1/160	6.348 e-5	2.219 e-5	3.844 e+1
1/40	1/320	7.982 e-6	2.785 e-6	2.760 e+2
1/80	1/640	1.006 e-6	3.546 e-7	2.267 e+3

Table 1.12. Error and CPU time for computing $\bar{u}_h$ and $\bar{B}_h$ with nonensemble BDF2 algorith.

h	Δt	$\|\bar{u} - \bar{u}_{en,h}\|_{\infty,0_{rel}}$	$\|\bar{B} - \bar{B}_{en,h}\|_{\infty,0_{rel}}$	CPU time (s)
1/10	1/80	4.962 e-4	1.750 e-4	1.674 e+1
1/20	1/160	6.348 e-5	2.219 e-5	1.152 e+2
1/40	1/320	7.982 e-6	2.785 e-6	8.233 e+2
1/80	1/640	1.006 e-6	3.549 e-7	6.720 e+3

1.6.3. STABILITY. Here we analyze the stability of the second order ensemble methods. For the test problem, we will exclude external energy and body forces so that in observation if the method is stable, the system energy should decay to zero as time passes. We also use the initial conditions,

$$\begin{cases} u_\epsilon^0 = (x^2(x-1)^2y(y-1)(2y-1), -y^2(y-1)^2x(x-1)(2x-1))(1+\epsilon), \\ p_\epsilon^0 = 0, \\ B_\epsilon^0 = (\sin(\pi x)\cos(\pi y), -\sin(\pi y)\cos(\pi x))(1+\epsilon). \end{cases}$$

We'll consider an ensemble of two perturbations, $\epsilon = 10^{-1}$ and $\epsilon = -10^{-1}$. We fix the coupling term $s = 1$ and choose two different sets of viscosity and magnetic viscosity to test, $\nu = \gamma = 0.1$ and $\nu = \gamma = 0.02$. The mesh discretization is fixed at $h = 1/50$ and several time steps are employed, with final time $T = 5$.

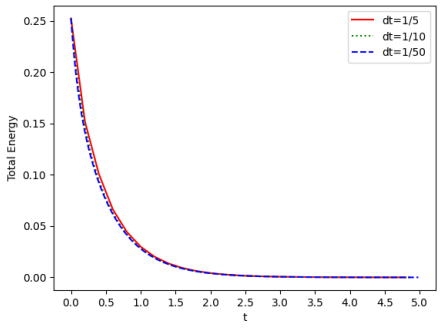

Decay of total system energy to $T = 5$ for Algorithm (1.3.1) with $\nu = \gamma = 0.1$.

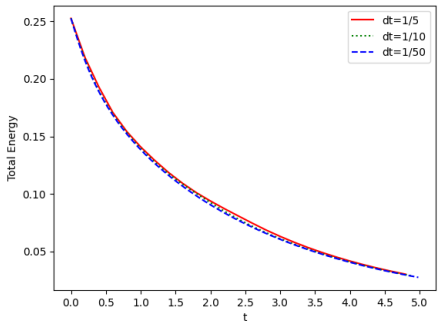

Decay of total system energy to $T = 5$ for Algorithm (1.3.1) with $\nu = \gamma = 0.02$.

Figure 1.1. Stability demonstrations of Crank-Nicolson Algorithm.

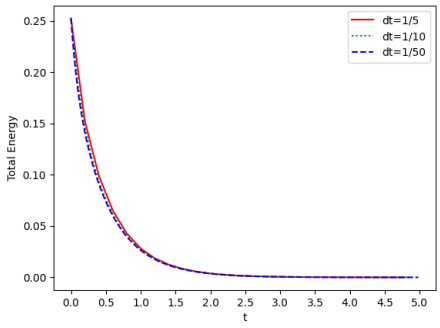

Decay of total system energy to $T = 5$ for Algorithm (1.3.1) with $\nu = \gamma = 0.1$.

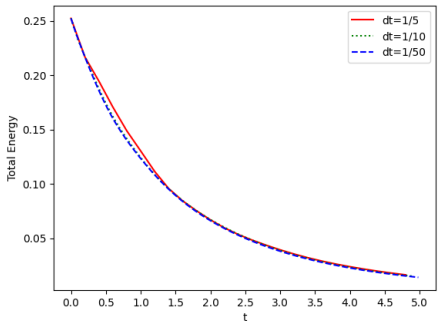

Decay of total system energy to $T = 5$ for Algorithm (1.3.1) with $\nu = \gamma = 0.02$.

Figure 1.2. Stability demonstrations of BDF2 Algorithm.

1.6.4. CHAMBER FLOW. In this numerical test, we consider a channel flow in a rectangular domain of length 2.2 units and height 0.41, with a cylinder of radius 0.05 centered at $(0.2, 0.2)$, in the presence of a magnetic field. On the walls and around the cylinder, a no-slip boundary condition is applied for velocity while magnetic field is kept

constant as $B =< 0, 0.1 >^T$. We set the inflow and outflow conditions equal, choosing $u =< 6y(0.41 - y)/0.41^2 \sin(\pi t/16.0), 0 >^T$ and $B =< 0, 0.1 >^T$. The coupling term is set to $s = 0.01$ and for all realizations we fix $\gamma = 0.1$ then consider two cases, $\nu = 1/50$ and $\nu = 1/1000$.

We'll use an ensemble of two different solutions with the initial and boundary conditions perturbed by multiplicative factors of $(1 \pm \epsilon)$. We simulate the flow with Algorithms (1.3.1) and (1.3.1) till final time $T = 8.8$ with a mesh discretization fixed at $h = 1/100$. We set $\alpha = \alpha_M = 0$ such that these tests are performed without the regularization terms involved. In order to maintain accurate results up unto $T = 8.8$, we find it necessary to choose a time step of roughly $\Delta t = 1/1000$ when $\nu = 1/50$ and $\Delta t = 1/2000$ when $\nu = 1/1000$. The solutions under each perturbation for velocity are shown in Figures (1.3)-(1.10) and for magnetic field in Figures (1.13)-(1.20). We also provide results for no perturbation, that is, $\epsilon = 0$. This is for comparison as we expect the ensemble solutions to converge to the unperturbed results as $\epsilon \to 0$.

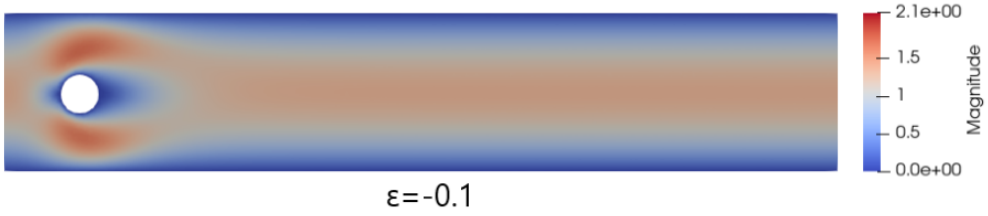

Figure 1.3. Ensemble solutions for first velocity member at time $T = 8.8$ for Algorithm (1.3.1) with $\nu = 0.02$, $\gamma = 0.1$ and $\Delta t = 0.001$.

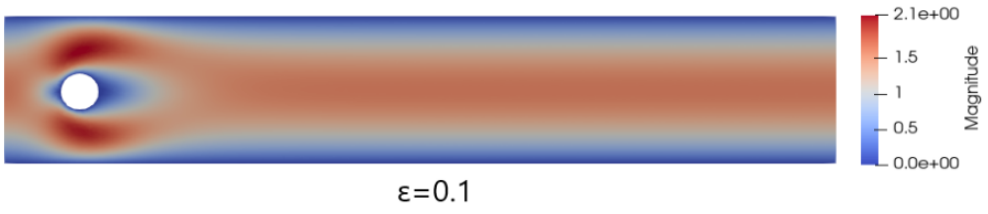

Figure 1.4. Ensemble solutions for second velocity member at time $T = 8.8$ for Algorithm (1.3.1) with $\nu = 0.02$, $\gamma = 0.1$ and $\Delta t = 0.001$.

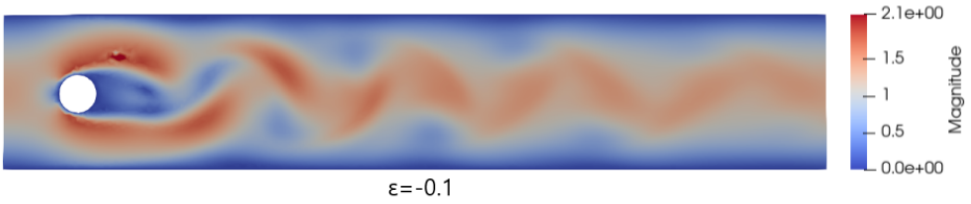

Figure 1.5. Ensemble solutions for first velocity member at time $T = 8.8$ for Algorithm (1.3.1) with $\nu = 0.001$, $\gamma = 0.1$ and $\Delta t = 0.0005$.

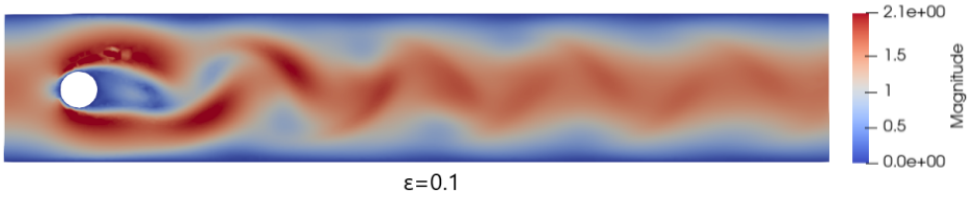

Figure 1.6. Ensemble solutions for second velocity member at time $T = 8.8$ for Algorithm (1.3.1) with $\nu = 0.001$, $\gamma = 0.1$ and $\Delta t = 0.0005$.

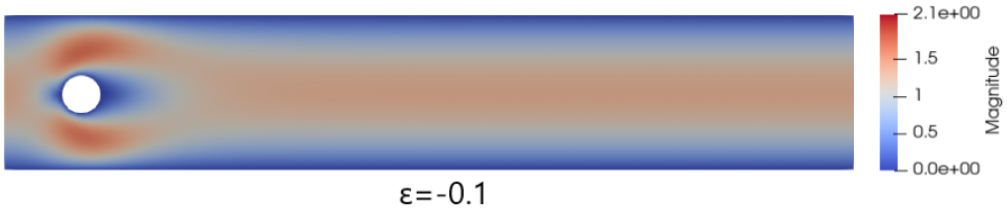

Figure 1.7. Ensemble solutions for first velocity member at time $T = 8.8$ for Algorithm (1.3.1) with $\nu = 0.02$, $\gamma = 0.1$ and $\Delta t = 0.001$.

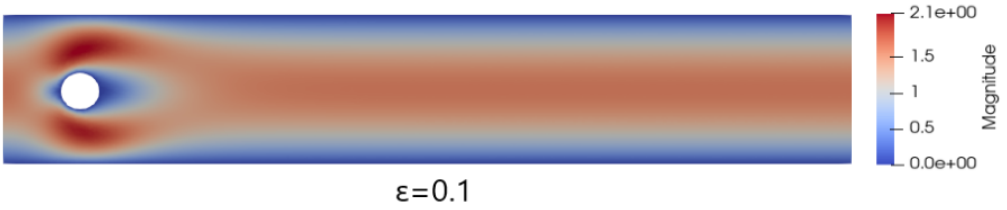

Figure 1.8. Ensemble solutions for second velocity member at time $T = 8.8$ for Algorithm (1.3.1) with $\nu = 0.02$, $\gamma = 0.1$ and $\Delta t = 0.001$.

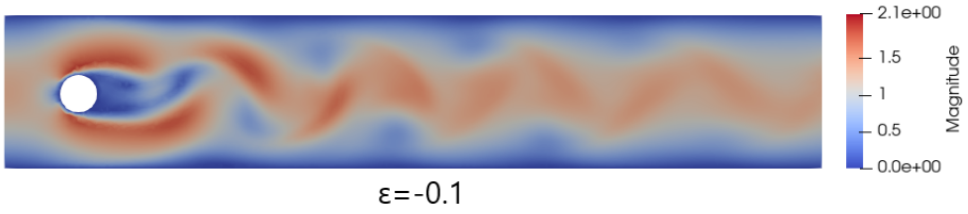

Figure 1.9. Ensemble solutions for first velocity member at time $T = 8.8$ for Algorithm (1.3.1) with $\nu = 0.001$, $\gamma = 0.1$ and $\Delta t = 0.0005$.

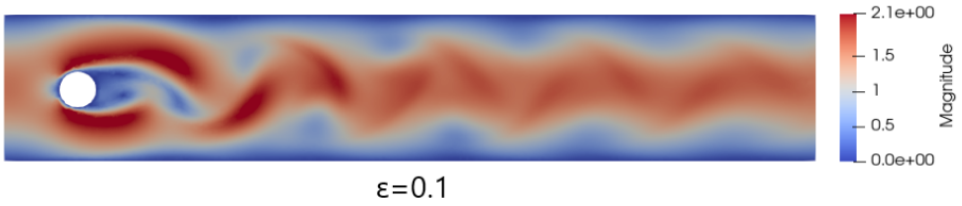

Figure 1.10. Ensemble solutions for second velocity member at time $T = 8.8$ for Algorithm (1.3.1) with $\nu = 0.001$, $\gamma = 0.1$ and $\Delta t = 0.0005$.

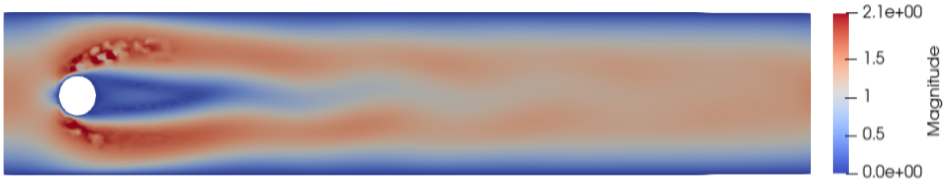

Figure 1.11. Algorithm (1.3.1) solution when $\epsilon = 0$ for velocity at time $T = 8.8$ with $\nu = 0.001$, $\gamma = 0.1$ and $\Delta t = 0.001$.

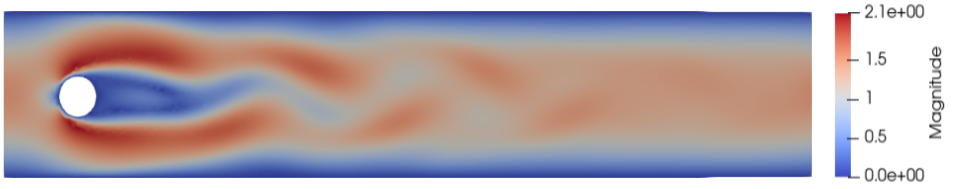

Figure 1.12. Algorithm (1.3.1) solution when $\epsilon = 0$ for velocity at time $T = 8.8$ with $\nu = 0.001$, $\gamma = 0.1$ and $\Delta t = 0.001$.

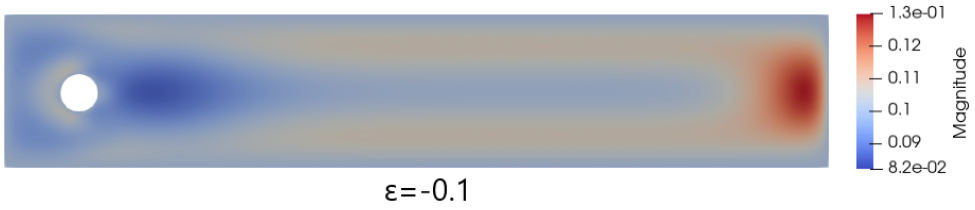

Figure 1.13. Ensemble solutions for first magnetic field member at time $T = 8.8$ for Algorithm (1.3.1) with $\nu = 0.02$, $\gamma = 0.1$ and $\Delta t = 0.001$.

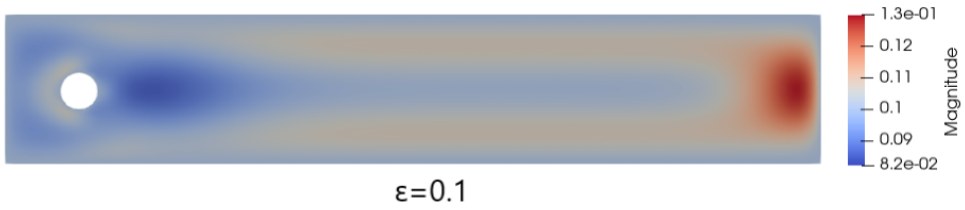

Figure 1.14. Ensemble solutions for second magnetic field member at time $T = 8.8$ for Algorithm (1.3.1) with $\nu = 0.02$, $\gamma = 0.1$ and $\Delta t = 0.001$.

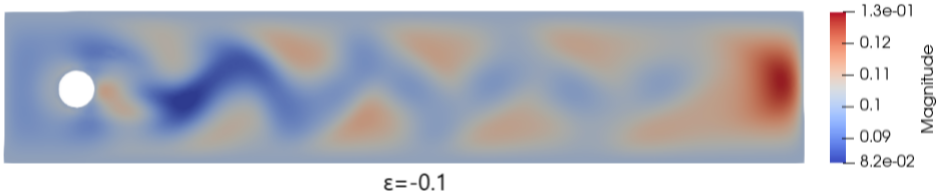

Figure 1.15. Ensemble solutions for first magnetic field member at time $T = 8.8$ for Algorithm (1.3.1) with $\nu = 0.001$, $\gamma = 0.1$ and $\Delta t = 0.0005$.

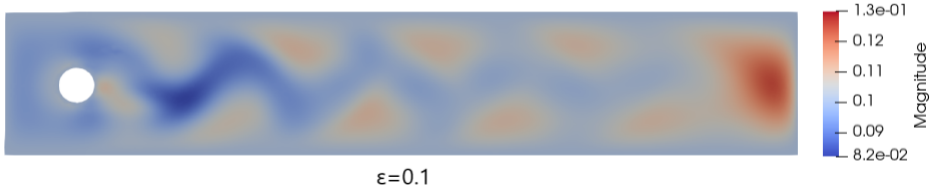

Figure 1.16. Ensemble solutions for second magnetic field member at time $T = 8.8$ for Algorithm (1.3.1) with $\nu = 0.001$, $\gamma = 0.1$ and $\Delta t = 0.0005$.

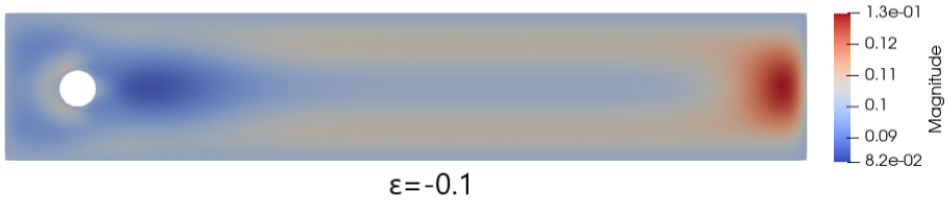

Figure 1.17. Ensemble solutions for first magnetic field member at time $T = 8.8$ for Algorithm (1.3.1) with $\nu = 0.02$, $\gamma = 0.1$ and $\Delta t = 0.001$.

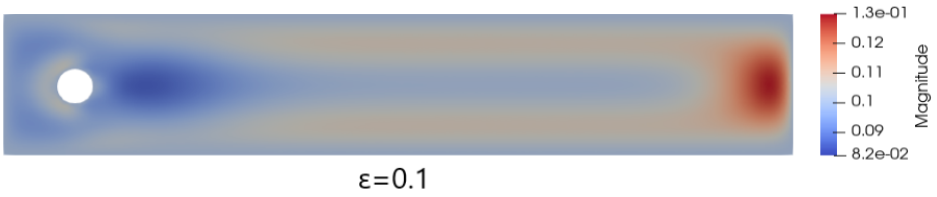

Figure 1.18. Ensemble solutions for second magnetic field member at time $T = 8.8$ for Algorithm (1.3.1) with $\nu = 0.02$, $\gamma = 0.1$ and $\Delta t = 0.001$.

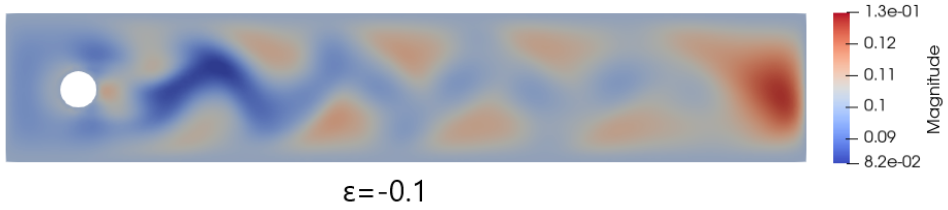

Figure 1.19. Ensemble solutions for first magnetic field member at time $T = 8.8$ for Algorithm (1.3.1) with $\nu = 0.001$, $\gamma = 0.1$ and $\Delta t = 0.0005$.

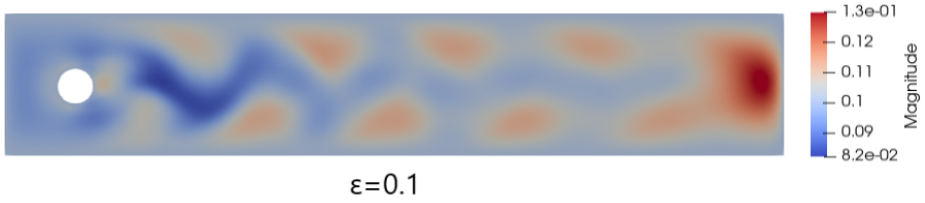

Figure 1.20. Ensemble solutions for second magnetic field member at time $T = 8.8$ for Algorithm (1.3.1) with $\nu = 0.001$, $\gamma = 0.1$ and $\Delta t = 0.0005$.

Figure 1.21. Algorithm (1.3.1) solution when $\epsilon = 0$ for magnetic field at time $T = 8.8$ with $\nu = 0.001$, $\gamma = 0.1$ and $\Delta t = 0.001$.

Figure 1.22. Algorithm (1.3.1) solution when $\epsilon = 0$ for magnetic field at time $T = 8.8$ with $\nu = 0.001$, $\gamma = 0.1$ and $\Delta t = 0.001$.

1.6.5. CHAMBER FLOW WITH REGULARIZATION. Here we present the same chamber flow problem implementing Algorithms (1.3.1) and (1.3.1) with nonzero regularization coefficients. We choose $\alpha = \nu$ and $\alpha_M = \gamma$ in each test. We're able to achieve similar accuracy to the previous section with coarser time step. The following numerical results are achieved:

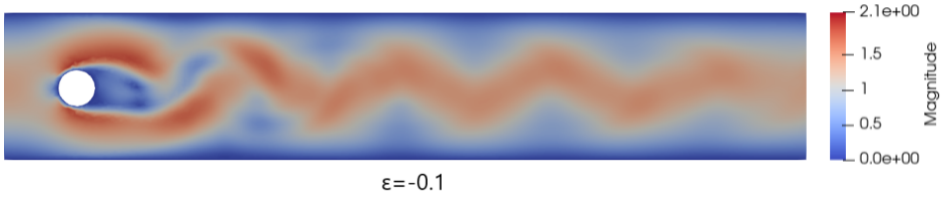

Figure 1.23. Ensemble solutions for first velocity member at time $T = 8.8$ for Algorithm (1.3.1) with regularization and $\nu = 0.001$, $\gamma = 0.1$ and $\Delta t = 0.001$.

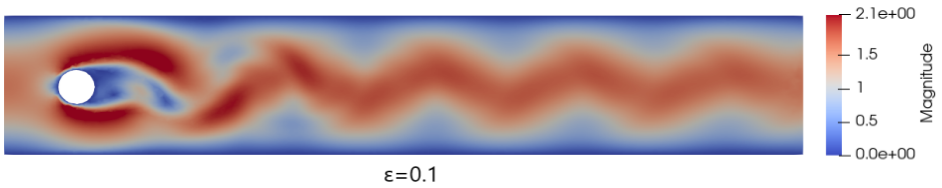

Figure 1.24. Ensemble solutions for second velocity member at time $T = 8.8$ for Algorithm (1.3.1) with regularization and $\nu = 0.001$, $\gamma = 0.1$ and $\Delta t = 0.001$.

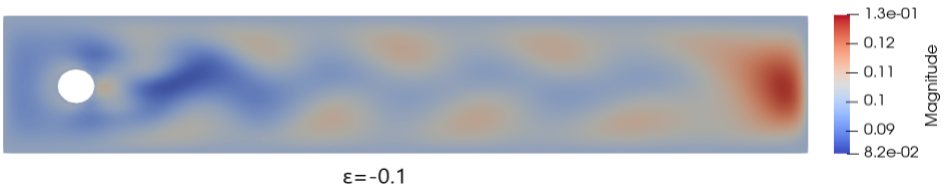

Figure 1.25. Ensemble solutions for first magnetic field member at time $T = 8.8$ for Algorithm (1.3.1) with regularization and $\nu = 0.001$, $\gamma = 0.1$ and $\Delta t = 0.001$.

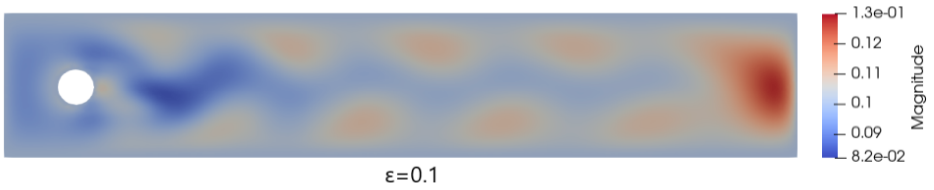

Figure 1.26. Ensemble solutions for second magnetic field member at time $T = 8.8$ for Algorithm (1.3.1) with regularization and $\nu = 0.001$, $\gamma = 0.1$ and $\Delta t = 0.001$.

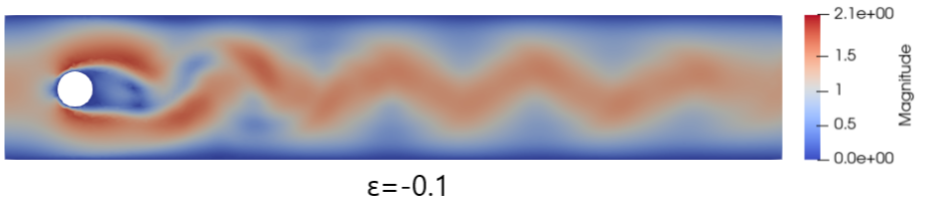

Figure 1.27. Ensemble solutions for first velocity member at time $T = 8.8$ for Algorithm (1.3.1) with regularization and $\nu = 0.001$, $\gamma = 0.1$ and $\Delta t = 0.001$.

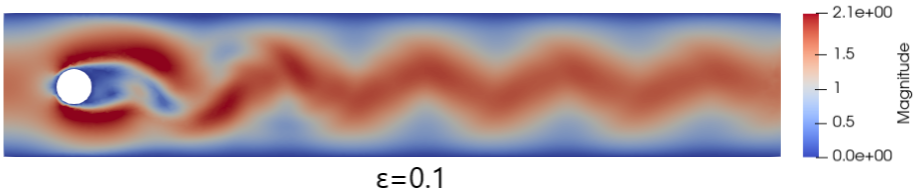

Figure 1.28. Ensemble solutions for second velocity member at time $T = 8.8$ for Algorithm (1.3.1) with regularization and $\nu = 0.001$, $\gamma = 0.1$ and $\Delta t = 0.001$.

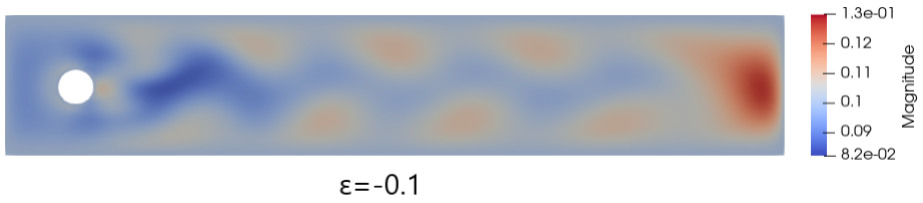

Figure 1.29. Ensemble solutions for first magnetic field member at time $T = 8.8$ for Algorithm (1.3.1) with regularization and $\nu = 0.001$, $\gamma = 0.1$ and $\Delta t = 0.001$.

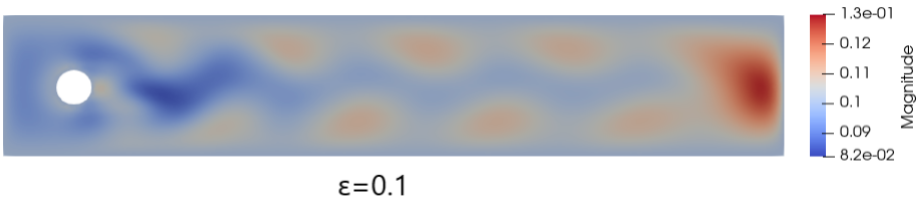

Figure 1.30. Ensemble solutions for second magnetic field member at time $T = 8.8$ for Algorithm (1.3.1) with regularization and $\nu = 0.001$, $\gamma = 0.1$ and $\Delta t = 0.001$.

1.6.6. ACCURACY COMPARISON. In this section we present a comparison test between the errors of the scheme with and without the regularization terms introduced in Section 1.6.5. We use the same test as in 1.6.1, except this time we set $\nu = 1.0$ and $\gamma = 0.2$. We choose two perturbations of $\epsilon = 0.1$ and $\epsilon = 0.2$, with final time $T = 2.5$. This time we use only the L^2 error norm of the result at final time T. For the stabilization coefficients α and α_M, we set them equal to the viscosity and magnetic resistivity correspondingly.

Table 1.13. Error for the first ensemble member in u_h.

h	Δt	SAV-CN	SAV-BDF2	Stab-SAV-CN	Stab-SAV-BDF2
1/100	1/8	1.398 e-2	3.789 e-2	6.485 e-6	1.823 e-5
1/100	1/16	8.242 e-2	6.229 e-2	3.467 e-6	4.143 e-6
1/100	1/32	3.369 e-2	3.664 e-2	1.907 e-6	9.296 e-7
1/100	1/64	2.230 e-2	9.960 e-3	7.120 e-7	1.902 e-7
1/100	1/128	4.517 e-2	2.383 e-3	1.093 e-6	5.102 e-8

Table 1.14. Error for the first ensemble member in B_h.

h	Δt	SAV-CN	SAV-BDF2	Stab-SAV-CN	Stab-SAV-BDF2
1/100	1/8	5.219 e-2	1.312 e-1	3.074 e-5	6.940 e-5
1/100	1/16	2.644 e-1	1.962 e-1	1.647 e-5	1.592 e-5
1/100	1/32	7.231 e-2	7.033 e-2	9.188 e-6	3.429 e-6
1/100	1/64	6.947 e-2	2.400 e-2	3.318 e-6	6.148 e-7
1/100	1/128	1.061 e-1	8.650 e-3	5.619 e-6	1.390 e-7

III. PARTITIONED, UNCONDITIONALLY STABLE, LINEAR ENSEMBLE ALGORITHMS FOR THE MAGNETOHYDRODYNAMICS EQUATIONS

J. A. Carter, D. Han, J. Nan
Department of Computational & Applied Mathematics
Missouri University of Science and Technology
Rolla, Missouri 65409–0050
Tel: 573–341–6622, Fax: 573–341–4115
Email: jachdm@mst.edu

ABSTRACT

We introduce an approach for solving the full Magnetohydrodynamics (MHD) equations that combines the Generalized Positive Auxiliary Variable (GPAV) approach, ensemble techniques and Artificial Compressibility (AC) method. The proposed scheme applies the ensemble method to the viscosity and magnetic resistivity coefficients, the GPAV to the nonlinear terms, and AC is used to update the pressure and solenoidal constraint on the magnetic field. The resulting scheme is second-order accurate and unconditionally stable with respect to the system energy.

Keywords: MHD, SAV, uncertainty quantification, ensemble algorithm, unconditional stability, artificial compressibility

1.1. INTRODUCTION

The governing equations for Magnetohydrodynamics (MHD) are highly nonlinear, and semi-implicit numerical schemes to solve these are notoriously unstable. Recently, Scalar Auxiliary Variable (SAV) techniques have been developed to remedy this issue by defining a type of lagrange multiplier in relation to the kinetic energy of the underlying equations. Generalized Positive Auxiliary Variable (GPAV) is a variant of SAV that guarantees the solutions to the numerical scalar equation are real and positive.

In this paper, we present a novel approach that combines an ensemble method, GPAV, and Artificial Compressibility (AC) to solve the full MHD equations. An ensemble mean is used to model the stochastic fluctuations in the viscosity and magnetic resistivity coefficients, while GPAV is applied to the nonlinear terms. The AC method is utilized to update the pressure and solenoidal constraint on the magnetic field.

The ensemble method allows for efficient and accurate simulations by sharing the same coefficient matrix across different realizations and time steps. The GPAV approach is flexible in handling complex boundary conditions. Though it lacks robustness, with the addition of some regularization terms it can perform well in advection-dominated flows. The AC method helps speed up computations by decoupling the pressure and solenoidal constraint equations from the velocity and magnetic field equations respectively.

We present extensive numerical tests to demonstrate the accuracy and stability.

1.1.1. GOVERNING EQUATIONS. we consider solving J times the following MHD equations: for $j = 1, 2, ..., J$,

$$\begin{cases} \boldsymbol{u}_{j,t} + \boldsymbol{u}_j \cdot \nabla \boldsymbol{u}_j - s\boldsymbol{B}_j \cdot \nabla \boldsymbol{B}_j - \nu_j \Delta \boldsymbol{u}_j + \nabla p_j = \boldsymbol{f}_j \text{ in } \Omega \times (0,T), \\ \nabla \cdot \boldsymbol{u}_j = 0, \text{ in } \Omega \times (0,T), \\ \boldsymbol{B}_{j,t} + \boldsymbol{u}_j \cdot \nabla \boldsymbol{B}_j - \boldsymbol{B}_j \cdot \nabla \boldsymbol{u}_j - \gamma_j \Delta \boldsymbol{B}_j + \nabla \lambda_j = \nabla \times \boldsymbol{g}_j \text{ in } \Omega \times (0,T), \\ \nabla \cdot \boldsymbol{B}_j = 0, \text{ in } \Omega \times (0,T), \\ \boldsymbol{u}_j(x,0) = \boldsymbol{u}_j^0(x), \text{ in } \Omega, \quad \boldsymbol{B}_j(x,0) = \boldsymbol{B}_j^0(x), \text{ in } \Omega. \end{cases} \tag{1.1}$$

Here $\boldsymbol{u}_j$ is the fluid velocity, p_j the pressure, $\boldsymbol{B}_j$ the magnetic field and λ_j is a Lagrange multiplier corresponding to the solenoidal constraint on $\boldsymbol{B}_j$ [41]. The body force $\boldsymbol{f}_j(x,t)$ and $\nabla \times \boldsymbol{g}_j$ are given, s is the coupling number, ν_j is the kinematic viscosity, and γ_j is the magnetic resistivity. This is an equivalent formulation of the MHD equations, cf. [41, 42, 60, 61].

1.2. PROBLEM FORMULATION

To start, we define the ensemble mean and the fluctuation of the viscosity terms ν_j^n and the electric potential γ_j^n at timestep n respectively

$$\bar{\nu}^n = \frac{1}{J}\sum_{j=1}^{J}\nu_j^n \quad \text{and} \quad \bar{\gamma}^n = \frac{1}{J}\sum_{j=1}^{J}\gamma_j^n, \tag{mean}$$

$$\nu_j'^n = \nu_j^n - \bar{\nu}^n \quad \text{and} \quad \gamma_j'^n = \gamma_j^n - \bar{\gamma}^n, \tag{fluctuation}$$

$$\nu'_{\max} = \max_j \max_{x\in\Omega} |\nu_j'^n(x)| \quad \text{and} \quad \gamma'_{\max} = \max_j \max_{x\in\Omega} |\gamma_j'^n(x)|,$$

where in our considerations $\nu_j^n = \nu_j$, $\gamma_j^n = \gamma_j$ are constants and $t_n = n\Delta t$ $(n = 0, 1, 2, ...)$. Define

$$\delta_t v^{n+1} = \frac{1}{2\Delta t}(3\boldsymbol{v}^{n+1} - 4\boldsymbol{v}^n + \boldsymbol{v}^{n-1}), \qquad \tilde{\boldsymbol{v}}^{n+1/2} = 2\boldsymbol{v}^{n-1/2} - \boldsymbol{v}^{n-3/2}, \tag{1.2}$$

$$\overset{*}{\boldsymbol{v}}^{n+1/2} = \frac{3}{2}\boldsymbol{v}^n - \frac{1}{2}\boldsymbol{v}^{n-1}, \qquad \tilde{\boldsymbol{v}}^{n+1} = 2\boldsymbol{v}^n - \boldsymbol{v}^{n-1}. \tag{1.3}$$

The pressure terms in (1.1) lead to a coupled saddle point problem. It is desireable to compute them seperately, especially in three dimension. For this purpose, we adopt the artificial compression technique. The divergence-free conditions are approximated by the following equations

$$\nabla \cdot \mathbf{u}_j + \epsilon p_{j,t} = 0, \tag{1.4}$$

$$\nabla \cdot \mathbf{B}_j + \epsilon \lambda_{j,t} = 0. \tag{1.5}$$

It is straightforward to verify that the modified system admits an energy

$$E_j(t) = \int_\Omega \frac{1}{2}|\boldsymbol{u}_j|^2 d\Omega + \int_\Omega \frac{s}{2}|\boldsymbol{B}_j|^2 d\Omega + \frac{\epsilon}{2}\int_\Omega (|p_j|^2 + |\lambda_j|^2) d\Omega. \tag{1.6}$$

Next, let $\mathcal{F}$ be any one-to-one increasing differentiable function with $\mathcal{F}^{-1} = \mathcal{G}$ such that

$$\begin{cases} \mathcal{F}(\chi) > 0, \quad \chi > 0, & (1.7) \\ \mathcal{G}(\chi) > 0, \quad \chi > 0. & (1.8) \end{cases}$$

The scalar variable $R_j(t)$ is defined by

$$R_j(t) = \mathcal{G}(E_j), \tag{1.9}$$

$$E_j(t) = \mathcal{F}(R_j). \tag{1.10}$$

Since $\frac{\mathcal{F}(R_j)}{E_j} = 1$ for all j, we may write

$$\begin{aligned} \mathcal{F}'(R_j)\frac{dR_j}{dt} = &\int_\Omega \left[\boldsymbol{u}_j \cdot \frac{\partial \boldsymbol{u}_j}{\partial t} + s\boldsymbol{B}_j \cdot \frac{\partial \boldsymbol{B}_j}{\partial t} + \epsilon p_j \frac{\partial p_j}{\partial t} + \epsilon \lambda_j \frac{\partial \lambda_j}{\partial t} \right] d\Omega \\ &- \int_\Omega \boldsymbol{u}_j \cdot \left(\nu_j \Delta \boldsymbol{u}_j - \nabla p_j + \frac{\mathcal{F}(R_j)}{E_j} [\boldsymbol{B}_j \cdot \nabla \boldsymbol{B}_j - \boldsymbol{u}_j \cdot \nabla \boldsymbol{u}_j] + \boldsymbol{f}_j \right) d\Omega \\ &- \int_\Omega s\boldsymbol{B}_j \cdot \left(\gamma_j \Delta \boldsymbol{B}_j - \nabla \lambda_j + \frac{\mathcal{F}(R_j)}{E_j} [\boldsymbol{B}_j \cdot \nabla \boldsymbol{u}_j - \boldsymbol{u}_j \cdot \nabla \boldsymbol{B}_j] + \nabla \times \boldsymbol{g}_j \right) d\Omega \\ &+ \int_\Omega p_j \nabla \cdot \mathbf{u}_j + \lambda_j \nabla \cdot \mathbf{B}_j d\Omega \\ &+ \frac{\mathcal{F}(R_j)}{E_j} \left[- \int_\Omega (\nu_j |\nabla \boldsymbol{u}_j|^2 + s\gamma_j |\nabla \boldsymbol{B}_j|^2) d\Omega \right. \\ &\left. + \int_\Omega (\boldsymbol{f}_j \cdot \boldsymbol{u}_j + s(\nabla \times \boldsymbol{g}_j) \cdot \boldsymbol{B}_j) d\Omega + \int_\Gamma B_S(\boldsymbol{u}_j, \boldsymbol{B}_j) d\Gamma \right] \\ &+ \left[1 - \frac{\mathcal{F}(R_j)}{E_j} \right] \left| \int_\Omega (\boldsymbol{f}_j \cdot \boldsymbol{u}_j + s(\nabla \times \boldsymbol{g}_j) \cdot \boldsymbol{B}_j) d\Omega + \int_\Gamma B_S(\boldsymbol{u}_j, \boldsymbol{B}_j) d\Gamma \right|, \end{aligned} \tag{1.11}$$

where $B_S(\boldsymbol{u}_j, \boldsymbol{B}_j)$ represents the forcing terms on the boundary, defined as

$$\begin{aligned} B_S(\boldsymbol{u}_j, \boldsymbol{B}_j) = \int_\Gamma \Bigg(&- \frac{1}{2}|\boldsymbol{u}_j|^2 \boldsymbol{u}_j - \frac{s}{2}|\boldsymbol{B}_j|^2 \boldsymbol{u}_j + \nu_j \nabla \boldsymbol{u}_j \cdot \boldsymbol{u}_j - p_j \boldsymbol{u}_j \\ &+ s(\boldsymbol{B}_j \cdot \boldsymbol{u}_j)\boldsymbol{B}_j + s\gamma_j \nabla \boldsymbol{B}_j \cdot \boldsymbol{B}_j - s\lambda_j \boldsymbol{B}_j \Bigg) \cdot \hat{n} \; d\Gamma \end{aligned} \tag{1.12}$$

and $\hat{n}$ is the unit normal vector to the boundary.

As will be seen later, we consider this reformulation (including the addition of the terms within absolute value brackets) as a means of constructing numerical schemes that inherit unconditional stability with respect to the modified energy $\mathcal{F}(R_j)$ and guaranteed positivity of a computed scalar variable ξ_j to be defined.

1.2.1. BDF2 ALGORITHM. Based on the system (1.1), the artificial compression formulation (1.4) and (1.5) with $\epsilon = (\Delta t)^2$, and the scalar equation (1.11), a (semi-discrete) second order backward differentiation scheme is as follows: Given $\boldsymbol{u}_j^{n-1}$, $\boldsymbol{u}_j^n$, $\boldsymbol{B}_j^{n-1}$, $\boldsymbol{B}_j^n$, find $\boldsymbol{u}_j^{n+1}$, $\boldsymbol{B}_j^{n+1}$, p_j^{n+1} and λ_j^{n+1} satisfying

$$\left(\frac{3u_j^{n+1} - 4u_j^n + u_j^{n-1}}{2\Delta t}\right) = -\xi_j \left(\tilde{\boldsymbol{u}}_j^{n+1} \cdot \nabla\right) \tilde{\boldsymbol{u}}_j^{n+1} + s\xi_j \left(\tilde{\boldsymbol{B}}_j^{n+1} \cdot \nabla\right) \tilde{\boldsymbol{B}}_j^{n+1} + \bar{\nu}^n \Delta u_j^{n+1} \tag{1.13}$$

$$+ \nu_j'^n \Delta \tilde{\boldsymbol{u}}_j^{n+1} - \nabla \tilde{p}_j^{n+1} + \boldsymbol{f}_j^{n+1},$$

$$\nabla \cdot u_j^{n+1} + (\Delta t)^2 \epsilon_p \left(\frac{3p_j^{n+1} - 4p_j^n + p_j^{n-1}}{2\Delta t}\right) = 0, \tag{1.14}$$

$$\left(\frac{3\boldsymbol{B}_j^{n+1} - 4\boldsymbol{B}_j^n + \boldsymbol{B}_j^{n-1}}{2\Delta t}\right) = \xi_j \left(\tilde{\boldsymbol{B}}_j^{n+1} \cdot \nabla\right) \tilde{\boldsymbol{u}}_j^{n+1} - \xi_j \left(\tilde{\boldsymbol{u}}_j^{n+1} \cdot \nabla\right) \tilde{\boldsymbol{B}}_j^{n+1} + \bar{\gamma}^n \Delta \boldsymbol{B}_j^{n+1} \tag{1.15}$$

$$+ \gamma_j'^n \Delta \tilde{\boldsymbol{B}}_j^{n+1} - \nabla \tilde{\lambda}_j^{n+1} + \nabla \times \boldsymbol{g}_j^{n+1},$$

$$\nabla \cdot \boldsymbol{B}_j^{n+1} + (\Delta t)^2 \epsilon_\lambda \left(\frac{3\lambda_j^{n+1} - 4\lambda_j^n + \lambda_j^{n-1}}{2\Delta t}\right) = 0, \tag{1.16}$$

$$\xi_j = \frac{\mathcal{F}(\overset{*}{R}_j^{n+3/2})}{E^{n+3/2}}, \tag{1.17}$$

$$E^{n+3/2} = \frac{1}{2}\|\bar{\boldsymbol{u}}_j^{n+3/2}\|^2 + \frac{s}{2}\|\bar{\boldsymbol{B}}_j^{n+3/2}\|^2 + \frac{(\Delta t)^2}{2}(\epsilon_p ||\bar{p}_j^{n+3/2}||^2 + \epsilon_\lambda ||\bar{\lambda}_j^{n+3/2}||^2) + C_0,$$

$$\frac{\mathcal{F}(\overset{*}{R}_j^{n+3/2}) - \mathcal{F}(\overset{*}{R}_j^{n+1/2})}{\Delta t} = \int_\Omega u_j^{n+1} \cdot \delta_t u_j^{n+1} + s\boldsymbol{B}_j^{n+1} \cdot \delta_t \boldsymbol{B}_j^{n+1} \tag{1.18}$$

$$+(\Delta t)^2(\epsilon_p p_j^{n+1} \delta_t p_j^{n+1} + \epsilon_\lambda \lambda_j^{n+1} \delta_t \lambda_j^{n+1}) d\Omega$$

$$
\begin{aligned}
&- \int_\Omega u_j^{n+1} \cdot \Big[- \xi_j \left(\tilde{\boldsymbol{u}}_j^{n+1} \cdot \nabla \right) \tilde{\boldsymbol{u}}_j^{n+1} + s\xi_j \left(\tilde{\boldsymbol{B}}_j^{n+1} \cdot \nabla \right) \tilde{\boldsymbol{B}}_j^{n+1} \\
&+ \bar{\nu}^n \Delta u_j^{n+1} + \nu_j'^n \Delta \tilde{\boldsymbol{u}}_j^{n+1} - \nabla \tilde{p}_j^{n+1} + \boldsymbol{f}_j^{n+1} \Big] d\Omega \\
&- \int_\Omega s\boldsymbol{B}_j^{n+1} \cdot \Big[\xi_j \left(\tilde{\boldsymbol{B}}_j^{n+1} \cdot \nabla \right) \tilde{\boldsymbol{u}}_j^{n+1} - \xi_j \left(\tilde{\boldsymbol{u}}_j^{n+1} \cdot \nabla \right) \tilde{\boldsymbol{B}}_j^{n+1} \\
&+ \bar{\gamma}^n \Delta \boldsymbol{B}_j^{n+1} + \gamma_j'^n \Delta \tilde{\boldsymbol{B}}_j^{n+1} - \nabla \tilde{\lambda}_j^{n+1} + \nabla \times \boldsymbol{g}_j^{n+1} \Big] d\Omega \\
&+ \int_\Omega p_j^{n+1} \nabla \cdot \mathbf{u}_j^{n+1} + \lambda_j^{n+1} \nabla \cdot \mathbf{B}_j^{n+1} d\Omega \\
&+ \xi_j \Big[- \int_\Omega \left(\nu_j |\nabla \bar{\boldsymbol{u}}_j^{n+1}|^2 + s\gamma_j |\nabla \bar{\boldsymbol{B}}_j^{n+1}|^2 \right) d\Omega + \int_\Omega \boldsymbol{f}_j^{n+1} \cdot \bar{\boldsymbol{u}}_j^{n+1} d\Omega \\
&+ \int_\Omega s(\nabla \times \boldsymbol{g}_j^{n+1}) \cdot \bar{\boldsymbol{B}}_j^{n+1} d\Omega + \int_\Gamma B_S(\bar{\boldsymbol{u}}_j^{n+1}, \bar{\boldsymbol{B}}_j^{n+1}) d\Gamma \Big] \\
&+ (1 - \xi_j) \Big| \int_\Omega \boldsymbol{f}_j^{n+1} \cdot \bar{\boldsymbol{u}}_j^{n+1} d\Omega + \int_\Omega s(\nabla \times \boldsymbol{g}_j^{n+1}) \cdot \bar{\boldsymbol{B}}_j^{n+1} d\Omega + \int_\Gamma B_S(\bar{\boldsymbol{u}}_j^{n+1}, \bar{\boldsymbol{B}}_j^{n+1}) d\Gamma \Big|.
\end{aligned}
$$

Here $\bar{\boldsymbol{u}}_j^{n+1}$, $\bar{\boldsymbol{u}}_j^{n+3/2}$, $\bar{\boldsymbol{B}}_j^{n+1}$ and $\bar{\boldsymbol{B}}_j^{n+3/2}$ are second order approximations of u_j^{n+1}, $u_j^{n+3/2}$, $\boldsymbol{B}_j^{n+1}$, and $\boldsymbol{B}_j^{n+3/2}$ to be defined later.

1.2.2. CRANK-NICOLSON ALGORITHM. With Dirichlet boundary conditions, a Crank-Nicolson scheme for 1.1 becomes: Given $\boldsymbol{u}_j^n$, $\boldsymbol{B}_j^n$, q_j^n and p_j^n, find $\boldsymbol{u}_j^{n+1}$, $\boldsymbol{B}_j^{n+1}$, q_j^{n+1} and p_j^{n+1} satisfying

$$
\begin{aligned}
\left(\frac{u_j^{n+1} - u_j^n}{\Delta t} \right) &= -\xi_j \left(\tilde{\boldsymbol{u}}_j^{n+1/2} \cdot \nabla \right) \tilde{\boldsymbol{u}}_j^{n+1/2} + s\xi_j \left(\tilde{\boldsymbol{B}}_j^{n+1/2} \cdot \nabla \right) \tilde{\boldsymbol{B}}_j^{n+1/2} + \bar{\nu}^n \Delta u_j^{n+1/2} \\
&\quad + \nu_j'^n \Delta \tilde{\boldsymbol{u}}_j^{n+1/2} - \nabla p_j^{n+1/2} + \boldsymbol{f}_j^{n+1/2}, \qquad (1.19)
\end{aligned}
$$

$$
\nabla \cdot u_j^n + (\Delta t)^2 \epsilon_p \left(\frac{p_j^{n+1} - p_j^n}{\Delta t} \right) = 0, \qquad (1.20)
$$

$$
\begin{aligned}
\left(\frac{\boldsymbol{B}_j^{n+1} - \boldsymbol{B}_j^n}{\Delta t} \right) &= \xi_j \left(\tilde{\boldsymbol{B}}_j^{n+1/2} \cdot \nabla \right) \tilde{\boldsymbol{u}}_j^{n+1/2} - \xi_j \left(\tilde{\boldsymbol{u}}_j^{n+1/2} \cdot \nabla \right) \tilde{\boldsymbol{B}}_j^{n+1/2} + \bar{\gamma}^n \Delta \boldsymbol{B}_j^{n+1/2} \\
&\quad + \gamma_j'^n \Delta \tilde{\boldsymbol{B}}_j^{n+1/2} - \nabla \lambda_j^{n+1/2} + \nabla \times \boldsymbol{g}_j^{n+1/2}, \qquad (1.21)
\end{aligned}
$$

$$\nabla \cdot \boldsymbol{B}_j^n + (\Delta t)^2 \epsilon_\lambda \left(\frac{\lambda_j^{n+1} - \lambda_j^n}{\Delta t} \right) = 0, \tag{1.22}$$

$$\xi_j = \frac{\mathcal{F}(R_j^{n+1})}{E(\bar{\boldsymbol{u}}_j^{n+1}, \bar{\boldsymbol{B}}_j^{n+1})}, \tag{1.23}$$

$$E(\bar{\boldsymbol{u}}_j^{n+1}, \bar{\boldsymbol{B}}_j^{n+1}) = \frac{1}{2}\|\bar{\boldsymbol{u}}_j^{n+1}\|^2 + \frac{s}{2}\|\bar{\boldsymbol{B}}_j^{n+1}\|^2 + \frac{(\Delta t)^2}{2}(\epsilon_p ||\bar{p}_j^{n+1}||^2 + \epsilon_\lambda ||\bar{\lambda}_j^{n+1}||^2) + C_0, \tag{1.24}$$

$$\begin{aligned}
\frac{\mathcal{F}(R_j^{n+1}) - \mathcal{F}(R_j^n)}{\Delta t} &= \int_\Omega u_j^{n+1/2} \cdot \left(\frac{u_j^{n+1} - u_j^n}{\Delta t} \right) d\Omega + \int_\Omega s\boldsymbol{B}_j^{n+1/2} \cdot \left(\frac{\boldsymbol{B}_j^{n+1} - \boldsymbol{B}_j^n}{\Delta t} \right) d\Omega \\
&- \int_\Omega u_j^{n+1/2} \cdot \Big[-\xi_j \left(\tilde{\boldsymbol{u}}_j^{n+1/2} \cdot \nabla \right) \tilde{\boldsymbol{u}}_j^{n+1/2} + s\xi_j \left(\tilde{\boldsymbol{B}}_j^{n+1/2} \cdot \nabla \right) \tilde{\boldsymbol{B}}_j^{n+1/2} \\
&+ \bar{\nu}^n \Delta u_j^{n+1/2} + \nu_j'^n \Delta \tilde{\boldsymbol{u}}_j^{n+1/2} - \nabla p_j^{n+1/2} + \boldsymbol{f}_j^{n+1/2} \Big] d\Omega \\
&- \int_\Omega s\boldsymbol{B}_j^{n+1/2} \cdot \Big[\xi_j \left(\tilde{\boldsymbol{B}}_j^{n+1/2} \cdot \nabla \right) \tilde{\boldsymbol{u}}_j^{n+1/2} - \xi_j \left(\tilde{\boldsymbol{u}}_j^{n+1/2} \cdot \nabla \right) \tilde{\boldsymbol{B}}_j^{n+1/2} \\
&+ \bar{\gamma}^n \Delta \boldsymbol{B}_j^{n+1/2} + \gamma_j'^n \Delta \tilde{\boldsymbol{B}}_j^{n+1/2} - \nabla \lambda_j^{n+1/2} + \nabla \times \boldsymbol{g}_j^{n+1/2} \Big] d\Omega \\
&+ \xi_j \Big[-\int_\Omega \left(\nu_j |\nabla \bar{\boldsymbol{u}}_j^{n+1/2}|^2 + s\gamma_j |\nabla \bar{\boldsymbol{B}}_j^{n+1/2}|^2 \right) d\Omega + \int_\Omega \boldsymbol{f}_j^{n+1/2} \cdot \bar{\boldsymbol{u}}_j^{n+1/2} d\Omega \\
&+ \int_\Omega s(\nabla \times \boldsymbol{g}_j^{n+1/2}) \cdot \bar{\boldsymbol{B}}_j^{n+1/2} d\Omega + \int_\Gamma B_S(\bar{\boldsymbol{u}}_j^{n+1/2}, \bar{\boldsymbol{B}}_j^{n+1/2}) d\Gamma \Big] \\
&+ (1 - \xi_j) \Big| \int_\Omega \boldsymbol{f}_j^{n+1/2} \cdot \bar{\boldsymbol{u}}_j^{n+1/2} d\Omega + \int_\Omega s(\nabla \times \boldsymbol{g}_j^{n+1/2}) \cdot \bar{\boldsymbol{B}}_j^{n+1/2} d\Omega \\
&+ \int_\Gamma B_S(\bar{\boldsymbol{u}}_j^{n+1/2}, \bar{\boldsymbol{B}}_j^{n+1/2}) d\Gamma \Big|.
\end{aligned} \tag{1.25}$$

Similarly $\bar{\boldsymbol{u}}_j^{n+1}$, $\bar{\boldsymbol{u}}_j^{n+1/2}$, $\bar{\boldsymbol{B}}_j^{n+1}$ and $\bar{\boldsymbol{B}}_j^{n+1/2}$ are second order approximations of u_j^{n+1}, $u_j^{n+1/2}$, $\boldsymbol{B}_j^{n+1}$, and $\boldsymbol{B}_j^{n+1/2}$ that will be defined later.

In practice, $(u_j^0, u_j^1, B_j^0, B_j^1)$ may be found from the initial conditions and using an algorithm without SAV, such as the aforementioned ensemble scheme in [41]. In our implementations, we used a primitive (without ensemble) first order scheme to initialize as the computational cost of solving each perturbation in these first steps is not significant.

1.3. IMPLEMENTATION

Since the schemes are linear and the auxiliary variables are scalar functions of time variable, the resulting systems can be solved conveniently by superposition of a series of Helmhotz equations. We illustrate the idea by presenting the algorithms in strong form.

With the splitting

$$\mathbf{u}_j^{n+1} = \hat{\boldsymbol{v}}_j^{n+1} + \xi_j \breve{\boldsymbol{v}}_j^{n+1}, \quad \mathbf{B}_j^{n+1} = \hat{\boldsymbol{B}}_j^{n+1} + \xi_j \breve{\boldsymbol{B}}_j^{n+1}, \tag{1.26}$$

Algorithm (1.2.1) is equivalent to solving the following linear equations

Sub-problem 1: find $\hat{\boldsymbol{u}}_j^{n+1}$, $\hat{\boldsymbol{B}}_j^{n+1}$, $\hat{p}_j^{n+1}$ and $\hat{\lambda}_j^{n+1}$ satisfying

$$\frac{3}{2\Delta t}\hat{\boldsymbol{u}}_j^{n+1} - \bar{\nu}^n \Delta \hat{\boldsymbol{u}}_j^{n+1} = -\nabla \bar{p}_j^{n+1} + \boldsymbol{f}_j^{n+1} + \frac{2}{\Delta t}u_j^n - \frac{1}{2\Delta t}u_j^{n-1} + \nu_j'^n \Delta \tilde{\boldsymbol{u}}_j^{n+1}, \tag{1.27a}$$

$$\frac{3}{2\Delta t}\hat{\boldsymbol{B}}_j^{n+1} - \bar{\gamma}^n \Delta \hat{\boldsymbol{B}}_j^{n+1} = -\nabla \bar{\lambda}_j^{n+1} + \nabla \times \boldsymbol{g}_j^{n+1} + \frac{2}{\Delta t}\boldsymbol{B}_j^n - \frac{1}{2\Delta t}\boldsymbol{B}_j^{n-1} + \gamma_j'^n \Delta \tilde{\boldsymbol{B}}_j^{n+1}, \tag{1.27b}$$

Sub-problem 2: find $\breve{\boldsymbol{u}}_j^{n+1}$, $\breve{\boldsymbol{B}}_j^{n+1}$, $\breve{p}_j^{n+1}$ and $\breve{\lambda}_j^{n+1}$ satisfying

$$\frac{3}{2\Delta t}\breve{\boldsymbol{u}}_j^{n+1} - \bar{\nu}^n \Delta \breve{\boldsymbol{u}}_j^{n+1} = s\left(\tilde{\boldsymbol{B}}_j^{n+1} \cdot \nabla\right)\tilde{\boldsymbol{B}}_j^{n+1} - \left(\tilde{\boldsymbol{u}}_j^{n+1} \cdot \nabla\right)\tilde{\boldsymbol{u}}_j^{n+1}, \tag{1.28a}$$

$$\frac{3}{2\Delta t}\breve{\boldsymbol{B}}_j^{n+1} - \bar{\gamma}^n \Delta \breve{\boldsymbol{B}}_j^{n+1} = \left(\tilde{\boldsymbol{B}}_j^{n+1} \cdot \nabla\right)\tilde{\boldsymbol{u}}_j^{n+1} - \left(\tilde{\boldsymbol{u}}_j^{n+1} \cdot \nabla\right)\tilde{\boldsymbol{B}}_j^{n+1}, \tag{1.28b}$$

Update of ξ_j:

$$\xi_j = \frac{\mathcal{F}(\overset{*}{R}_j^{n+1/2}) + |S_0|\Delta t}{E^{n+3/2} + \Delta t \int_\Omega \left(\nu|\nabla \bar{\boldsymbol{u}}_j^{n+1}|^2 + s\gamma|\nabla \bar{\boldsymbol{B}}_j^{n+1}|^2\right) d\Omega + \Delta t(|S_0| - S_0)}, \tag{1.29}$$

where

$$S_0 = \int_\Omega \boldsymbol{f}_j^{n+1} \cdot \bar{\boldsymbol{u}}_j^{n+1} d\Omega + \int_\Omega s(\nabla \times \boldsymbol{g}_j^{n+1}) \cdot \bar{\boldsymbol{B}}_j^{n+1} d\Omega + \int_\Gamma B_S(\bar{\boldsymbol{u}}_j^{n+1}, \bar{\boldsymbol{B}}_j^{n+1}) d\Gamma, \tag{1.30}$$

with the second approximations:

$$\begin{cases} \bar{\boldsymbol{v}}_j^{n+1} & = \hat{\boldsymbol{v}}_j^{n+1} + \check{\boldsymbol{v}}_j^{n+1}, \quad (1.31) \\ \bar{\boldsymbol{v}}_j^{n+3/2} & = \frac{3}{2}\bar{\boldsymbol{v}}_j^{n+1} - \frac{1}{2}\boldsymbol{v}^n. \quad (1.32) \end{cases}$$

Once we have ξ_j we update R_j^{n+1} as follows:

$$\begin{cases} \overset{*}{R}_j^{n+3/2} & = \mathcal{G}\left(\xi_j E(\bar{\boldsymbol{u}}_j^{n+3/2}, \bar{\boldsymbol{B}}_j^{n+3/2})\right), \quad (1.33) \\ R_j^{n+1} & = \frac{2}{3}\overset{*}{R}_j^{n+3/2} + \frac{1}{3}R_j^n. \quad (1.34) \end{cases}$$

Finally, the pressure is updated by L^2 projection:

$$\left(\nabla \cdot \mathbf{u}_j^{n+1}, (\Delta t)^2 \delta_t p_j^{n+1}, l\right) = 0, \quad (1.35a)$$

$$\left(\nabla \cdot \mathbf{B}_j^{n+1}, (\Delta t)^2 \delta_t \lambda_j^{n+1}, \psi\right) = 0. \quad (1.35b)$$

Algorithm (1.2.2) can be implemented in a similar fashion.

1.4. NUMERICAL TESTS

This section will present numerical results for Algorithms (1.2.2) and (1.2.1) to demonstrate the expected convergence rates and the stability. We set $\mathcal{F}(\chi) = \chi^2$ and the corresponding $\mathcal{G}(\chi) = \sqrt{\chi}$ in every experiment. Throughout these tests we'll use the finite element triplet (P^2–P^1–P^2), and the finite element software package FEniCS [24].

1.4.1. CONVERGENCE TEST. To verify the expected convergence rates, we will use a variation of the test problem in [65]. Take the time interval $0 \leq t \leq 1$ and domain $\Omega = [0, 1]^2$. Define the true solution (u, p, B) as

$$\begin{cases} u_\epsilon = \left(y^5 + t^2, x^5 + t^2\right)(1+\epsilon), \\ p_\epsilon = 10(2x-1)(2y-1)(1+t^2)(1+\epsilon), \\ B_\epsilon = \left(\sin(\pi y) + t^2, \sin(\pi x) + t^2\right)(1+\epsilon), \end{cases} \tag{1.36}$$

where ϵ is a given perturbation. For this problem we will consider two perturbations $\epsilon_1 = 10^{-1}$ and $\epsilon_2 = -10^{-1}$. The kinematic viscosity and magnetic resistivity are defined as $\nu_\epsilon = 0.5 \cdot (1+\epsilon)$ and $\gamma_\epsilon = 0.5 \cdot (1+\epsilon)$. Regularization coefficients are set as $\alpha = \alpha_M = 0.5$. The pressure and solenoidal constraint scalars are set as $\epsilon_p = \epsilon_\lambda = 10$ in each test. The source terms and initial conditions correspond with the exact solution for the given perturbation. For each algorithm we initialize u_j, B_j, p_j or λ_j using the exact solution. The results are displayed in tables (1.1)-(1.8) with regularization. Under this test, we indeed observe second order convergence with and without regularization. In this particular test on a short time interval, we also observe the algorithm with regularization achieves relatively similar accuracy to the algorithm without.

Table 1.1. Crank-Nicolson error and convergence rates for the first ensemble member in u_h and ∇u_h.

h	Δt	$\|u_1 - u_{1,h}\|_{\infty,0_{rel}}$	Rate	$\|\nabla u_1 - \nabla u_{1,h}\|_{2,0_{rel}}$	Rate
1/10	1/8	2.313 e-2	—	6.688 e-2	—
1/20	1/16	9.126 e-3	1.342	2.242 e-2	1.577
1/40	1/32	2.364 e-3	1.949	6.435 e-3	1.801
1/80	1/64	6.633 e-4	1.833	1.750 e-3	1.879
1/160	1/128	1.760 e-4	1.914	4.591 e-4	1.930

Table 1.2. Crank-Nicolson error and convergence rates for the first ensemble member in B_h and ∇B_h.

h	Δt	$\|B_1 - B_{1,h}\|_{\infty,0_{rel}}$	Rate	$\|\nabla B_1 - \nabla B_{1,h}\|_{2,0_{rel}}$	Rate
1/10	1/8	7.328 e-4	—	3.986 e-3	—
1/20	1/16	1.816 e-4	2.012	1.098 e-3	1.861
1/40	1/32	4.918 e-5	1.885	2.845 e-4	1.948
1/80	1/64	1.347 e-5	1.868	7.294 e-5	1.964
1/160	1/128	3.575 e-6	1.914	1.852 e-5	1.978

Table 1.3. Crank-Nicolson error and convergence rates for the second ensemble member in u_h and ∇u_h.

h	Δt	$\|u_2 - u_{2,h}\|_{\infty,0_{rel}}$	Rate	$\|\nabla u_2 - \nabla u_{2,h}\|_{2,0_{rel}}$	Rate
1/10	1/8	2.271 e-2	—	6.562 e-2	—
1/20	1/16	9.028 e-3	1.331	2.236 e-2	1.553
1/40	1/32	2.358 e-3	1.937	6.431 e-3	1.798
1/80	1/64	6.626 e-4	1.831	1.750 e-3	1.878
1/160	1/128	1.759 e-4	1.914	4.591 e-4	1.930

Table 1.4. Crank-Nicolson error and convergence rates for the second ensemble member in B_h and ∇B_h.

h	Δt	$\|B_2 - B_{2,h}\|_{\infty,0_{rel}}$	Rate	$\|\nabla B_2 - \nabla B_{2,h}\|_{2,0_{rel}}$	Rate
1/10	1/8	8.214 e-4	—	4.102 e-3	—
1/20	1/16	2.056 e-4	1.998	1.146 e-3	1.840
1/40	1/32	5.682 e-5	1.855	3.000 e-4	1.934
1/80	1/64	1.565 e-5	1.861	7.752 e-5	1.953
1/160	1/128	4.153 e-6	1.913	1.977 e-5	1.971

Table 1.5. BDF2 error and convergence rates for the first ensemble member in u_h and ∇u_h.

h	Δt	$\|u_1 - u_{1,h}\|_{\infty,0_{rel}}$	Rate	$\|\nabla u_1 - \nabla u_{1,h}\|_{2,0_{rel}}$	Rate
1/10	1/8	2.551 e-2	—	7.735 e-2	—
1/20	1/16	8.397 e-3	1.603	2.341 e-2	1.725
1/40	1/32	2.401 e-3	1.807	6.598 e-3	1.827
1/80	1/64	6.495 e-4	1.886	1.773 e-3	1.896
1/160	1/128	1.720 e-4	1.917	4.620 e-4	1.940

Table 1.6. BDF2 error and convergence rates for the first ensemble member in B_h and ∇B_h.

h	Δt	$\|B_1 - B_{1,h}\|_{\infty,0_{rel}}$	Rate	$\|\nabla B_1 - \nabla B_{1,h}\|_{2,0_{rel}}$	Rate
1/10	1/8	1.277 e-3	—	5.457 e-3	—
1/20	1/16	3.477 e-4	1.877	1.415 e-3	1.948
1/40	1/32	9.311 e-5	1.901	3.731 e-4	1.923
1/80	1/64	2.448 e-5	1.928	9.686 e-5	1.946
1/160	1/128	6.289 e-6	1.961	2.477 e-5	1.967

Table 1.7. BDF2 error and convergence rates for the second ensemble member in u_h and ∇u_h.

h	Δt	$\|u_2 - u_{2,h}\|_{\infty,0_{rel}}$	Rate	$\|\nabla u_2 - \nabla u_{2,h}\|_{2,0_{rel}}$	Rate
1/10	1/8	2.480 e-2	—	7.575 e-2	—
1/20	1/16	8.288 e-3	1.581	2.327 e-2	1.703
1/40	1/32	2.391 e-3	1.794	6.591 e-3	1.820
1/80	1/64	6.495 e-4	1.880	1.772 e-3	1.895
1/160	1/128	1.721 e-4	1.916	4.619 e-4	1.940

Table 1.8. BDF2 error and convergence rates for the second ensemble member in B_h and ∇B_h.

h	Δt	$\|B_2 - B_{2,h}\|_{\infty,0_{rel}}$	Rate	$\|\nabla B_2 - \nabla B_{2,h}\|_{2,0_{rel}}$	Rate
1/10	1/8	1.462 e-3	—	6.222 e-3	—
1/20	1/16	3.995 e-4	1.872	1.589 e-3	1.970
1/40	1/32	1.065 e-4	1.908	4.167 e-4	1.931
1/80	1/64	2.806 e-5	1.924	1.081 e-4	1.947
1/160	1/128	7.218 e-6	1.959	2.766 e-5	1.967

1.4.2. STABILITY. In this section, we analyze the stability of our ensemble methods. We consider a problem without external energy and body forces, so that the system energy should decay to zero as time passes. The initial conditions used are given by:

$$\begin{cases} u_\epsilon^0 = (x^2(x-1)^2y(y-1)(2y-1), -y^2(y-1)^2x(x-1)(2x-1))(1+\epsilon), \\ p_\epsilon^0 = 0, \quad \lambda_\epsilon^0 = 0, \\ B_\epsilon^0 = (\sin(\pi x)\cos(\pi y), -\sin(\pi y)\cos(\pi x))(1+\epsilon). \end{cases} \tag{1.37}$$

We consider an ensemble of two perturbations, $\epsilon = 10^{-1}$ and $\epsilon = -10^{-1}$. We fix the coupling term $s = 1$ and test two different sets of viscosity and magnetic viscosity, $\nu = \gamma = 0.1$ and $\nu = \gamma = 0.02$. We again set $\epsilon_p = \epsilon_\lambda = 10$. The mesh discretization is fixed at $h = 1/50$, and we use several time step refinements, with a final time of $T = 1$.

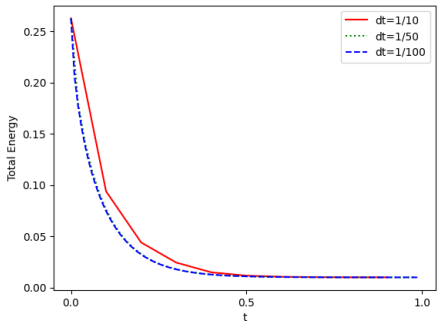

(a) Decay of total system energy to $T = 1$ with $\nu = \gamma = 0.1$.

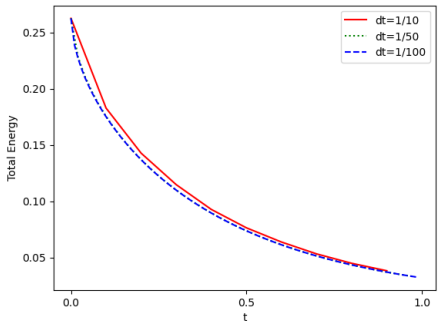

(b) Decay of total system energy to $T = 1$ with $\nu = \gamma = 0.02$.

Figure 1.1. Stability demonstrations of Crank-Nicolson Algorithm (1.2.2)

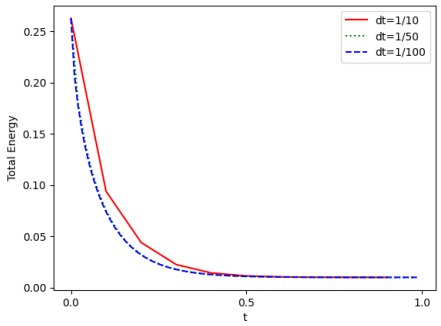

(a) Decay of total system energy to $T = 1$ with $\nu = \gamma = 0.1$.

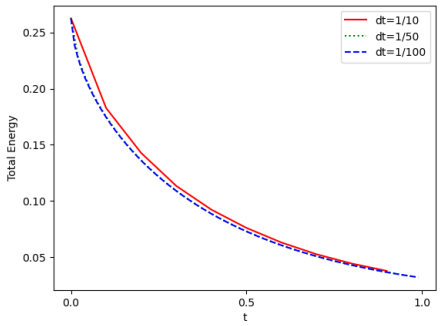

(b) Decay of total system energy to $T = 1$ with $\nu = \gamma = 0.02$.

Figure 1.2. Stability demonstrations of BDF2 Algorithm (1.2.1)

These figures accurately portray the decay of the total system energy to $T = 1$ for Algorithm (1.2.2) with $\nu = \gamma = 0.1$ and $\nu = \gamma = 0.02$, respectively. Figures 1.2a and 1.2b also show decay to $T = 1$ for Algorithm (1.2.1) with $\nu = \gamma = 0.1$ and $\nu = \gamma = 0.02$.

2. SUMMARY AND CONCLUSIONS

In conclusion, we've presented efficient second-order ensemble methods for fluid flow simulations using SAV and artificial compressibility techniques. With regularization, the proposed methods demonstrate significant improvements in stability, long-time accuracy, and efficiency over existing methods, as demonstrated by simulations such as the channel flow about a cylinder.

Our findings contribute to the advancement of numerical methods for fluid flow simulations and have important practical use for a variety of scientists and engineers studying MHD flows. The use of ensemble methods offers a promising means of achieving efficient predictions for problems such as atmospheric modelling, and the use of artificial compressibility techniques stack even greater efficiency in-tandum with the ensemble methods.

Future work in this area could explore the use of different types of compressibility and pressure correction techniques and the extension of the methods to more complex flow scenarios. We hope that the results presented in this thesis will inspire further research in this exciting field and lead to new developments in the use of ensemble methods for fluid flow simulations.

REFERENCES

[1] P. R. Amestoy, I. S. Duff, J. Y. L'Excellent, and J. Koster, "A fully asynchronous multifrontal solver using distributed dynamic scheduling," *SIAM Journal on Matrix Analysis and Applications*, vol. 23, no. 1, pp. 15–41, 2001.

[2] N. Jiang and W. Layton, "Numerical analysis of two ensemble eddy viscosity numerical regularizations of fluid motion," *Numerical Methods for Partial Differential Equations*, vol. 31, no. 3, pp. 630–651, 2015.

[3] A. Takhirov, M. Neda, and J. Waters, "Time relaxation algorithm for flow ensembles," *Numerical Methods for Partial Differential Equations*, vol. 32, no. 3, pp. 757–777, 2016.

[4] J. Connors, "An ensemble-based conventional turbulence model for fluid-fluid interactions," *INTERNATIONAL JOURNAL OF NUMERICAL ANALYSIS AND MODELING*, vol. 15, no. 4-5, pp. 492–519, 2018.

[5] N. Jiang, S. Kaya, and W. Layton, "Analysis of model variance for ensemble based turbulence modeling," *Computational Methods in Applied Mathematics*, vol. 15, no. 4-5, pp. 173–188, 2015.

[6] J. A. Fiordilino, "A second order ensemble timestepping algorithm for natural convection," *SIAM Journal on Numerical Analysis*, vol. 56, no. 2, pp. 816–837, 2018.

[7] N. Jiang, "A pressure-correction ensemble scheme for computing evolutionary Boussinesq equations," *J. Sci. Comput.*, vol. 80, no. 1, pp. 315–350, 2019.

[8] N. Jiang and C. Qiu, "An efficient ensemble algorithm for numerical approximation of stochastic stokes–darcy equations," *Computer Methods in Applied Mechanics and Engineering*, vol. 343, pp. 249–275, 2019.

[9] N. Jiang and M. Schneier, "An efficient, partitioned ensemble algorithm for simulating ensembles of evolutionary mhd flows at low magnetic reynolds number," *Numerical Methods for Partial Differential Equations*, vol. 34, no. 6, pp. 2129–2152, 2018.

[10] M. Mohebujjaman and L. G. Rebholz, "An efficient algorithm for computation of mhd flow ensembles," *Computational Methods in Applied Mathematics*, vol. 17, no. 1, pp. 121–137, 2017.

[11] X. He, N. Jiang, and C. Qiu, "An artificial compressibility ensemble algorithm for a stochastic stokes-darcy model with random hydraulic conductivity and interface conditions," *International Journal for Numerical Methods in Engineering*, vol. 121, no. 4, pp. 712–739, 2020.

[12] Y. Luo and Z. Wang, "An ensemble algorithm for numerical solutions to deterministic and random parabolic pdes," *SIAM Journal on Numerical Analysis*, vol. 56, no. 2, pp. 859–876, 2018.

[13] Y. Luo and Z. Wang, "A multilevel monte carlo ensemble scheme for random parabolic pdes," *SIAM Journal on Scientific Computing*, vol. 41, no. 1, pp. A622–A642, 2019.

[14] N. Li, J. Fiordilino, and X. Feng, "Ensemble time-stepping algorithm for the convection-diffusion equation with random diffusivity," *Journal of Scientific Computing*, vol. 79, no. 2, pp. 1271–1293, 2019.

[15] M. Gunzburger, T. Iliescu, and M. Schneier, "A Leray regularized ensemble-proper orthogonal decomposition method for parameterized convection-dominated flows," *IMA Journal of Numerical Analysis*, vol. 40, pp. 886–913, 01 2019.

[16] M. Gunzburger, N. Jiang, and M. Schneier, "An ensemble-proper orthogonal decomposition method for the nonstationary navier–stokes equations," *SIAM Journal on Numerical Analysis*, vol. 55, no. 1, pp. 286–304, 2017.

[17] M. Gunzburger, N. Jiang, and M. Schneier, "A higher-order ensemble/proper orthogonal decomposition method for the nonstationary navier-stokes equations," *International Journal of Numerical Analysis and Modeling*, vol. 15, no. 4-5, pp. 608–627, 2018.

[18] M. D. Gunzburger, *Finite Element Methods for Viscous Incompressible Flows*. San Diego: Academic Press, 1989.

[19] S. Brenner and R. Scott, *The Mathematical Theory of Finite Element Methods*. New York, NY: Springer, 2008.

[20] W. Layton, *Introduction to the Numerical Analysis of Incompressible Viscous Flows*. Philadelphia, PA: Society for Industrial and Applied Mathematics, 2008.

[21] J. G. Heywood and R. Rannacher, "Finite-element approximation of the nonstationary navier-stokes problem part iv: Error analysis for second-order time discretization," *SIAM Journal on Numerical Analysis*, vol. 27, no. 2, pp. 353–384, 1990.

[22] V. Girault and P. A. Raviart, *Finite Element Approximation of the Navier-Stokes Equations*. Berlin, Heidelberg: Springer, 1979.

[23] V. Girault and P. A. Raviart, *Finite Element Methods for Navier-Stokes Equations*. Berlin, Heidelberg: Springer, 1986.

[24] M. Alnæs, J. Blechta, J. Hake, A. Johansson, B. Kehlet, A. Logg, C. Richardson, J. Ring, M. Rognes, and G. Wells, "The fenics project version 1.5," vol. 3, 01 2015.

[25] W. Layton, H. Tran, and C. Trenchea, "Numerical analysis of two partitioned methods for uncoupling evolutionary mhd flows," *Numerical Methods for Partial Differential Equations*, vol. 30, no. 4, pp. 1083–1102, 2014.

[26] P. R. Amestoy, I. S. Duff, J. Y. L'Excellent, and J. Koster, "A fully asynchronous multifrontal solver using distributed dynamic scheduling," *SIAM Journal on Matrix Analysis and Applications*, vol. 23, no. 1, pp. 15–41, 2001.

[27] P. R. Amestoy, A. Guermouche, J. Y. L'Excellent, and S. Pralet, "Hybrid scheduling for the parallel solution of linear systems," *Parallel Computing*, vol. 32, no. 2, pp. 136–156, 2006. Parallel Matrix Algorithms and Applications (PMAA'04).

[28] W. Layton, H. Tran, and C. Trenchea, "Stability of partitioned methods for magneto-hydrodynamics flows at small magnetic reynolds number," *Contemp Math*, vol. 586, 04 2013.

[29] N. Jiang and W. Layton, "An algorithm for fast calculation of flow ensembles," *Int. J. Uncertain. Quantif.*, vol. 4, no. 4, pp. 273–301, 2014.

[30] N. Jiang and W. Layton, "Numerical analysis of two ensemble eddy viscosity numerical regularizations of fluid motion," *Numer. Methods Partial Differential Equations*, vol. 31, no. 3, pp. 630–651, 2015.

[31] N. Jiang, "A higher order ensemble simulation algorithm for fluid flows," *J. Sci. Comput.*, vol. 64, no. 1, pp. 264–288, 2015.

[32] N. Jiang, "A second-order ensemble method based on a blended backward differentiation formula timestepping scheme for time-dependent Navier-Stokes equations," *Numer. Methods Partial Differential Equations*, vol. 33, no. 1, pp. 34–61, 2017.

[33] M. Gunzburger, N. Jiang, and M. Schneier, "An ensemble-proper orthogonal decomposition method for the nonstationary Navier-Stokes equations," *SIAM J. Numer. Anal.*, vol. 55, no. 1, pp. 286–304, 2017.

[34] J. A. Fiordilino, "A second order ensemble timestepping algorithm for natural convection," *SIAM J. Numer. Anal.*, vol. 56, no. 2, pp. 816–837, 2018.

[35] M. Gunzburger, N. Jiang, and Z. Wang, "An efficient algorithm for simulating ensembles of parameterized flow problems," *IMA J. Numer. Anal.*, vol. 39, no. 3, pp. 1180–1205, 2019.

[36] N. Jiang and C. Qiu, "An efficient ensemble algorithm for numerical approximation of stochastic Stokes-Darcy equations," *Comput. Methods Appl. Mech. Engrg.*, vol. 343, pp. 249–275, 2019.

[37] N. Jiang, Y. Li, and H. Yang, "An artificial compressibility Crank-Nicolson leap-frog method for the Stokes-Darcy model and application in ensemble simulations," *SIAM J. Numer. Anal.*, vol. 59, no. 1, pp. 401–428, 2021.

[38] N. Jiang and M. Schneier, "An efficient, partitioned ensemble algorithm for simulating ensembles of evolutionary MHD flows at low magnetic Reynolds number," *Numer. Methods Partial Differential Equations*, vol. 34, no. 6, pp. 2129–2152, 2018.

[39] J. Carter and N. Jiang, "Numerical analysis of a second order ensemble method for evolutionary magnetohydrodynamics equations at small magnetic reynolds number," *Numer. Methods Partial Differ. Eq.*, 2022.

[40] W. M. Elsasser, "The hydromagnetic equations," *Phys. Rev.*, vol. 79, pp. 183–183, Jul 1950.

[41] M. Mohebujjaman and L. G. Rebholz, "An efficient algorithm for computation of MHD flow ensembles," *Comput. Methods Appl. Math.*, vol. 17, no. 1, pp. 121–137, 2017.

[42] M. Mohebujjaman, H. Wang, L. G. Rebholz, and M. A. A. Mahbub, "An efficient algorithm for simulating ensembles of parameterized mhd flow problems," 2021.

[43] F. Guillén-González and G. Tierra, "On linear schemes for a Cahn-Hilliard diffuse interface model," *J. Comput. Phys.*, vol. 234, pp. 140–171, 2013.

[44] X. Yang, J. Zhao, and Q. Wang, "Numerical approximations for the molecular beam epitaxial growth model based on the invariant energy quadratization method," *J. Comput. Phys.*, vol. 333, pp. 104–127, 2017.

[45] X. Yang and L. Ju, "Linear and unconditionally energy stable schemes for the binary fluid-surfactant phase field model," *Comput. Methods Appl. Mech. Engrg.*, vol. 318, pp. 1005–1029, 2017.

[46] Y. Gong, J. Zhao, and Q. Wang, "Arbitrarily high-order linear energy stable schemes for gradient flow models," *J. Comput. Phys.*, vol. 419, pp. 109610, 20, 2020.

[47] J. Shen, J. Xu, and J. Yang, "The scalar auxiliary variable (SAV) approach for gradient flows," *J. Comput. Phys.*, vol. 353, pp. 407–416, 2018.

[48] J. Shen, J. Xu, and J. Yang, "A new class of efficient and robust energy stable schemes for gradient flows," *SIAM Rev.*, vol. 61, no. 3, pp. 474–506, 2019.

[49] Z. Yang and S. Dong, "An unconditionally energy-stable scheme based on an implicit auxiliary energy variable for incompressible two-phase flows with different densities involving only precomputable coefficient matrices," *J. Comput. Phys.*, vol. 393, pp. 229–257, 2019.

[50] Z. Yang and S. Dong, "A roadmap for discretely energy-stable schemes for dissipative systems based on a generalized auxiliary variable with guaranteed positivity," *J. Comput. Phys.*, vol. 404, pp. 109121, 46, 2020.

[51] X. Yang, "A novel fully-decoupled, second-order and energy stable numerical scheme of the conserved Allen-Cahn type flow-coupled binary surfactant model," *Comput. Methods Appl. Mech. Engrg.*, vol. 373, p. 113502, 2021.

[52] W. Chen, X. Wang, Y. Yan, and Z. Zhang, "New sav-pressure correction methods for the navier-stokes equations: Stability and error analysis," *Math. Comp.*, 2021.

[53] N. Jiang and H. Yang, "SAV decoupled ensemble algorithms for fast computation of Stokes-Darcy flow ensembles," *Comput. Methods Appl. Mech. Engrg.*, vol. 387, pp. Paper No. 114150, 34, 2021.

[54] A. Labovsky, W. J. Layton, C. C. Manica, M. Neda, and L. G. Rebholz, "The stabilized extrapolated trapezoidal finite-element method for the Navier-Stokes equations," *Comput. Methods Appl. Mech. Engrg.*, vol. 198, no. 9-12, pp. 958–974, 2009.

[55] X. Li, W. Wang, and J. Shen, "Stability and Error Analysis of IMEX SAV Schemes for the Magneto-Hydrodynamic Equations," *SIAM J. Numer. Anal.*, vol. 60, no. 3, pp. 1026–1054, 2022.

[56] C. Zhang, J. Ouyang, C. Wang, and S. M. Wise, "Numerical comparison of modified-energy stable SAV-type schemes and classical BDF methods on benchmark problems for the functionalized Cahn-Hilliard equation," *J. Comput. Phys.*, vol. 423, pp. 109772, 35, 2020.

[57] M. Jiang, Z. Zhang, and J. Zhao, "Improving the accuracy and consistency of the scalar auxiliary variable (SAV) method with relaxation," *J. Comput. Phys.*, vol. 456, p. Paper No. 110954, 2022.

[58] C. Foias, D. D. Holm, and E. S. Titi, "The Navier-Stokes-alpha model of fluid turbulence," vol. 152/153, pp. 505–519, 2001. Advances in nonlinear mathematics and science.

[59] S. Chen, D. D. Holm, L. G. Margolin, and R. Zhang, "Direct numerical simulations of the Navier-Stokes alpha model," vol. 133, pp. 66–83, 1999. Predictability: quantifying uncertainty in models of complex phenomena (Los Alamos, NM, 1998).

[60] D. Wei and Z. Zhang, "Global well-posedness of the MHD equations in a homogeneous magnetic field," *Anal. PDE*, vol. 10, no. 6, pp. 1361–1406, 2017.

[61] C. Trenchea, "Unconditional stability of a partitioned IMEX method for magnetohydrodynamic flows," *Appl. Math. Lett.*, vol. 27, pp. 97–100, 2014.

[62] M. D. Gunzburger, *Finite Element Methods for Viscous Incompressible Flows*. Computer Science and Scientific Computing, San Diego: Academic Press, 1989.

[63] S. Brenner and R. Scott, *The Mathematical Theory of Finite Element Methods*. Texts in Applied Mathematics, Springer New York, 2007.

[64] R. H. Kraichnan, "Inertial ranges in two-dimensional turbulence," *The Physics of Fluids*, vol. 10, no. 7, pp. 1417–1423, 1967.

[65] G. Zhang, X. He, and X. Yang, "Fully decoupled, linear and unconditionally energy stable time discretization scheme for solving the magneto-hydrodynamic equations," *Journal of Computational and Applied Mathematics*, vol. 369, p. 112636, 12 2019.

VITA

John Carter was raised in Ellsinore, a small town near the bootheel of Missouri. He grew up there and graduated from East Carter high school before leaving for Springfield, MO to attend Missouri State University (MSU). He received his bachelor degree in mathematics there, then completed a masters degree in pure mathematics while working part time as a software developer at the headquarters of O'Reilly Automotives. From Fall 2018, he started his Ph.D studies in applied and computational mathematics at Missouri University of Science and Technology (S&T) under the supervision of Dr. Han Daozhi and Dr. Nan Jiang. His research was focused on partial differential equations that model physical systems, numerical methods via analysis, scientific computing, ensemble and regularization techniques. In July 2023, he received his PhD in Mathematics with Applied and Computational Mathematics emphasis from Missouri S&T.

John enjoys a variety of sports, weightlifting, science fiction, Dungeons and Dragons, and computer architecture.